X chromosome as a polarising signal in asymmetric cell division

by

Talal Ali Mohammed AL Yazeedi

A thesis submitted in partial fullfuilment of
the requirments for the degree
of Doctor of Philosophy

University of Warwick, School of life Sciences
Februaury, 2020

Table of Contents

List of Tables

List of Figures

List of Abbreviations:

abs aberrant spermatocyte

ACD Asymmetric Cell Division

AI Anaphase I

AII Anaphase II

ASE Autosomal signal elements

Asym Asymmetric

ATP Adenosine Triphosphate

ATPB ATP synthase beta subunit

B Big DNA mass, Big DPI surface area

Bam Binary equivalent of sam

Blast Basic local alignment search tool

BSA Bulk Segregant Analysis

BWA Burrow-Wheeler Aligner for short reads

CI Confidence Intervals

cRB central Residual Body

DAPI 4′,6-diamidino-2-phenylindole, a florescent stain used to visualise DNA

DIC Differential Interference Contrast microscopy

DNA Deoxy Ribonucleic Acid

DP Depth Coverage

EMS

Eq Equal

FastQC Fasta Quality Check, a quality control software for high throughput sequencing

F_n Filial, n = Generation number

GATK Genomic Analysis Tool Kit

GO Gene Ontology

GQ Genotype Quality

H-pool DNA pool from lines producing high number of males

HB High Bulk, DNA bulk from high male lines

HM High Male

IA Inbreeding Avoidance

K Keimbahn, germline-limited chromosome in *Acricotopus lucidu*

L-pool DNA pool from lines producing low number of males

L1-L4 Larvae stages 1-4

LB Low Bulk, DNA bulk from low male lines

LG, lg Linkage Group

LM Low Male

MQ RMSMapping Quality

MQRankSum Mapping Quality RankSum Test

mRNA messenger Ribonucleic Acid

MSP Major Sperm Protein

mtDNA mitochondrial DNA

NCBI National Center for Biotechnology Information

nDNA nuclear DNA

NGS Next Generation Sequencing

P_0 Parental generation

PCR Polymerase Chain Reaction

QD Quality Depth

QTL Quantitative Trait Loci

QUAL quality score on Phred-scale

RB Residual Body

ReadPosRankSum Read Position RankSum Test

RIAILs Recombinant Inbred Advance Intercross Lines

RILs Recombinant Inbred Lines

ROS Reactive Oxygen Species

RT Restriction Enzyme

S Small DNA mass, Small DAPI surface area

S Somatic chromosome in *Acricotopus lucidu*

Sam Sequence alignment/map

SLC Stem-Like Cells

SNP Single Nucleotide Polymorphism

SOR Strand Odds Ratio

sp spermatid

spI primary spermatocyte

spII secondary spermatocyte

SWD Single Worm Decent

Sym Symmetric

tra Transformer

Uneq unequal

VCF Variant Calling Files

wt, WT wildtype

XSE X signal elements

GSD Genotypic sex determination

ESD Environmental sex determination

List of Units:

h Hour(s)

min minute

s second

g Gram

µg microgram

ng nanogram

L Litter

ml Millilitre

M Molar

mM Millimolar

µM Micromolar

mg Milligram

$_{o}$C degree Celsius

µg/ml microgram per millilitre

mg/ml milligram per millilitre

cm centimetre

µm micrometre

mm millimetre

µl microliter

N Normality of a solution
bp base pair
Mbp, **Mb** Mega base pair, Mega base
Kb Kilobase pair

Acknowledgments

First and foremost, I would like to give my special thanks to my supervisor, Dr Andre Pires da Silva. I really could not ask for a better mentor. Thank you for your support, encouragement, understanding and immense Knowledge.

Thank you for all the members of Pires lab, both past and present, who made time during my postgraduate so memorable. My sincere thanks go to all my lab colleagues, past and present, especially, Sally Adams, Pedro Robels, Henry Ancell, Giusy Zuco, Anisa Turner and Panagiota Paganopoulou.

I am grateful to my advisory panel, Prof. Robin Allaby and Dr. Patrick Schafer, for their scientific discussion and insights. I am also thankful for my collaborators Dr. Diane Shakes, especially her lab member Emily Xu, and Jun Kim for their great experimental and technical help.

Finally, I would like to thank my family for their unwavering limitless support, optimism and love.

Declaration

This thesis has been submitted to the University of Warwick in support of my application for a degree of Doctor of philosophy. It has been composed by myself and has not been submitted to support the application of any other degree.

The work presented (including data generated and data analysis) were carried out by the author except in the cases outlined below:

- Figure 1.11 was provided by collaborator Anna Schwarz.
- *A. rhodensis* X chromosome markers used in Chapter 3 was created by Sophie Tandonnet.
- Genotyping of some masculiniser progeny in figure 3.1 was conducted by Jasmin Kaur.
- Immunostaining of masculiniser spermatogenesis in figure 3.12 and 3.13 was conducted in collaboration with Emily Xu from Prof. Diane Shakes laboratory.
- *A. freiburgensis clear-1* mutant in figure 5.5 was created by Thomas Murrell.
- The schematic meiosis on figure 1.12 and 4.15 were adapted from figures created by Andre Pires da Silva.
- *A. freiburgensis* X chromosome marker in table C.1 was created by Sally Adams.

Abstract

In the nematode genus of *Auanema*, sex is determined by X chromosome dosage, females and self-fertilising hermaphrodites are XX and males are XO. Surprisingly, cross between XX female and XO male results in mostly XX progeny. This occurs because males only produce one functional sperm bearing an X chromosome, whereas nullo-X sperm is discarded. The exclusive formation of X-bearing sperm by males is attributed to the asymmetric segregation of essential sperm components, necessary for sperm function and motility, with the X chromosome. Whereas non-essential cytoplasmic materials (e.g., Golgi complex, ribosomes) disposed of in the nullo-X cell that takes the role of a residual body. This unique system permits easy-to-score phenotype on the organismal level to study asymmetric cell division; because the sex ratio of a cross-progeny can be used to monitor the type of divisions occurring during male spermatogenesis. Here I report that during *Auanema* spermatogenesis, the X chromosome acts as a polarising signal for sperm components to segregate with the cell inheriting the X chromosome.

Sperm components also segregate with the X chromosomes in other *A. rhodensis* spermatogenesis models. During the spermatogenesis of *A. rhodensis* XX hermaphrodites, sperm components segregate to the cell inheriting the X chromosome. Similarly, I identified that during the spermatogenesis of *A. rhodensis* masculiniser mutant *Arh-mas-1* (Genetically XX but with a male morphology), sperm components co-segregate with X chromosomes in asymmetric division or equally with X chromosomes to both daughter cells in symmetric division.

I demonstrated that shuffling X chromosome haplotype blocks in *A. freiburgensis* RIAILs from two strains with different genetic background resulted in a new transgressive phenotype. Where, males from RIAILs produced a high number of males, due to their ability to form a functional nullo-X sperm. Genetic mapping using BSA analysis identified four candidate regions on the X chromosome involved in the spatial localisation of cytoplasmic components. Those findings led to hypothesised that interaction between a group of polygenes on the X chromosome in *Auanema* polarises sperm components to segregate with the X chromosome.

Mechanisms describing how intrinsic factors regulate cell polarity are poorly understood, mostly because it is difficult to establish in the absence of extrinsic factors influence. Here, I present a novel mechanism for an intrinsic polarisation of asymmetrically dividing cells initiated by the X chromosome.

Chapter 1

Introduction

1.1. Asymmetric cell division

Asymmetric cell division (ACD) is any cell division in which resulting sister cells have different fates [1]. The fate of cells resulting from asymmetric cell division is determined by size, shape, morphology or inheritance of biochemical fate determinants [2-5]. Asymmetric cell division is a fundamental biological process that is prevalent in nature from basic unicellular organisms, to higher multi-cellular organisms [6]. Asymmetric cell division is crucial for multi-cellular organisms' embryonic development, cellular differentiation and cellular diversity [4, 6]. The asymmetric cell division process is characterised by differential segregation of cytoplasmic components known as fate determinant factors to descendant cells, resulting in the formation of two distinct daughter cells. Two basic mechanisms are controlling the polarity of an asymmetrically dividing cell; an intrinsic or an extrinsic mechanisms [2, 7, 8]. Cytoplasmic fate-determining factors diffusion in the dividing mother cell in a polarised manner is an intrinsic mechanism to determine the fate of resulting cells (Figure 1.1) [9, 10]. On the other hand, polarising signals provided by the surrounding environment to the mother cell or daughter cells demonstrate an extrinsic mechanism to determine the fate of resulting cells (Figure 1.1) [7, 11].

Our understanding of the importance and mechanism orchestrating asymmetric cell division is gathered from a variety of model organisms throughout history. Whitman's study on leech egg *clepsine marginata* in (1878) established the hypothesis that asymmetric segregation of cytoplasmic components during cell division produces two intrinsically different daughter cells [12]. His investigation on leech cell lineages illustrated that leech egg cytoplasmic components differential segregation to descending cells determines the fate of those cells [2, 12]. Subsequently, the hypothesis was further consolidated in (1905) Conklin's study on ascidian *Styela partita* cell lineage. Conklin investigation revealed that

ascidian egg pigmented cytoplasmic determinants segregate differentially to daughter cells giving rise to five different tissues [9, 13]. Subsequent, studies complemented those classical findings of asymmetric segregation of fate-determining factor. However, the molecular characterisation of the first cell fate determinant (Numb) was not known until 1994 [14]. To date, many cell fate determinants that establish the polarity of ACD have been characterized including, proteins, transcription factors, mRNA, histone DNA and organelles such as mitochondria [9].

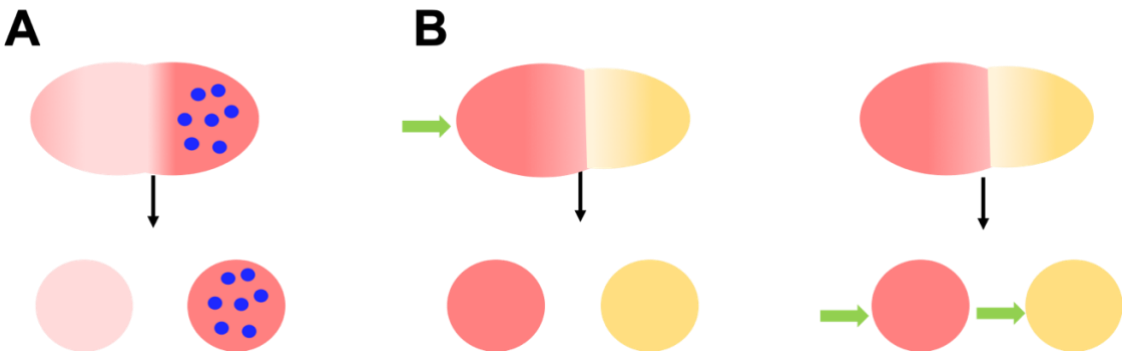

Figure 1.1: Mechanisms of asymmetric cell division.
(A) When intrinsic, cytoplasmic determinants diffuse asymmetrically to one side of the dividing mother cell. Asymmetric segregation of fate-determining factors results in two different daughter cells. (B) External signals (green arrow) from the mother's neighbouring environment cause polarisation of the cytoplasm to segregate differentially. Besides, daughter cells differentiate as a result of an external signal from their surrounding environment or bias towards specific fate by interaction with the sister cell.

1.2. Importance of Asymmetric cell division

ACD is crucial in multicellular organisms for stem cells differentiation, specification, development, and tissue renewal [4, 9, 15]. However, dysregulation of ACD causes severe defects to tissue growth, manifested in cancer tumorigenesis [16-19]. A defining feature of stem cells is their ability to self-renew and differentiate into specific tissue types, and asymmetric cell division is the core mechanism that gives stem cells their unique properties [3, 20-22]. Generally, stem cells differentiate daughter cells by asymmetric segregation of molecular fate determinants to resulting daughter cells [8, 15, 21]. Mouse mammary gland stem cells, purified from wild-type mammary glands into a laboratory culture, segregate fate determinant (Numb) asymmetrically to one of their daughter cells [23]. Dysregulation of asymmetric segregation of Numb leads

to severe consequences and the development of a tumour [23]. The number of stem cells in mouse mammary tumour model increased and divided symmetrically with Numb being uniformly distributed in daughter cells [23]. In a P53-mutant mice model, a similar observation was made [23]. Numb is a major repressor of breast cancer. Asymmetric segregation of Numb regulates the activity of tumour suppressor protein p53 by preventing its degradation and restricting the stemness to only one daughter cell [24].

Moreover, epithelial stem-like cells (SLCs) identified from immortalised human mammary epithelial cells cultures, asymmetrically segregate mitochondria depending on age to daughter cells [25]. Stem-like mother cells contain both old and new mitochondria. However, upon division SLCs asymmetrically sorts new young mitochondria and passes them preferentially into the stem cell, and daughter cell undergoing specification inherits a mix of the two [25]. Age-selective asymmetric segregation of mitochondria during SLCs division suggests a stem cell-specific mechanism to allocate young mitochondria asymmetrically to one daughter cell to maintain stemness properties [25]. Mitochondria is the powerhouse of the cell, the centre of its metabolism, regulates programmed cell death (apoptosis) and regulates signalling activity such as calcium signalling [26-29]. A build-up of mitochondrial damage leads to severe consequences and aging-related diseases such as muscle myopathies and neurodegenerative diseases [30-32]. Accumulation of mitochondrial damage leads to dysfunction in mitochondrial cellular function, affects mitochondria membrane potential and reduces its energy production of ATP, leads to built-up of reactive oxygen species (ROS), and damages mitochondrial genome [33-35]. Investigation of mitochondrial function based on the level of reactive oxygen species (ROS) in living yeast indicates that ROS in the mitochondria of buds is significantly lower than in mother cells [36]. Accordingly, in budding yeast mitochondria undergo age-dependent asymmetric segregation based on their level of ROS [36]. Asymmetrical inheritance of young mitochondria in SLC and budding yeast maintains youthhood and increases life expectancy, by preventing the accumulation of mitochondrial damage contributed by old mitochondria [36].

1.3. Mechanisms controlling asymmetric cell division in model organisms

Mechanisms describing intrinsic factors controlling the polarity of an asymmetric dividing cell are poorly understood, mainly because it is difficult to develop in the absence of an extrinsic factor [2]. Our detailed understanding of asymmetric cell division in vertebrates and stem cells reliant on transferring the knowledge gained from studying asymmetric cell division in yeast, *c. elegans* and *D. melanogaster* [5, 16, 19, 37]. Almost all asymmetrically inherited fate determinant proteins are conserved but sometimes act differently. Most progress in understanding asymmetric cell division in *Drosophila* originates from neuroblast studies [22]. The mechanism of asymmetric cell division in *D. melanogaster* neuroblast is mediated by asymmetric localization of basal fate determinant factors [22, 38]. Between prophase and metaphase (prometaphase), basal determinant factors Numb and Brat (a translational inhibitor) localise at the basal plasma membrane [14, 38-41]. Localization of basal determinant factors is mediated by two other proteins; Miranda facilitates the localization of Brat and adaptor protein Pon mediates the localization of Numb [40, 42]. Asymmetric accumulation of basal determinants proceeds the localization of PDZ domain-containing proteins at the apical cell cortex to establish *Drosophila* neuroblast apical-basal polarity [4, 16]. PDZ domain-containing proteins, include Par-3, Par-6 and aPKC proteinase kinase, which is a *D. melanogaster* homolog of *c. elegans* PKC-3 [43-45]. Apical accumulation of PDZ domain-containing proteins in neuroblasts is originated from apical localization of Par-3, Par-6 and aPKC in epithelial cells of the ventral neuroectoderm during neuroblast delamination [45]. Apical asymmetric localization of Par-3, Par-6, and aPKC proteins is required to establish the apical/dorsal polarity in *Drosophila* neuroblast mitosis (Figure 1.2) [45]. In other Asymmetric cell division models, Par-proteins and their homologs are crucial to establish and maintain apical-basal polarity and influence the asymmetric localization of cell fare determinants [16]. However, localization of Par-proteins asymmetrically requires the influence of an extrinsic factor; such as in the one-celled embryo of *c. elegans*, where polarity is influenced by sperm entry.

Anterior-posterior axis in *c. elegans* zygote is generated during fertilization by sperm entry in an event known as symmetry-breaking [46-49]. The contribution

of sperm centrosome during fertilization and its localization posteriorly close to the male pronucleus initiates the polarisation of the zygote [46, 50]. Sperm entry polarises the actomyosin network; cortical non-muscle myosin (NMY-2) and F-actin migrates towards the anterior pole [51]. As a result of the cortical actomyosin flow, Par-proteins asymmetry is established, where Par-3, Par-6, and PKC-3 are localized in the anterior half [51]. Cortical actomyosin surface contractions that were consistent throughout the cell before sperm entry become confined anteriorly following sperm entry [51]. Posterior localization of Par-2 inhibits localization NMY-2 in the posterior cell cortex confining the actomyosin contractions anteriorly and the posterior end becomes smooth (Figure 1.2) [51].

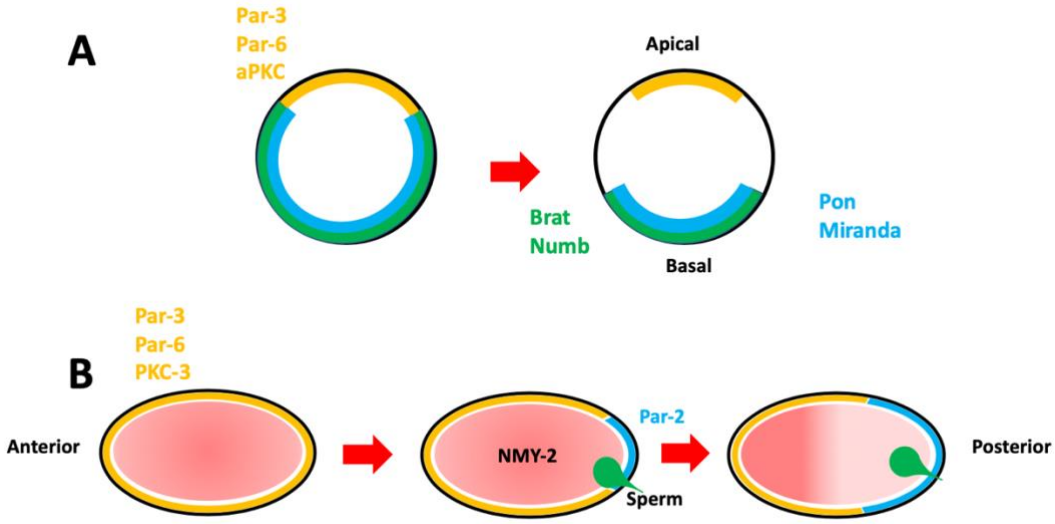

Figure 1.1: Mechanism of asymmetric cell divisions in multicellular organisms.
(**A**) Apical localization of Par-3, Par-6, and aPKC is essential to establish the apical/basal polarity in *D. melanogaster* neuroblast asymmetric cell division. Basal fate determinant factors Brat and Numb accumulate in the basal membrane following the apical localization of PDZ domain-containing proteins. Basal localization of Brat and Numb is facilitated by two other proteins, Miranda and Pon. **(B**) Anterior-posterior axis of *c. elegans* zygote is determined after sperm entry in an event known as symmetry breaking. Sperm entry polarises cytoplasm causing the actomyosin network to contract anteriorly. Following sperm entry Par proteins polarise where Par-3, Par-6, and PKC-3 accumulate anteriorly and Par-2 localises to the posterior side. Par-2 inhibits the contractility of the actomyosin posteriorly confining its contraction to the anterior side of the zygote.

Until recently, the mechanism driving asymmetric localization of fate determinant factors in *c. elegans* and *D. melanogaster* remained a mystery. Different models were established to suggest a process facilitating asymmetric localization of future fate determinants [16]. Initial models suggested that localization of fate determinant in *D. melanogaster* neuroblasts depends on actomyosin contraction [52-54]. Asymmetric movement of actomyosin segregated basal fate determinants proteins asymmetrically to the basal side of dividing *D. melanogaster* neuroblasts [55]. However, this model has been challenged in recent findings that suggest Aurora-A dependent phosphorylation mechanism initiates the actomyosin flow and asymmetric localisation of fate determinants [56]. Moreover, in *c. elegans* zygote asymmetry breaking, Aurora-A regulates actomyosin network cortical flow by inhibiting its contractility from the proximal cortex and promoting its anterior cortical flow [57]. Therefore, the model of actomyosin cortical flow that asymmetrically segregate fate determinants by directional transport was substituted with other models that suggest a dynamic association with cortical proteins or cellular components facilitate the asymmetric localization of fate determinants [16].

In lines with the above-mentioned examples of asymmetric cell division, intrinsic factors that establish cellular polarity are poorly understood without the influence of extrinsic polarising factors [2, 16]. In this thesis, we will discuss a new mechanism of intrinsic polarisation of asymmetrically dividing cell, found in the male spermatogenesis of *Auanema* nematode. During the male spermatogenesis of *Auanema* nematode daughter cell that inherits sex chromosome (X chromosome) inherits mitochondria and cytoskeletal proteins important for sperm function [58, 59]. The other daughter cell without sex chromosome inherits discarded components, such as Golgi complex and ribosomes (Figure 1.3).

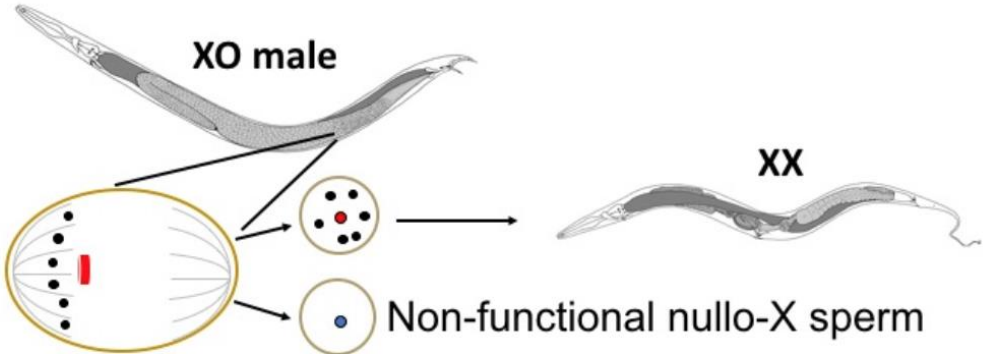

Figure 1.3: Asymmetry in *Auanema* spermatogenesis.
Cytoplasmic components, such as mitochondria (Black dots), asymmetric co-segregation of with the X chromosome (red). This results in the production of exclusively X-bearing sperm by males and subsequent increase in XX progeny after a cross with a female.

This thesis will investigate a new polarising signal during cell division caused by the sex chromosome to influence asymmetric segregation of cell fate determinants. One of few mechanism described in the literature where DNA causes cytoplasmic polarisation is in the fission yeast [60, 61]. The mechanism suggests that the fate of daughter cells is determined by the inheritance of either of the two parental chromatids (leading or lagging) [62]. Similarly, spatial arrangement and cytoplasmic localization of mitochondria caused by unequal chromosomes segregation was investigated in the gonadal mitosis of *Acricotopus lucidus*, a non-biting midges belonging to the bloodworm family Chironomidae [63]. In species of the Orthocladiinae, a superfamily of Chironomidae, germline soma were detected to have different karyotypes by Bauer and Beermann [64]. A varying number of germline-limited chromosomes (Ks) in addition to somatic chromosomes (S) were detected in the germline of both sexes [64, 65]. Name of the germline-limited chromosomes Ks derived from the German word Keimbahn, meaning germline [66]. All Ks chromosomes are eliminated from the future somatic nuclei of the early syncytial embryo, at the stage of cell polarisation, by remaining in the equatorial plane during mitotic cell division, while S chromosomes segregate equally [65, 67]. Similarly, about half of the Ks chromosomes are eliminated in a similar scheme in the first mitosis of the primordial germ cell [63, 65, 67]. However, in the last gonadal mitosis a differential segregation of chromosome occur; all Ks undivided migrate to only cell pole, while S chromosomes separate and segregate equally [65]. Daughter

cell that receives only S chromosomes differentiate into an aberrant spermatocyte in male and a nurse cell in female, whereas daughter cell inheriting all the Ks and Ss differentiate into a primary spermatocyte in male a and into the oocyte in female [65, 67]. Both daughter cells remain connected with cytoplasmic bridge, even while meiosis is undertaken [65]. In the germline of *A. lucidus*, differential monopolar movement of Ks to one pole is accompanied by asymmetric distribution of mitochondria to the cell opposite to the Ks segregation [63]. In *A. lucidus*, as result of the unequal unipolar segregation of Ks to the primary spermatocyte majority of mitochondria segregate to the aberrant spermatocyte (Figure 1.4) [63]. Mitochondria are transported back from the aberrant to the primary spermatocyte via a permanent cytoplasmic bridge (Figure 1.4) [63]. This indicate the role of aberrant spermatocyte to nourish the primary spermatocyte with cytoplasmic components during growth and meiosis division [63].

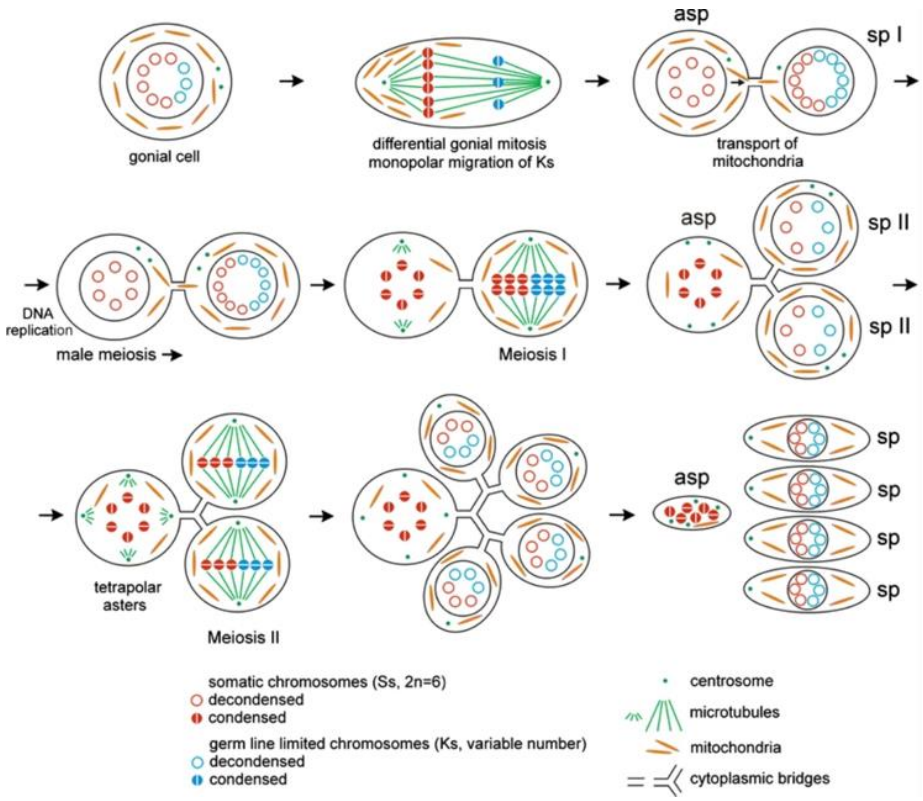

Figure 1.4: Representation illustrates chromosomes segregation and mitochondria distribution in *A. lucidus* male germline.
Mitochondria segregate opposite to the poleward-moving Ks exclusively to the aberrant spermatocyte in the last gonial mitosis. Later mitochondria are transported to the primary spermatocyte through a cytoplasmic bridge. Abbreviations in the figure; abs aberrant spermatocyte, *spI* primary spermatocyte, *spII* secondary spermatocyte and *sp* spermatid. The Figure was copied from [67].

Asymmetric polarisation of cytoplasm by chromosome segregation is poorly understood and has a little description in literature. The work in this thesis will aim to fill-in that literature gap and introduce a new mechanism of polarising mother cells in the event of asymmetric cell division. However, before detailing the asymmetric segregation of sperm components exclusively with the X chromosome during *Auanema* male spermatogenesis and its subsequent effect on broad sex ratio. I will first describe nematode species from the *Auanema* genus used in this research.

1.4. Auanema as a model system to study asymmetric cell division

Recently two free-living nematode species *Auanema rhodensis* and *Aunema freiburgensis* were discovered [68, 69]. The scientific name of the recently discovered genus with generic epithet 'aua' derived from indigenous South America Tupi language meaning 'hair' [69]. *Auanema* are trioecious free-living nematodes were male, female and hermaphrodite co-exist simultaneously[69]. Nematoda phylum is vast and diverse containing a variety of reproductive modes [70, 71]. Predominantly nematodes reproduce sexually male/female in a reproductive mode known as dioecy [72]. Several other reproductive modes have evolved independently in other clades including hermaphrodite/male reproductive mode in the popular nematode *c. elegans*, known as (androdioecy) [73-75]. Trioecy is a good reproductive model to study the evolution of new mating systems. The co-existence of males, females, and hermaphrodites in a rare trioecious mating system is considered to be an evolutionary intermediate state. It is believed that sexually reproducing nematodes (dioecy) have evolved through the trioecious transient state to an androdioecy mating system [69].

1.4.1. *Auanema rhodensis* and *Auanema freiburgensis* isolation and maintenance

Auanema resembles *c. elegans* as a laboratory model; it can be easily handled and maintained in the lab, these species are transparent with a short life cycle, and they produce a large number of progeny [69]. *Auanema* nematodes were first isolated from their natural environment; subsequently, they were inbred under laboratory conditions for several generations. *Auanema rhodensis* n. sp. (strain SB347) was isolated from deer ticks (*Ixodes scapularis*), that were used as a trap

for nematodes. Ticks were dropped on the upper layer of the soil in Kingston (Rhod Island), United States by Dr. Elyes Zhioua (W. Sudhaus, personal communication) [68]. *Auanema rhodensis n. sp.* (strain TMG33) was isolated from a dead tiger beetle on an AVT trail in West Virginia by Theresa Grana (University of Mary Washington). SB347 was subjected to 50 generations of inbreeding, subsequently, it was renamed APS4. TMG33 strain inbred for 11 generations was renamed APS6. *A. freiburgensis* SB372 strain was isolated in Freiburg, Germany, by W. Sudhaus from a dung pile [69]. *A. freiburgensis* SB372 strain was inbred in the lab for several generations to produce the inbred strain APS7. *A. freiburgensis* JU1782 strain was isolated from a rotting Petasites stem sampled in Ivry (Val-de-Marne, France). The JU1782 strain was inbred in laboratory conditions for several generations and was renamed inbred strain APS14. All strains were cultured at 20 ^{o}C in laboratory conditions, in NGM plates seeded with *Escherichia coli* OP50, as for *c. elegans*.

1.5. Sex determination and sex description in trioecious *Auanema* species

In most of multicellular organisms, sexual reproduction has led to the formation of two separate sexes, males and females. However, the evolution of two separate sexes across lineages is not inescapable, almost 94% of flowering plants are hermaphrodites containing both male and female organs within the same flower or within the same individual plant [76]. Meanwhile in animals, hermaphroditism is rare compared to plants about 5% of all species [76]. The small representations of hermaphroditism in animals is attributed to its absence in the species-rich insects group, however it is common in other animal taxa, such as fish, and other invertebrates including barnacles, snails, corals and nematodes [76]. In most species in the animal kingdom with known sex determination mechanism sex is determined with genotypic sex determination mechanism (GSD), where genetic elements determine whether an individual develop into a male or a female [76]. In mammals, sex is determined by sex chromosomes, where males are XY and females are XX. In many animals the development of sex does not lie within genes, but an external stimulus determines the sex of the individual. This form of sex determination is known as environmental sex determination (ESD), such as the temperature-dependent sex determination in reptiles [77]. In other animals, sex is determined by the whole genome in a system known as haploidploidy,

where fertilised eggs develop into diploid females and unfertilised eggs develop to haploid males. This mechanism of sex determination found in about 12% of animal species, especially hymenopterans [77]. In other animals, there is only one sex chromosome, referred to as X chromosome. Sex on those animals determined by the dosage of X chromosome, females are diploid for the sex chromosome (XX) and males are haploid for the sex chromosome (XO), in a system known as XX:XO sex determination system [76]. This system exist in all apterygote and Plecopteran insects (e.g. dragon flies and silverfish), most exopterygote insects, (e.g. cockroaches, grasshoppers and crickets), some crustaceans, bony fish and nematodes [76].

Sex in *Auanema* is chromosomally determined as most nematode species. There is only one sex chromosome in nematodes (X chromosome) and sex determination depends on the X chromosome dosage [78, 79]. Males are a hetero-gametic (XO) inheriting six pairs of autosomes and a single X chromosome (O indicates the absence of sex chromosome), whereas females/hermaphrodite are homo-gametic (XX) inheriting six pairs of autosomes and two X chromosomes [59] [72]. The mechanism for sex determination in *Auanema* is generally known as the XX: XO mechanism [69, 72]. The primary Sex determination signal in *Auanema* relies on the ratio between sets of autosomes and X chromosome [78]. Diploid animals resulting from fertilization between two X-bearing gametes (XX: AA ratio 1) develop to females or hermaphrodites depending on environmental conditions, whereas animals resulting from fertilization between nullo-X gamete (A gamete without sex chromosome) and X-bearing gamete (X: AA ratio 0.5) develop as a male [59].

1.5.1. Difference between hermaphrodites and females

Both species *A. rhodensis* and *A. freiburgensis* are generally morphologically similar, with a cylindric body covered with a fine annulation cuticle [69]. *Auanema* hermaphrodite produces all of the three sexes, males, females, and hermaphrodites, in varying ratios (Table 1.1) (Figure 1.7) [80]. Hermaphrodites and females are genetically similar and morphologically indistinguishable. The difference between females and hermaphrodites is environmentally determined, characterised during the larval developmental stages when hermaphrodites pass

through compulsory non-feeding dauer stage (Figure 1.5) [68]. Nematodes before adulthood naturally pass through four juvenile larval molts called (L1-L4) (Figure 1.5) [68]. Independent of the environmental conditions specific proportion of L1 larva are predetermined to form non-feeding and stress-resistant third larval morph called dauer [68, 81]. Dauer larvae are characterised by their ability to stand up on their tail and display a tube waving behaviour potentially searching for invertebrate carrier [68, 69]. In favourable growth conditions, dauers remain in their resistant non-feeding form for ~24h after they exit the dauer stage [68]. *A. rhodensis* Juveniles L1 hermaphrodites are distinguished by their small gonad primordium in comparison to other L1 female siblings that don't pass through the stress-resistant juvenile stage [68, 81]. In *A. rhodensis* sex determination and dauer formation are linked only hermaphrodites develop from dauer (Figure 1.5) [68, 80]. The link between hermaphroditism and dauer formation was determined by isolating only *A. rhodensis* dauers and killing all *A. rhodensis* non-dauer worms by 1% sodium dodecyl sulfate solution. All the 1,015 dauers developed into self-reproducing hermaphrodites [80]. *A. rhodensis* self-reproducing hermaphrodite throughout their reproductive life predominantly produces more hermaphrodites than female progeny (Table 1.1) [80, 81]. However, In standard culture conditions, eggs laid within the first 15h develop into mostly females [80]. Despite hermaphrodites and females being genetically identically dauer formation is environmentally determined. Manipulating hormones responsible for dauer formations can induce a pre-determined larvae as a female to undergo dauer formation, then develop to hermaphrodite, and vice versa [80, 81]. *A. rhodensis* L1 larvae that typically develop into females in standard culture conditions can be induced to become a dauer and redirected to develop as a hermaphrodite by the removal of cholesterol when cultured in low supply of food [69, 80]. Furthermore, dauer formation is inhibited in L1 larva with a small gonad primordium destined to become hermaphrodites and redirected to females development by the addition of the hormone dafachronic acid [69, 80].

A. freiburgensis predominantly produce females in isolation (8.7% males, 91.1% females, 0.2% hermaphrodites) (Table 1.1) [69]. Whereas, In response to crowding conditions *A. freiburgensis* produce mostly hermaphrodites (80.1% hermaphrodites, 6.2% females, 13.6% males) [69]. In contrast to *A.*

rhodesnis, hermaphrodite and female juveniles (L2) are indistinguishable by the size of their gonad primordium. Similar to *A. rhodensis*, *A. freiburgensis* dauer formation, and hermaphroditism is linked, only juveniles that undergo dauer stage develop into hermaphrodites [69].

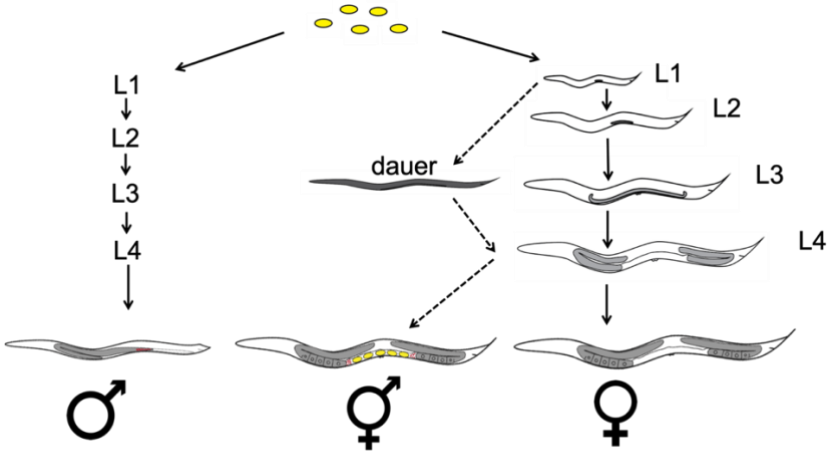

Figure 1.5: *Auanema* life cycle.
Auanema males and females before adulthood pass through four juvenile larvae molt (L1-L4). Sex determination and dauer formation is linked in *Auanema* only L1 passes through a compulsory dauer stage, in response to stress signals, develop as a hermaphrodite

1.5.2. Males relatively rare in *Auanema*

Males in *Aunema* are generally smaller in size compared to their female/hermaphrodite counterparts. Males are characterized morphologically at the posterior end by the bluntness of the tail and the presence of copulatory spicules [69]. Males in *Auanema* are relatively rare, do not go through a dauer stage, and produced in a low percentage from self-fertilizing hermaphrodite. *A. rhodensis* hermaphrodite produce (9-13%) males and (8.7-13.6%) males produced from *A. freibrugesnis* hermaphrodite [80, 81]. Furthermore, *Auanema* male mated with a female produce cross-progeny with a remarkably skewed sex ratio [59, 68, 69, 81]. *A. rhodensis* male outcross with a female produces a significantly skewed sex ratio, males are only (1.6-2.3 %) of the total cross progeny [59, 68]. Similarly, *A. freibrugesnis* male outcross with a female produces a low percentage of males (18%) (Table 1.1) [69]. The low percentage of males, in *Auanema*, produced during an outcross is particularly peculiar because it stands against Mendel's first law that predicts a cross between an (XO) male and an (XX) female should produce equal 1:1 ratio of males to females [82]. The unequal transmission of X

chromosome and subsequent production of skewed sex ratio in *Auanema* outcrosses is attributed to the near absence of motile nullo-X sperms [59]. *A. rhodensis* hermaphrodite self-fertilisation predominantly produce XX animals, because it generally produces duplo-X sperm and nullo-X oocyte (Figure 1.6C and D). In rare occasions during hermaphrodite spermatogenesis, when both X chromosomes fail to segregate together an X-bearing sperm is formed leading to the production of males from selfing (Figure 1.7). On the other hand, *A. rhodensis* females generally produce X-bearing oocyte and in rare occasions produce nullo-X oocytes (Figure 1.6A). Since males only produce a one kind of sperm an X-bearing sperm, a cross between male and female will result in mostly XX progeny and a rare number of males (Figure 1. 6) [83]. As a result of the unique gametogenesis in *A. rhodensis*, X chromosome in sons is inherited paternally (Figure 1.7). This non-canonical inheritance pattern of X chromosome is explained by *A. rhodensis* male exclusive production of X-bearing sperm and females/hermaphrodite production of nullo-X oocyte [83]. It is not yet clear why there is a difference in outcross male brood ratio between *A. freibrugesnis* and *A. rhodensis*. But since males exclusively produce X-bearing sperm, it is likely that the difference is due to the rate of X chromosome non-disjunction in female leading to the production of nullo-X oocytes. i.e. the rate of X chromosome non-disjunction in *A. freibrugesnis* female is higher than in *A. rhodensis*, therefore the former produces more nullo-X oocytes and hence more male progeny during an outcross (Figure 1.7).

Table 1.1. Sex ratio of *A. rhodensis* and *A. freibrugesnis* progeny of whole broods from selfing and outcross.
Some percentages are presented in a ratio depending on different experiments reported in different publications. Percentages with similar colour (blue) are from the same experiment.

Species	Reproduction	(XO) Males %	(XX) Females %	(XX) Hermaphrodite %
***Rhodensis* (APS4)**	Selfing in isolation (uncrowded condition)	9-13 (10)	44	46
	outcross	1.6-2.3	98.4-97.7 (total XX progeny)	
***Freiburgensis* (APS7)**	Selfing in isolation (uncrowded condition)	8.7-13.6	91.1	0.2
	outcross	18	82 (total XX progeny)	

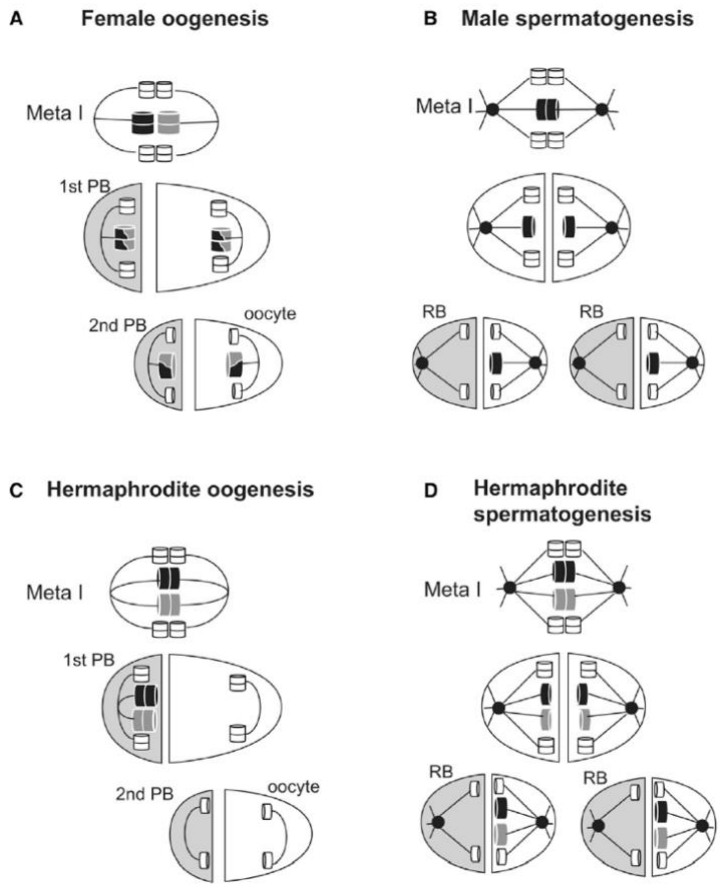

Figure 1.6: X chromosome segregation in *A. rhodensis* meiosis.
The figure represents meiosis of F1s resulting from a cross between two polymorphic *A. rhodensis* strains copied from [83]. (A) female oogenesis produces X-bearing oocytes, and X chromosome recombines during the process. Autosomes in white and X chromosome in grey and black, representing inheritance of an X chromosome from each parental strain. (B) Male spermatogenesis exclusively produces an X-bearing oocyte. In the first meiosis, Autosomes segregate to different daughter cells, while unpaired single X chromatids separate and segregate equally to daughter cells. In the second meiosis, X chromatid segregates exclusively to one daughter cell. (C) hermaphrodite oogenesis exclusively produces an X bearing oocyte. Unpaired X chromosomes segregate to the polar body during the first meiosis. (D) hermaphrodite spermatogenesis produces duplo-X sperms. Chromatids of unpaired X chromosomes separate equally to both daughter cells during the first meiosis. In the second meiosis, both X chromosomes segregate to the future functional sperm.

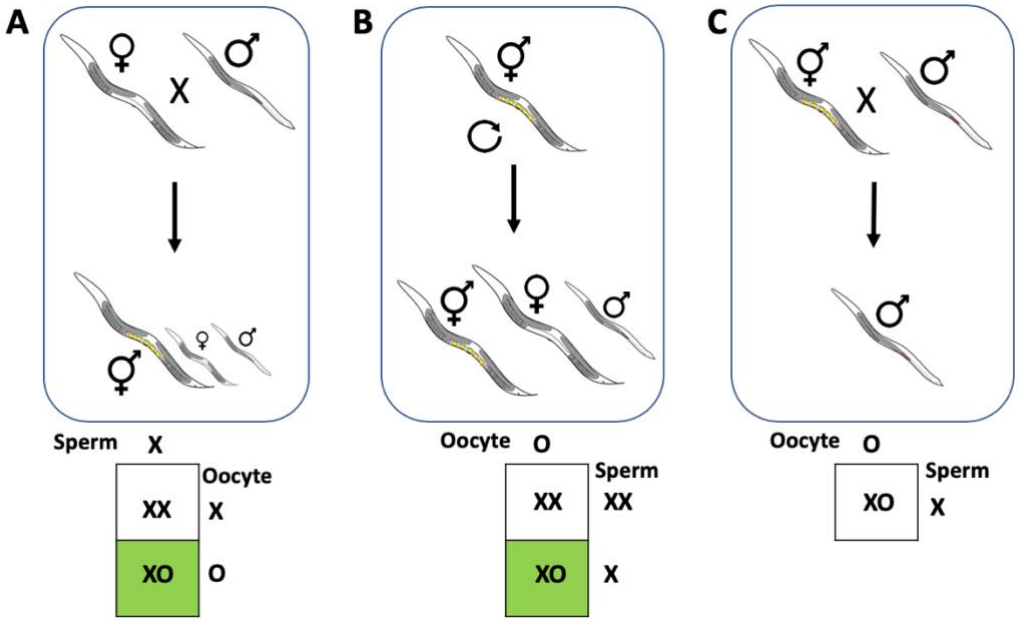

Figure 1.7: *Auanema* mating dynamics.
(A) A cross between a male and a female generally produces XX animals that develop to either female or hermaphrodites depending on environmental conditions. In the event of nondisjunction during female oogenesis, a nullo-X oocyte is produced, leading to the generation of male cross progeny. **(B)** hermaphrodites generally produce XX animals from selfing due to its overall predominant production of nullo-X oocytes and duplo-X sperm. However, on rare occasions, single X-bearing sperm are produced, leading to the male formation. **(C)** Since hermaphrodites produce nullo-X oocytes and males exclusively produces X-bearing sperm, a cross between hermaphrodite and a male only produces male cross progeny.

During male spermatogenesis, subcellular components important for sperm function and motility co-segregate asymmetrically with the X chromatid exclusively producing functional X-bearing sperm, whereas nullo-X sperm is discarded [59]. Modifications to the spermatogenesis scheme in *Auanema* male, in contrast to *c. elegans* male (XO), results in the exclusive production of X-bearing sperm. The absence of nullo-X sperm in *Auanema* males helps explain the low percentage of males produced during an outcross [59]. To understand the importance of this asymmetric X chromosome transmission and its subsequent co-segregation with sperm components in producing skewed sex ratio we first need to understand male spermatogenesis in the popular nematode model *c. elegans*.

1.6. Spermatogenesis in *Auanema* compared to *c. elegans*

A remarkable feature of *Auanema* male spermatogenesis is the exclusive production of X-bearing sperms and the near absence of motile nullo-X sperms in contrast to *c. elegans* [59]. Males in *c. elegans* (XO) produce functional X-bearing and nulllo-X sperms; both sperms are transmitted equally in the event of an outcross. In the dividing *c. elegans* spermatocyte during the second anapahse, sperm component important for sperm function and motility segregate equally from the central residual body to the budding spermatids resulting in the production of a nullo-X and X-bearing motile spermatozoa [84]. The difference between *Auanema* male and *c.elegans* spermatogenesis is clear in the second anaphase, however in the first anaphase cytoplasmic components segregate equally in both species.

1.6.1. physiology and cytology of *c. elegans* male spermatogenesis

Primary *c.elegans* spermatocyte divides equally to generates two secondary spermatocytes during meiosis I of *c. elegans* spermatogenesis [85]. During meiosis II from each secondary spermatocyte, two haploid sperm segregate from a central residual body [85]. Spermatids budding from the central residual body will contain essential components important for sperm function and motility, including centriole pair, mitochondria and major sperm protein (MSP) [86]. On the other hand, discarded cytoplasmic materials, including Cytoskeletal components (myosin, actin, and tubulin) the Golgi apparatus, endoplasmic reticulum (ER) and all ribosomes, segregate to the central residual body (Figure 1.8) [85, 87]. MSP is an important protein for nematode sperm motility. It forms an elaborate filament system that enables amoeboid crawling motility [88-90]. In *c. elegance* spermatogenesis, MSP is initially synthesized and assembled into a fibrous body in the primary spermatocyte. Fibrous body (FB) accumulates inside a membranous organelle (MO) assembling into a doubled-membrane organelle known as fibrous body membranous organelle (FB-MO) [91]. The assembly of the FB-MO complex ensures the segregation of MSP into the budding spermatids [91]. FB-MO complex separates after spermatids segregation, fibrous filaments depolymerize depositing MSP into the spermatid cytoplasm and the membranous organelle fuse with the spermatid plasma membrane [91]. Activation of MSP inside the sperm enables amoebae-like crawling motility [91].

In total, *c. elegans* spermatogenesis produces two X-bearing sperms, two nullo-X sperms and two residual bodies (RB). Essential components important for sperm function and motility segregate with the spermatids, unwanted cellular components discarded into a central residual body [85]. The primary spermatocyte contains a single unpaired X chromosome that lags during the first meiosis and segregates to either of the two secondary spermatocytes. When the secondary spermatocyte containing the X undergoes meiosis II, sister chromatids of the X chromosome separate equally to the budding spermatids producing two X-bearing sperms and a central residual body (RB). Meanwhile, in the other secondary spermatocyte without the X, cellular components essential for sperm function segregate to the budding spermatids and non-sperm cellular materials discarded to a central residual body (Figure 1.8) [59, 92, 93].

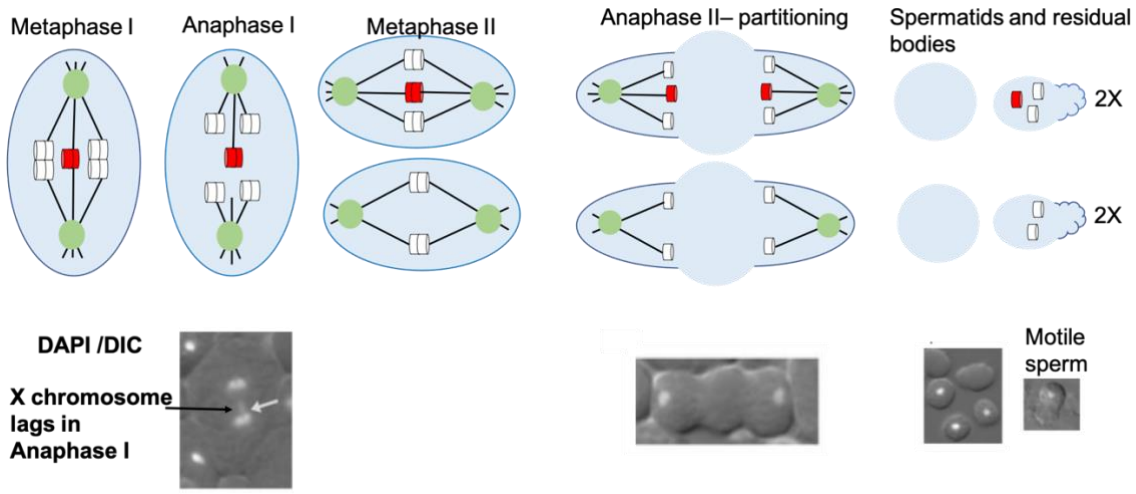

Figure 1.8: X chromosome segregation in *c. elegans* male spermatogenesis. *c. elegans* primary spermatocyte contains a single unpaired X chromosome (red). X chromosome lags during *c. elegance* Anaphase I, then segregates to one of the two secondary spermatocytes. Cellular components important for sperm function and motility segregate equally in meiosis I irrespective of the direction of the lagging X. During anaphase II of secondary spermatocyte with the X, sister chromatids of the X chromosome split and segregate equally to budding spermatids, producing two X-bearing sperms and a central residual body. On the other secondary spermatocyte, sperm components segregate equally to budding spermatids producing two nullo-X sperms and a central residual body. DAPI staining merged with DIC (differential interference contrast) microscopy image illustrates the shape of the dividing cell in correspondent stages and lagging of the X chromosome in Anaphase I. DAPI and DIC cytology images adopted from [58].

1.6.2. *Auanema* male spermatogenesis exclusively produces X bearing sperm

Primary *Auanema* male spermatocyte divides equally during meiosis I, similar to *c. elegans*. In contrast to *c. elegans* meiosis I no lagging of the unpaired X chromosome is observed, X chromatids of the unpaired X segregate equally to both secondary spermatocyte [59]. However, during meiosis II, The lone X chromatid lags and reductionally segregate to either pole of the dividing secondary spermatocyte (Figure 1.9) [59]. In contrast to *c. elegans* spermatogenesis, lagging X chromosome in *Auanema* is observed during meiosis II. During meiosis II, cellular components important for sperm function and motility, including MSP and mitochondria, segregate exclusively to the X bearing sperm (Figure 1.9) [58, 59]. In the first meiosis, fibrous bodies (later depolymerizing to MSP) and mitochondria segregate equally to secondary spermatocytes. However, in the second anaphase, they segregate exclusively with the X-bearing spermatid. As a result, only the X-bearing sperm will contain essential cellular components important for sperm function and mature to motile spermatozoa [59]. Cellular components unnecessary for sperm function, including Golgi-apparatus and cytoskeletal proteins segregate to the nullo-X pole of the dividing secondary spermatocyte, suggesting that nullo-X cell undertake the function of the residual body (Figure 1.10). In contrast to *c. elegans* spermatogenesis, no central residual body is formed, rather the nullo-X cell inherits discarded materials and function as disposal residual body with DNA [59].

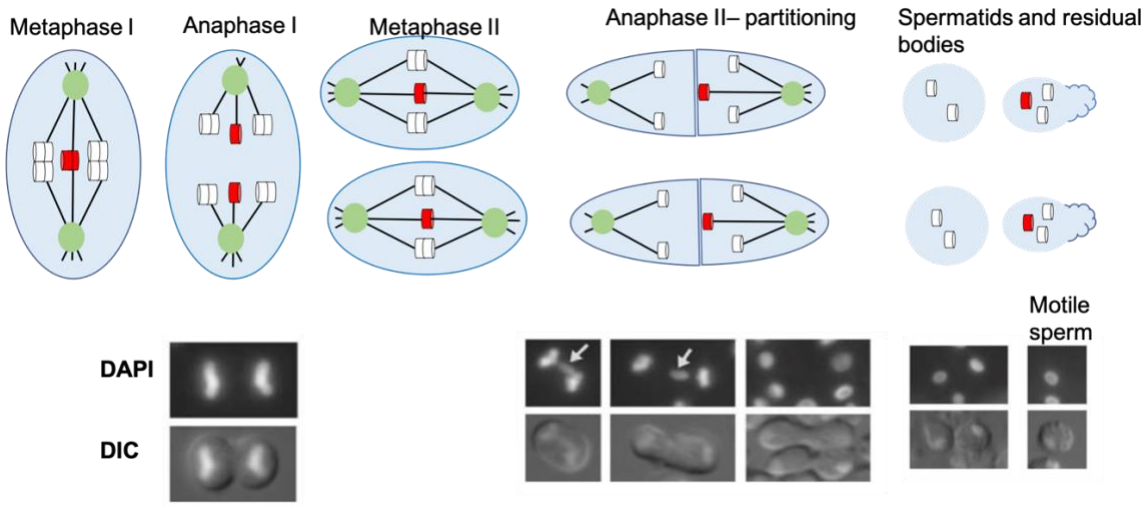

Figure 1.9: X chromosomes segregation in *A. rhodensis* male spermatogenesis.
During Anaphase I X chromatids of the unpaired X chromosome (red cylinder) splits and segregate equally to both secondary spermatocytes. During anaphase II, X chromosome lags then segregate exclusively to one pole of the dividing secondary spermatocytes. Sperm components important for sperm function and motility segregate exclusively to the X-bearing pole. DAPI and DIC images illustrate chromosomes and the shape of the dividing cells for the corresponding phase. DAPI staining illustrates lagging X chromosome in the second anaphase segregating exclusively to one pole of the dividing spermatocyte. There is no formation of a central residual body when spermatids partitioned. Daughter cells without the X undertake the role of a residual body with DNA. DAPI and DIC adopted from [58].

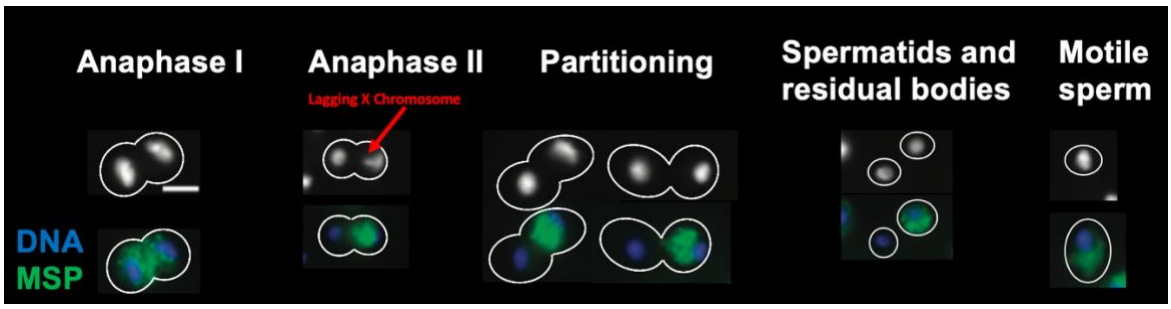

Figure 1.10: Segregation of MSP (green) to the X-bearing pole during *A. rhodensis* male spermatogenesis.
Images illustrate the segregation of MSP (green) and DAPI (blue) in corresponding spermatogenesis phases. Lagging X chromosome in anaphase II is indicated by the red arrow. MSP segregates exclusively with the X bearing pole in meiosis II. Producing an X bearing sperm and a residual body with DNA. Cytology images adopted from [58].

Major changes in male spermatocyte microtubule organization cause a unipolar portioning towards the X-bearing pole. During the first meiotic division organisation of microtubules is asymmetric leading to equal segregation of X chromatids and sperm components to the secondary spermatocytes. During the second anaphase, microtubules were assembled symmetrically as long as the X chromosome is centrally located. However, this symmetry shifts as soon as the X chromosome physically contacted one anaphase plate without being fully incorporated, spindles were asymmetric with longer microtubules emerged from the X-bearing pole [58]. In the second anaphase, sperm components, including MSP, initially remain centrally positioned regardless of the direction of the lagging X chromosome. However, when the X chromosome is fully incorporated into one anaphase plate, MSP partitioned unipolarly towards the X-bearing pole.

Electron Microscopy analysis followed by electron tomography analysis of dividing *A. rhodensis* spermatocyte revealed that the partitioning of sperm components in anaphase II occurred briefly after the X segregation [58]. MSP and mitochondria were centrally positioned as long as the X chromatid remained centrally located during metaphase II. However, briefly, after X chromosome segregation to one pole, mitochondria and MSP segregate exclusively to the X-bearing pole (Figure 1.11) [58]. As a result of asymmetric co-segregation of sperm components with the X chromosome and exclusive production of X-bearing sperm, a cross between *Auanema* and females produces a significantly skewed sex ratio, with predominantly female progeny [59]. *Auanema* XX females generally produce X bearing oocyte, but in the event of X chromosome nondisjunction, females produce nullo-X oocytes in a very low percentage [83]. The near absence of null-X sperm produced by *Auanema* male and rarity of nullo-X oocytes produced by females explains the low number of male progeny resulting from an outcross (Figure 1.12) [59, 81, 83].

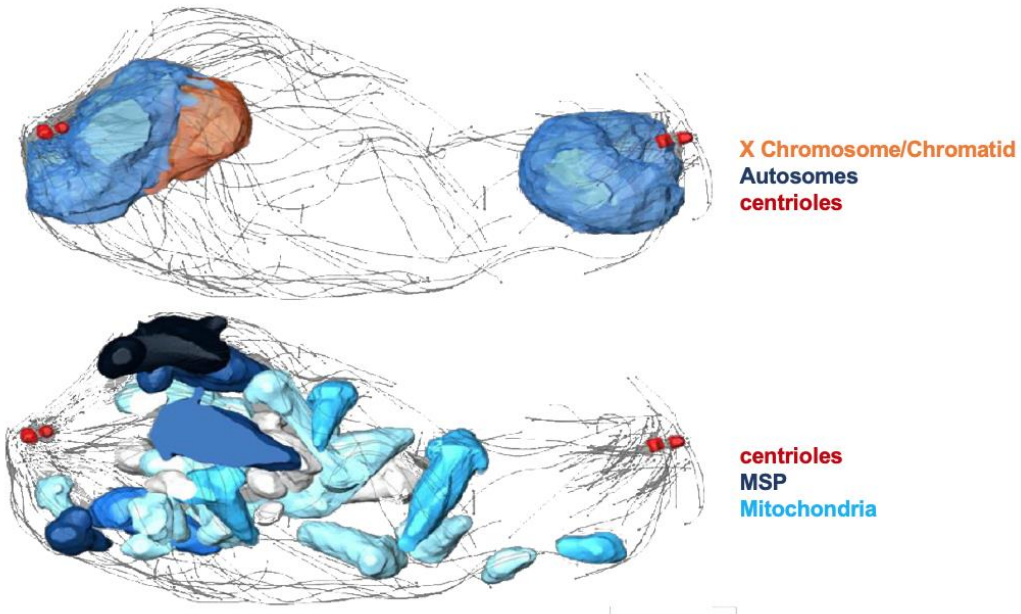

Figure 1.11: Electron tomography of anaphase II of *A. rhodensis* male spermatogenesis.
X chromosome segregates exclusively to one pole of the dividing secondary spermatocytes. As soon as the X chromosome is incorporated into one anaphase plate sperm components, MSP and mitochondria, segregate towards the X-bearing pole. Figure provided by Anna Schwarz (personal communication).

Since there is a correlation between sperm components and X chromosome segregation, we hypothesised that *Auanema* X chromosome guides and reorganise the cytoplasm during meiosis II. This thesis will investigate the internal polarising signal initiated by the X chromosome causing asymmetric segregation of subcellular compartments. *Auanema* offers a unique easy-to-score phenotype, where the type of division occurring during male spermatogenesis can be determined from the sex progeny of that male.

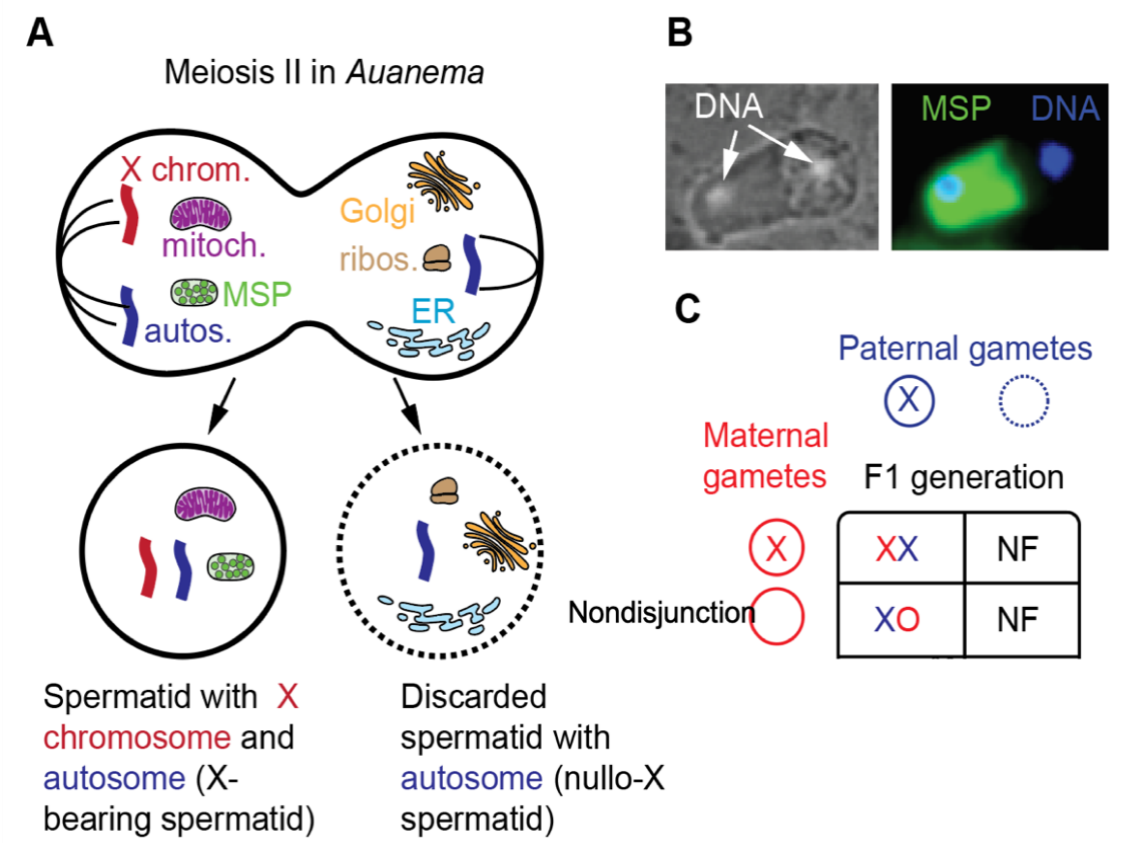

Figure 1.12: Asymmetric cell division in anaphase II of *A. rhodensis* spermatogenesis.
(A) a schematic representation illustrates a cytological observation. Sperm components, including mitochondria and MSP, segregate exclusively with the X chromosome. The sister cell inheriting the X chromosome is viable, whereas the sister cell inherits discarded components, including ribosomes, Golgi-complex, and endoplasmic reticulum. It undertakes the role of a residual body that contains DNA. **(B)** Antibody staining of anaphase II illustrates MSP (green) segregates exclusively to the X-bearing pole. DAPI staining of DNA (blue) indicates that the residual body will contain DNA. **(C)** A cross between an XX female and an XO male will produce predominantly XX progeny since only the paternal gamete with the X viable and the nullo-X gamete is non-viable. In the rare event of nondisjunction in females (N.D.) in females, nullo-X oocytes will be produced. Maternal nullo-oocyte fertilization with paternal X sperm will produce an XO male. The rarity of nullo-oocytes and the near absence of nullo-X sperms explains the low number of the male population in *Auanema*.

1.7. Scope of the thesis

The Thesis investigate if the X chromosome is a polarising signal during the spermatogenesis of *Auanema* male.

First, I will investigate the hypothesis if the X chromosome is a polarising signal during the spermatogenesis of an XX masculiniser mutant, pseudo-male (chapter 3). An *A. rhodensis* XX male mutant was isolated from a chemical mutagenesis screen. This mutant, called *masculiniser* (*Arh-mas-1*), has the XX karyotype, but the morphology of a male. In this chapter, I will investigate the spermatogenesis of XX masculinisers to determine if the X chromosome is also a polarising signal directing cytoplasmic components segregation.

Secondly, in the 4th chapter, I will discuss the generation of *A. freibrugesnis* recombinant advanced intercross lines (RIAILs) using two *A. freiburgensis* polymorphic strains. *A. freiburgensis* RIAILs were constructed to determine if mosaic shuffling from two different parental genomes will give rise to a new extreme phenotype (transgression), males that are able to produce functional nullo-X sperm. Then, genome from RIAILs will be used for genetic mapping analysis to identify candidate regions involved in the X chromosome segregation and the spatial localisation of cytoplasmic components during *Auanema* spermatogenesis.

Finally, I will discuss the introgression of the X chromosome from one strain into the genetic and cellular background of another (Chapter 5. The unique X chromosome inheritance pattern in *Auanema*, where the X chromosomes in sons is inherited paternally, will enable the generation of males with an X chromosome from one strain while autosomes and the cellular background will be from another strain. Spermatogenesis of those males will provide a model system to study mito-nuclear interactions. Since I hypothesized that the X chromosome is a polarising signal in *Auanema* male spermatogenesis, incompatibility between X chromosomes, autosomes and mitochondria in those males is expected.

Chapter 2

General materials and methods

General materials and methods for this thesis will be detailed here unless stated otherwise in each chapter's materials and methods. Pre-prepared materials are provided by the University of Warwick school of life science preparation room.

2.1. Materials

2.1.1. Reagents

1N M9 Buffer

For 1 litter of M 9, 3 g of KH_2PO_4, 6 g of Na_2HPO_4, 5 g of NaCl, dissolved into 1 L of dH_2O. Autoclaved, then 1 ml of 1 M $MgSO_4$ was added.

1M NaOH:

To make up one litter of 1 M of sodium hydroxide. 40 g of NaOH was dissolved into a 1 litter of dH_2O. Solution mixed well until NaOH fully dissolved using a magnetic stirrer.

1M Sodium azide

65 mg of powder sodium azide was dissolved into 1 ml of dH_2O. Stored at 4 ^oC.

Nematode freezing solution

For 1 Litre of the liquid freezing solution, 5.85 g of NaCl, 6.8 g of KH_2PO_4, 300 ml of glycerol was added to 600 ml of dH_2O and autoclaved. After autoclaving, 3 ml of sterile 0.1M $MgSO_4$ was added.

Lysis buffer

100 mM Tris(pH 8.5), 100 mM NaCl, 50 mM EDTA, 1% SDS and 1% beta-Mercaptoethanol added fresh to the lysis mix when required. Then 2.5 µl of proteinase K (20mg/ml) was added to each tube containing 500 µl of lysis buffer.

3 M sodium acetate (CH_3COONa)

24.61 g of CH_3COONa were dissolved in 80 ml of water to make up a total of ~100 ml solution. The solution was mixed using a magnetic stirrer.

1 M Tris-HCl

To make one litter of 1 M Tris-HCl, 121.14 g of Tris dissolved in 800 ml dH_2O. pH adjusted to 7.0 by adding an appropriate volume of concentrated HCl. dH_2O was added to bring the solution to 1 liter. Generally, Tris-HCl is prepared by the Warwick school of life science preparation room. Stored at room temperature.

Alkaline hypochlorite solution (bleach solution)

1.5 ml of sodium hypochlorite and 2 ml of 4 N NaOH were added to 7.5 ml of dH_2O.

1 M KPO_4 (Potassium phosphate) buffer

to prepare 1 liter of 1 M KPO_4, 108.3 g of KH_2PO_4 ,35.6 g of K_2HPO_4, and dH_2O was added to 1 liter. The solution was autoclaved then mixed well until completely dissolved.

5 mg/ml cholesterol

0.5 g of cholesterol mixed in 100 ml of 100% ethanol. The solution was mixed well in a magnetic stirrer.

1 M $MgSO_4$ Magnesium sulfate

98.59 g of MgSO4 was mixed in 400 ml of dH_2O. The solution was mixed well using a magnetic stirrer.

1M $CaCl_2$ calcium chloride

58.8 g of $CaCl_2$ was mixed in 400 ml of dH_2O. The solution was mixed well using a magnetic stirrer.

Nystatin 10mg/ml

0.25 g of Nystatin was mixed with 25 ml of 70% ethanol in a 50 ml falcon tube and Stored at -20.

50X TAE

242 g of Tris-base dissolved in 700 ml of dH_2O. 57.1 ml of acetic acid and 100 ml of 0.5 M EDTA (pH 8.0) were added, the pH of the buffer is not adjusted and should be ~8.5. The solution is adjusted to a final volume of 1L by adding dH_2O. Generally, 50X TAE is prepared by Warwick school of life science preparation room. Stored at room temperature.

2.1.2. LB plates

LB plates are prepared by mixing the following items; 10 g of Bacto-tryptone, 5 g of Bacto-yeast, 5 g of NaCL, and 15 g of agar to 1 L dH_2O, the pH is adjusted to 7.5 by adding 1 M of NaOH [94]. LB solution was sterilized by autoclaving, then when cooled, was poured into plates. Once solidified plates are ready to use. LB plates were prepared by Warwick school of life science preparation room.

2.1.3. L-Broth

LB broth is made by mixing the following items; 10g of Bacto-tryptone, 5g of Bacto-yeast, 5g of NaCl, and dH_2O added to 1L, pH adjusted to 7.0 using 1 M NaOH. L-Broth was prepared by Warwick school of life science preparation room.

2.1.4. Nematode and bacterial Strains

Table 2.1. Nematode and bacterial strains used in the study.

Strain	Species	Mutant or wildtype	Genotype	Allele
APS4	*A. rhodensis* strain SB347, inbred 50x.	wildtype		
APS6	*A. rhodensis* strain TMG33, inbred 11x.	Wild type		
APS20	*A. rhodensis*	Mutant (EMS)	*mas-1*	*brz-3*
APS7	*A. freiburgensis* SB372, inbred 10X	Wild Type		

APS14	*A. freiburgensis* JU1782, inbred 10X	Wild Type		
APS28	*A. freiburgensis*	Mutant (EMS)	*clr-1*	*brz-4*
OP50-1	*E. coli*	Wildtype		

2.2. Methods

2.2.1. preparation of bacterial food source

Auanema nematodes can be maintained axenically. However, it is difficult to maintain it alone over a long period; it will develop very slowly due to the formation of dauer in the absence of food source [69, 95]. Therefore, it is maintained monoxenically in laboratory conditions, as *c. elegans*, with *E. coli* strain OP50-1 used as a food source [96]. Initially, *E. coli* strain OP50-1 from glycerol stock was streaked for a single colony on a pre-prepared LB agar plate. Bacterial culture grew by incubation at 37 ^{o}C overnight. A rich pre-prepared L-broth containing Streptomycin with a final concentration of 50 µg/ml was inculcated aseptically using a single colony from a streak plate. Inoculated LB medium with *E. coli* OP50-1 was allowed to grow overnight at 37 ^{o}C. The *E. coli* OP50-1 streak plate and the liquid culture were moved to 4 ^{o}C for a long period of incubation.

2.2.2. preparation of nematode growth medium (NGM)

Materials and reagents:

NaCl, Agar, peptone, 5 mg/ml of cholesterol in ethanol, 1 M of KPO_4 buffer (potassium phosphate buffer), 1 M of $MgSO_4$, Streptomycin, Nystatin, dH_2O. See the reagent section for the recipe. The amount and concentration of each component to make up a final volume of 400 ml and 1 L of NGM are outlined in table (2.2).

Table 2.2. Components required to prepare NGM.

component	Stock concentration	Final concentration	Final Volume 400 ml	Final Volume 1 L
NaCl			1.2 g	3 g
Bacto-peptone			1 g	2.5
Agar			6.8 g	17

Magnesium sulphate	1 M	1 mM	400 ul	1 ml
Cholesterol	5 mg/ml	5mg/l	400 ul	1 ml
Calcium chloride	1 M	1 mM	400 ul	1 ml
Potassium phosphate ph6	1 M	25 mM	10 ml	25 ml
Streptomycin	50mg/ml	50 ug/ml	400 ul	1 ml
Nystatin	10 mg/ml 75% Ethanol	0.01 mg/ml	400 µl	1 ml
Water			390 ml	975 ml

Method

To make up a final volume of 1 L of NGM, 3 g of NaCl, 17 g of agar, and 2.5 g of peptone in a 2 L Erlenmeyer flask. 975 ml of dH_2O was added. The mouth of the flask was covered with aluminium foil and autoclaved. Once cooled, the following components were added; 1 ml of 1 M $CaCl_2$, 1 ml of 5 mg/ml cholesterol in ethanol, 1 ml of 1 M $MgSO_4$, and 25 ml of 1 M KPO_4 buffer. Anti-bacterial streptomycin and anti-fungal nystatin were added. Then, the NGM solution was mixed well.

2.2.3. Preparation of NGM Petri plates

With a careful sterile procedure, NGM solution was dispensed into Petri plates using a peristaltic pump filling Petri plates 2/3 full of agar. Plates were left at room temperature overnight to allow for the detection of contaminants, and to allow excess moisture to evaporate.

2.2.4. Seeding NGM plates

Using a sterile technique, 1 ml of the OP50-1 *E. coli* liquid culture is pipetted to 6 cm NGM plates, 3-5 ml in 10cm plates, and ~100 ul to each well of 24 multi-well plates. *E. coli* OP50-1 lawn was allowed to grow overnight at room temperature.

2.2.5. Nematodes handling and maintenance of stock

Several methods were used to transfer nematodes and maintenance of different *Auanema* stocks. A convenient method used often to maintain stocks was chunking, where a sterilised spatula was used to chunk agar from an old plate with hundreds of worms to a fresh plate.

The second method was picking individual worms using a platinum wire, a worm-picker. Platinum wire worm-picker is made by mounting a piece of 2-3 inches of platinum wire to the narrow tip of a pasture pipet. The tip of the platinum wire was shaped into a hook, and sandpaper was used to smooth sharp edges. Under a dissecting microscope, individual worms were picked from plates and released to new plates. Sometimes the stickiness of the OP50-1 *E. coli* lawn was used to form a blob at the end of the worm-picker, then individual worms were selected by touching the top of the worm.

Auanema nematode culture was generally incubated at 20 ^{o}C. However, sometimes they were moved to 15 ^{o}C to slow down the growth of the culture.

2.2.6. Isolating *Auanema* hermaphrodites and females

Under a dissecting microscope, Adult males are generally easily distinguished by their blunt tail and almost transparent body. However, Adult hermaphrodites and females are morphologically indistinguishable in the *Auanema* population unless females were isolated before impregnation by males. *Auanema* hermaphrodites can be separated by isolating stress-resistant dauers from crowded plates. Dauers are characterised by their ability to stand on their tails and display a tube waving behaviour. In favourable growth conditions, dauers exit their resistance non-feeding state and develop to adult hermaphrodites in ~24 h [69].

In isolation, *A. rhodensis* hermaphrodite produced a mixture of dauers and non-dauers [80]. It is relatively difficult to isolate the non-dauers under a dissecting microscope. Therefore, to efficiently separate XX larvae that will develop into females, eggs laid by a hermaphrodite were separated into individual plates; usually, a multi-well plate is used. *A. rhodensis* hermaphrodite was left to lay eggs for ~24 h before moving it to a fresh new plate. Eggs laid on the same day will be synchronised and grow relatively at the same age. Once they exit the second larval stage after 2-3 days, XX larvae destined to be females will proceed to the 3rd larvae, and those predetermined to be hermaphrodites will develop into non-feeding dauer. At this stage, individual animals were separated into separate wells of a multi-well plate. At adulthood, hermaphrodites will be distinguished

from unimpregnated females by their ability to self-fertalise and lay fertilised eggs.

On the other hand, *A. freiburgensis* hermaphrodites generally produce females in isolation. *A. freiburgensis* hermaphrodites are left to lay eggs for ~24 h to synchronise the age of the developing larvae. Once larvae exit the second larval stage after 2-3 days, *A. freiburgensis* dauers are distinguished by their distinctive long then body and small gonad. 3rd larvae females can be isolated by the shape of their body and the size of their gonads compared to dauers. At adulthood, *A. freiburgensis* females that are not impregnated will lay unfertilised eggs.

2.2.7. Cleaning contaminated stocks using sodium hypochlorite treatment

In a fresh seeded NGM plate, 5 ul of bleach solution was pipetted to form a spot on the side of the bacterial loan. A mixture of adults and eggs from contaminated culture were added to the spot using the pick to break up any bacterial clumps. 2-3 spots of bleach added in separate locations adjacent to the lawn, and a mixture of adults and eggs were added to each of them. Once the bleach is soaked, and bacterial contamination is still visible, another 5 ul of bleach is added to the same spot. The plate was left at room temperature for ~5 h until eggs hatched and larvae crawled back to the OP50-1 loan. Healthy contamination-free larvae were moved to a fresh NGM plate to establish a new culture.

2.2.8. Freezing nematodes

Nematodes were cultured into two 10 cm NGM plates. Nematodes were let until plates have just been starved of food at this stage; there should be numerous L1 and L2 larvae, as those are the nematodes that would survive freezing most readily. Plates were washed with 5-10 ml of M9 buffer or dH_2O and swirled around to loosen worms. The solution was carefully pipetted into 15 ml conical tubes. Tubes were centrifuged, and worms were collected at the bottom of the tube. The supernatant was removed, and worms were resuspended in 3 ml of M9. 1ml was pipetted to screwcap cryogenic tube to make triplicate of each line. An equal volume freezing solution was added to each tube. Tubes were then placed inside a styrofoam box and put inside -80 incubator and left overnight to help

freezing worms slowly before moving worms' stock to the final liquid nitrogen storage.

2.2.9. EMS mutagenesis

Three Petri plates of 6 cm diameter containing a few hundred *Auanema* nematodes at the early adult stage were washed off using 2-3 ml of sterile M9 buffer per plate. The M9 nematode suspension was collected in a sterile, disposable 15 ml centrifuge tube. The tube was then centrifuged at maximum speed for 7 minutes, and nematodes were re-suspended in 2 ml of M9. 20 µl of EMS was then added to the tube using filtered tips. The tube was gently swirled to allow EMS to dissolve, to a final concentration of 47 mM. EMS is a potent mutagen, and thus all materials (gloves, pipette, tips) that were in contact with the EMS were treated with 1N NaOH to inactivate it. The tube was covered with parafilm, and the nematode suspension was incubated at room temperature (20 $_{o}$C) on a low-speed rack for 3.5 h. The tube was then incubated vertically until nematodes sank and formed a pellet. The supernatant was then discarded into the 1 N NaOH beaker. Nematodes were washed three times using 5 ml of M9. The tube was inverted 25-30 times and left to form a pellet. The supernatant was discarded into the 1 N NaOH baker. After the final wash, nematodes were resuspended into ~500 µl of M9 and pipetted out into two NGM plates containing a lawn of Escherichia coli OP50-1. The liquid was let to dry. Healthy-looking adults were transferred to a new plate to be used as the P0 generation.

2.2.10. Single worm genotyping

DNA extraction

Single nematodes were picked into a 200 µl PCR tube, each containing 10-20 µl of 1X PCR buffer mix. Tubes containing nematodes were frozen at -80 °C. Frozen samples were thawed, and 0.5 µl of proteinase K was added. Samples were incubated at 65 °C for 60 minutes, and the enzyme was deactivated at 95 °C for 15 minutes. Then, DNA was stored at -80 °C to be used when required.

PCR

DNA fragment harbouring genetic markers were amplified by adding 2 µl of forward primer, 2 µl of reverse primers, 10 µl of PCR green master mix (Promega

2X), 4 µl of water and 2 µl of DNA in each PCR reaction. Samples were run for 30-35 cycles, with initial denaturation for 7min at 95 °C. Cycling conditions were as following; denaturation at 94 °C for 15 s, primers annealing at 55 °C for 30 s, and elongation at 72 °C for 1 min.

2.2.11. Restriction enzyme digestion

PCR products were digested by adding 0.5 µl of a restriction enzyme to the PCR product. Samples were incubated for 1-2 h at 37 °C.

2.2.12. Gel electrophoresis and UV imaging

Digested products were loaded into 1.8% agarose gel covered with 10X TAE buffer inside an electrophoresis apparatus, and samples were run at 70 Volts for ~40 min. Individuals' genotype was determined from gel images by matching them with wildtype genotypes.

2.2.13. Agarose pad slides preparation

First of all, 3 g of agarose powder was added to 100 ml of dH_2O. The solution was heated for 1min in a microwave and mixed thoroughly until the solution was clear with no bubbles. Two microscope slides with tape wrapped in the middle for a thickness of ~1 mm were prepared. One microscope slide was placed between the two microscope slides with the tape aligning all three slides next to each other. A small drop of 3% agarose using a plastic pipette was placed on the clear microscope slide. Quickly it was covered with another clear slide forming a cross with both of its sides are elevated slightly by the thickness of the tape forming a 1 mm thick pad. After left to cool at room temperature, slides were dissembled apart with the agarose pad stuck on one of the clear slides.

2.2.14. Immobilization of nematode for imaging

Nematodes were immobilized by picking them directly into 5 ul of 1 M sodium azide drop placed on agarose pad slide or unseeded NGM plate. The agarose pad slide was covered with a coverslip and pressed gently to remove air bubbles before being placed on an inverted microscope. On the surface of an unseeded NGM plate, nematodes were manually aligned using a platinum wire pick.

2.2.15. Microscopy

Auanema nematode was generally maintained, crossed, and screened for mutants using an Olympus SZ61 stereomicroscope. For high magnification and imaging, Olympus SZX7 was regularly used. For high-resolution imaging of nematodes, a Zeiss Axio Zoom V16 fluorescence microscope was used.

Cytology images throughout the thesis were acquired on an Olympus BX60 epifluorescence microscope with a QImaging EXi Aqua cooled CCD camera. An Olympus PlanApo 60X objective lens and iVision software were used to take images. Z-stacks through the whole gonad was acquired, 10-15µm in 90-120 z-planes. Finally, images were minimally processed using Adobe Photoshop.

Chapter 3

Investigating spermatogenesis of *A. rhodensis* XX spermatocyte

Summary

In this chapter, I investigated the spermatogenesis of *A. rhodensis* XX male to determine if the X chromosome polarises specific cytoplasmic components. An *A. rhodensis* XX male mutant was isolated from a chemical mutagenesis screen. This mutant, called *masculiniser* (*Arh-mas-1*), has the XX karyotype, but the morphology of a male. Sexing and genotyping of *Arh-mas-1* broods following an outcross with a wildtype *A. rhodensis* female indicates that masculinisers produce X-bearing sperm, nullo-X sperm, and diplo-X sperm. Immunostaining analysis of *Arh-mas-1* spermatogenesis revealed that sperm components essential for sperm function and motility segregate equally with X chromosomes in a symmetric division, or co-segregate with both X chromosomes in an asymmetric division (as a result of chromosome non-disjunction). Segregation of sperm components specifically to the cell inheriting X chromosomes during asymmetric divisions supports the hypothesis that sperm components segregate exclusively to the cell inheriting the X chromosome.

3.1. Introduction

A defining feature of the *A. rhodensis* male spermatogenesis is the exclusive production of one type of sperm containing an X chromosome. The complete absence of nullo-X sperm in the male explains the low proportion of XO male progeny produced after a cross with an XX female. This occurs because, in the final cell division of spermatogenesis, only the spermatid inheriting the X chromosome becomes viable and motile sperm. The sister spermatid nullo-X cell

(the cell without the X) becomes non-viable and is discarded by programmed cell death (Figure 3.1).

Since there is a correlation between the X chromosome and sperm components segregation, we hypothesised that the *Auanema* X chromosome acts as a polarising signal that guides and reorganise the cytoplasm during spermatogenesis. To test if the X chromosome is a polarising signal, the spermatogenesis pattern in XX spermatocytes was investigated. According to our hypothesis, I expect that sperm components essential for sperm function and motility in the secondary XX spermatocyte should segregate to both daughter cells, each with an X chromosome. The *A. rhodensis* XX hermaphrodite produces spermatocytes and oocytes throughout their reproductive life simultaneously and continuously (Figure 1.6) [97, 98]. Therefore, XX spermatocytes in *A. rhodensis* hermaphrodite provide a good initial model to investigate if the X chromosome acts as a polarising signal in *Auanema* spermatogenesis.

3.1.1. Spermatogenesis in *A. rhodensis* hermaphrodite

When *A. rhodensis* hermaphrodites self-fertilise, they usually produce XX animals. In principle, an XX spermatocyte in *A. rhodensis* hermaphrodite would be expected to produce four sperm cells, each with an X chromosome. *A. rhodensis* hermaphrodites were thought to produce 1 X-bearing oocyte and 1 X-bearing sperm to be able to produce XX progeny predominantly. However, the cytological analysis revealed that during hermaphrodite oogenesis, both X chromosomes segregate to the first polar body during the first meiotic division, yielding a nullo X oocyte (Figure 1.6) [83]. Since the *A. rhodensis* hermaphrodite usually produces nullo-X oocytes, its predominant production of XX progeny through self-fertilisation suggests that hermaphrodite spermatogenesis regularly produces diplo-X sperm (instead of haplo-X sperm) [81] [80]. Genetic analysis of *A. rhodensis* hybrid $X_{APS4}X_{APS6}$ hermaphrodite progeny illustrates that the X chromosome in hermaphrodite does not recombine, and progeny resulting from hermaphrodite selfing were heterozygote for all X chromosomes markers [83]. The complete absence of homozygous X chromosome markers at all loci suggests that, in addition to the production of diplo-X sperm, there is no recombination

event between X chromosomes during hermaphrodite spermatogenesis (Figure 1.6) [83].

Cytological analysis of hermaphrodite spermatogenesis revealed that cytoplasmic components essential for sperm function and motility (e.g., mitochondria and MSP) segregate asymmetrically exclusively to the side inheriting both X chromosomes; the sister nullo-X cell becomes a residual body with DNA inheriting discarded material and proteins (e.g., tubulin) (Figure 3.1). As in *A. rhodensis,* wildtype males, the X chromosomes lags in the second anaphase; subsequently, cellular components necessary for sperm function segregate to the pole inheriting both X chromosomes. The chromatin mass revealed by the DAPI staining was approximate twice the size of those observed in anaphase II of male spermatogenesis, suggesting that the two X chromosomes segregate to the same pole (Figure 3.1) [83]. Similar to male spermatogenesis, X chromosomes and cytoplasmic components essential for sperm function segregate together in the hermaphrodite. However, in contrast to male spermatogenesis, cytological and genetics studies suggest that hermaphrodite spermatogenesis produces diplo-X sperm rather than haplo-X sperm. The asymmetric segregation of cytoplasmic components important for sperm function and motility, together with both X chromosomes in hermaphrodite spermatogenesis, are consistent with our hypothesis that the X is involved in cytoplasmic polarisation and subsequent asymmetric segregation of cytoplasmic components. To confirm that the X is involved in organising the cytoplasm during spermatogenesis, I generated a masculinising mutation in *A. rhodensis*. Sex determination in *A. rhodensis* XX animal was disrupted by ethyl methanesulfonate (EMS) chemical mutagenesis, causing the appearance of a masculine phenotype. Since the recovered mutation causes an XX animal to exhibit masculine appearance, it was called masculiniser and abbreviated to *Arh-mas-1(brz-3).*

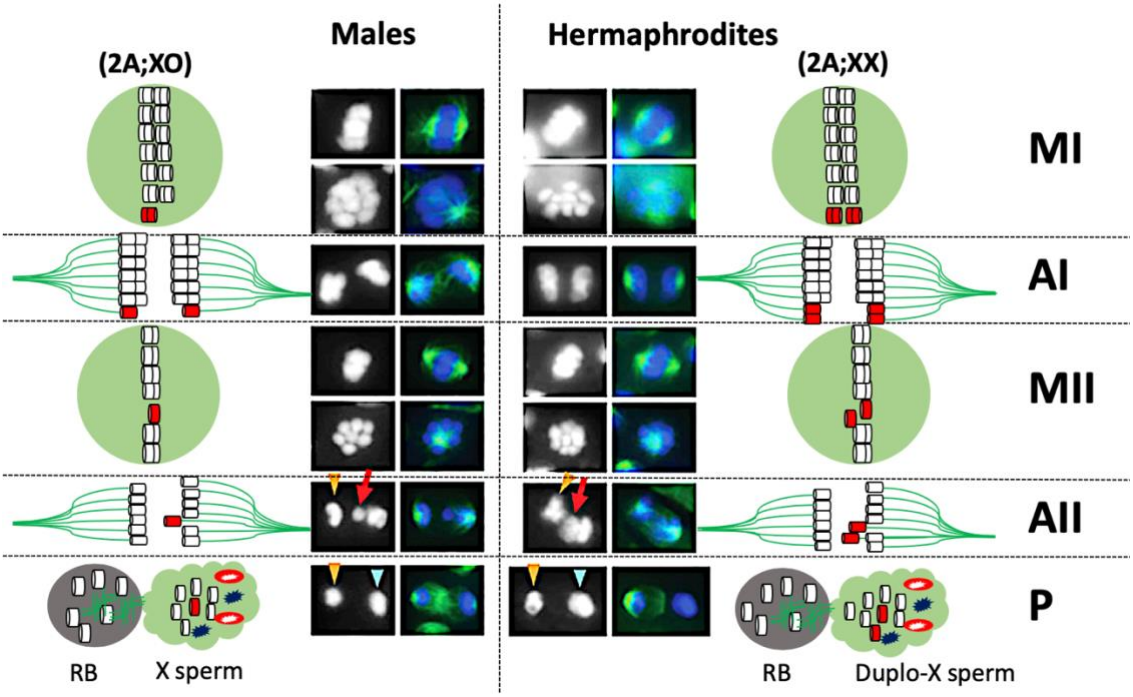

Figure 3.1: *A. rhodensis* XX spermatocyte segregate asymmetrically producing diplo-X sperm.
chromosomes were stained with DAPI (blue), and microtubules were stained with anti-tubulin antibody. A schematic diagram representing autosomes (white cylinders) and X chromosome (red cylinders) segregation during spermatogenesis is shown alongside the immunostaining images. Spindles in green are shown in both orientations representing the two poles of the dividing spermatocyte. In the second anaphase, X chromosomes lag (red arrow) and segregate exclusively to one pole of the dividing secondary spermatocyte. In the second anaphase, the intensity of the lagging X chromosome DAPI staining in hermaphrodite in comparison to males indicates the segregation of two X chromosomes producing diplo-X sperm rather than haplo-X sperm. Tubulin segregates to the residual body with the smaller chromatin mass (orange arrow), whereas cellular components (mitochondria and MSP) essential for sperm function and motility segregates with the cell inheriting X chromosomes (blue arrow). Staining and schematic representation of chromosomes segregation were adapted from [83].

2.1.2. The masculinising mutation converts a genetically XX female to have the phenotype of a male

A. rhodensis males contain six pairs of autosomes and a single X chromosome (2A; XO), whereas hermaphrodites/females contain six pairs of autosomes and two X chromosomes (2A; XX) [69, 99, 100]. In *c. elegans*, the X chromosome ploidy ratio controls sex determination; individuals inheriting a single X chromosome develop into males (0.5 ratio), and individuals inheriting two X chromosomes develop into hermaphrodite (ratio of 1) [78, 100-103]. However, mutations in autosomal genes involved in sex determination can cause a reversal

to the normal process, where animals with XX karyotype develop a masculinised phenotype and animals with XO karyotype develop a feminised phenotype [99, 100, 104-106]. Earlier studies in *c. elegans* showed that the autosomal genes *tra-1*, *tra-2*, and *tra-3* are essential for both the somatic and germline development of females/hermaphrodites: loss-of-function mutation on those genes transforms a genetically XX animal to exhibit masculine phenotypes. Hence, they were named transformers genes and abbreviated to *tra* [99, 104-106] (Figure 3.2).

The difference in X chromosome dosage between XX female and XO male, unless regulated, causes a difference in the expression of genes located on the X chromosome [78]. Since females and hermaphrodites inherit two X chromosomes, they can potentially produce X-linked genes product twice as much as in males [102]. However, the amount of X-linked gene products in hermaphrodites are reduced by half to equalise the expression of X-linked genes between the two sexes [107, 108]. Somatic and germline cells in hermaphrodites evolved a molecular mechanism known as "dosage compensation" to deal with the X chromosome dosage challenge, whereby in XX animals, the expression of genes located on the X down-regulated by twofold [78]. Cells determine the number of X chromosomes by the expression of X-linked genes on the X chromosome, known as the X signal elements (XSEs) [78]. High expression of XSEs represses the activity of *her-1* gene, an essential gene for hermaphrodite development in the sex determination pathway [78, 109-111]. Mutation in *the her-1* gene converts XO embryos to hermaphrodites [100]. During embryonic development, the expression of *her-1* in XX embryo is much lower than in XO embryo, because XSEs in XX embryo are expressed twice as much [78]. Antagonistic action on the upstream global sex regulation by the Autosomal signal elements (ASEs) counterbalances XSEs [78]. The HER-1 level in diploid XX embryo is kept low because the double dose of XSE genes products outweigh the antagonistic activity of ASEs [78, 102].

On the other hand, HER-1 level in XO embryos is high because a single dosage of XSEs is insufficient to override the antagonistic activity of ASEs, leading to failure to implement dosage compensation [78]. In XO embryos, a high level of HER-1 represses the activity of downstream *tra* genes leading to the development

of males [78]. On the other hand, low expression of *her-1* in XX embryos will be insufficient to inhibit the activity of downstream *tra* genes leading to the development of hermaphrodites/females (Figure 3.2).

Epistasis genetic interactions between other sex determination genes and *tra-1* in a regulatory pathway illustrate their wildtype role of mediating between the key *tra-1* gene and the initial sex determination signal caused by the ratio of X chromosome to autosomes [104]. *tra-1* is a critical gene in nematode sex determination. It is function is essential and solely sufficient to induce the development of females, whereas loss-of-function of *tra-1* gene is sufficient for males development [104]. In XX hermaphrodites/females, a cascade of genes acting upstream of *tra-1* activate the transcription factor TRA-1 to be translocated to the nucleus to activate transcription of tissue-specific sex determination gene [104]. In XX animals, cleavage of transmembrane TRA-2 protein by TRA-3 producing (TRA-2ic) inhibits the activity of FEM protein [104, 106]. Therefore, TRA-1 is translocated to the nucleus, where it activates the transcription of downstream local sex determination genes. In XO males where XSEs dosage is low TRA-1 is inhibited by FEM protein and retained in the cytoplasm. Initially, HER-1 inhibits the cleavage of TRA-2 by TRA-3; consequently, TRA-1 is inhabited by FEM protein (Figure 3.2) [104, 106]. Sex determination genes acting upstream of *tra-1* are global sex determination factors; mutation on those genes transform the sex of the animal completely, irrespective of the X chromosome to autosomes ratio [106].

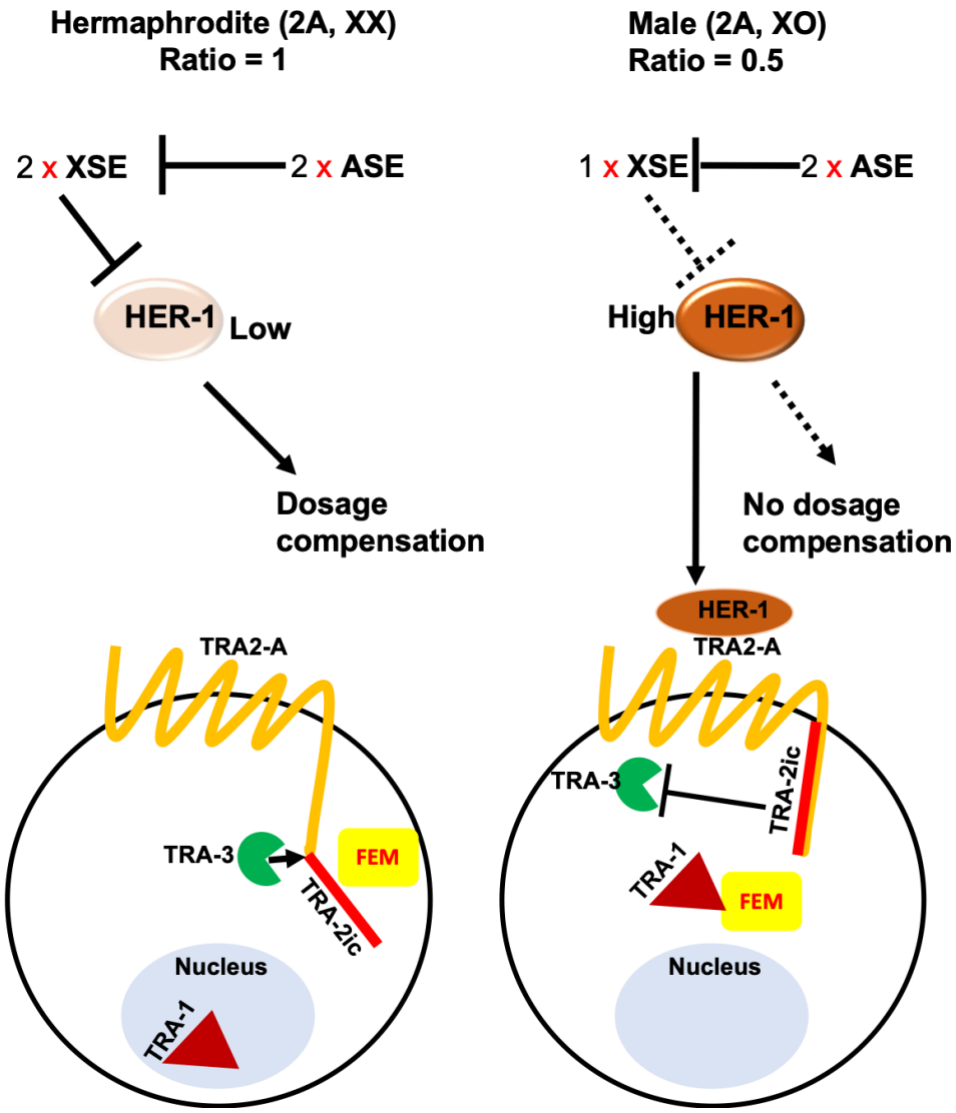

Figure 3.2: Regulatory pathway of sex determination in nematodes.
The figure is adapted from [78, 106]. Initially, sex is determined by the ratio of X chromosomes to autosomes. The double dosage of XSE negatively regulates the activity of HER-1. Low level of HER-1 initiates a cascade of interactions that result in the activation of TRA-1 to be translocated to the nucleus to activate the transcription of local sex determination genes. TRA-3 cleaves the intracellular domain of TRA-2 (TRA-2ic), which inhibits the activity of FEM protein. In males, a single dosage of XSE is not sufficient to block the activity of HER-1, leading to a high level of *her-2* expression. The activity of HER-1 protein inhibits cleavage of TRA-2 intracellular domain; as a result, the activity of TRA-1 is inhibited by FEM protein and retained in the cytoplasm.

Loss-of-function (*lf*) mutations in any one of the three genes (*tra-1*, *tra-2*, and *tra-3*) causes genotypically XX animals to masculinise into pseudo-male, a sex determination mutant with both a male soma and germline phenotype [99, 100, 104, 105, 112]. *A. rhodensis* sex determination mutant *Arh-mas-1* (masculiniser) that is phenotypically male but with an XX karyotype was isolated from (EMS)

mutagenesis. It is likely that the *A. rhodensis* sex determination mutant *Arh-mas-1* is a result of Loss-of-function (*lf*) mutations of one of the *tra* genes during the EMS mutagenesis. However, in this thesis the cause of the sex determination mutation was not fully explored. In this chapter, I will investigate the spermatogenesis of XX masculinisers to determine if the X chromosome is a polarising signal causing asymmetric segregation of cytoplasmic components in *A. rhodensis* wild type male spermatogenesis. If the hypothesis is correct, we predict that each X chromosome will segregate to opposite poles of the dividing cell. Sperm components essential for sperm function and motility will segregate symmetrically, generating functional X-bearing sperm in every instance.

3.2. Materials and Methods

3.2.1. Post-mutagenesis screening for *A. rhodensis* APS4 *masculiniser* (*Arh-mas-1*) mutant

Mutagenised P0 of early adult *A. rhodensis* APS4 hermaphrodites were let to lay eggs on a fresh plate for ~24 h to decrease the number of females. An *A. rhodensis* (APS4) self-fertilising hermaphrodite produces a higher percentage of female and male progeny during the first day of adulthood, which interferes with the screen design [81]. However, the percentage of male and female progeny drops considerably by the second day, where the ratio of hermaphrodite progeny is at its peak [81]. Because we wanted to find XX animals with male morphology, the eggs laid during the first ~24h from P0s and F1s were discarded. After 24 hours, hermaphrodites were moved into a new separate plate each. P0 mutagenised nematodes were left to self-fertilise, in a separate plate each, to produce F1 Progeny. F1 self-fertilising hermaphrodites were then moved to a single plate each and left to lay eggs for ~24 hours to reduce the number of females. Later, F_1 hermaphrodites were moved to a separate plate each to lay F2 progeny. Finally, F2 progeny from 521 F1 were screened for phenotype of *masculiniser* recessive mutation (Figure 3.3). The mutation was maintained by propagating potential heterozygote *mas-1* +/- sibling hermaphrodites (Figure 3.3).

3.2.2 *A. rhodensis masculiniser* (*Arh-mas-1*) backcross with APS4 and polymorphic APS6

Backcrossing with APS4 strain was conducted to remove any potential mutations that might have arisen alongside the *mas-1* mutation during EMS wide mutagenesis. Masculiniser strain backcrossing with polymorphic APS6 strain generates hybrid $X_{APS4}X_{APS6}$ masculinisers, when genotyped provides genetic evidence that the mutant is masculinised XX. The masculiniser strain was backcrossed with *A. rhodensis* APS4 strain in two separate experiments. In the first experiment, five rounds of backcrosses were performed using males that were heterozygote for the *mas-1* mutation. However, this backcrossed strain was lost. Therefore, a second experiment was conducted after discovering that masculinisers are fertile, where three rounds of backcrosses were conducted.

3.2.2.1. Using males that were heterozygote for the *mas-1* mutation *mas-1 +/-*

In the first experiment, ten P0 males from a heterozygote plate for the masculinising mutation were crossed with 10 *A. rhodensis* wildtype females, in separate crosses. Crossed individuals were left to cross for almost ~24 h before males were removed. Then 10 F1 dauers were picked from each plate and moved to a new fresh plate each to make a total of 100 F1 individuals. Masculiniser phenotype was screened for in the F2 progeny and recovered for the next round of backcross. This backcrossing scheme was repeated five times with APS4 strain. However, backcrossed masculiniser strain with APS4 strain using this experiment was lost during maintenance. Masculiniser strain recovered from the chemical mutagenesis was backcrossed with APS6 females using a similar backcrossing scheme to generate a hybrid $X_{APS4}X_{APS6}$ masculiniser mutants. Hybrids $X_{APS4}X_{APS6}$ were isolated to be genotyped.

3.2.2.2. Backcrossing using *A. rhodensis masculinises*

The second experiment of backcross with (APS4) strain was conducted after discovering that masculinisers are fertile. In the second experiment, five P0 masculinisers (XX males) were crossed with five wildtype females in 5 separate crosses. Masculinisers and females were kept together throughout their entire life to ensure fertilisation of the female. Then, ten F1 early adult XX individuals were moved from each cross to a fresh new plate to make a total of 50 F1 individuals. masculiniser phenotype was screened for in the F2 progeny. This procedure was repeated three times. The strain, after three times backcross to APS4, was renamed to APS20 [*Arh-mas-1* (brz-3)]. The APS20 was backcrossed with polymorphic APS6 strain to generate a hybrid $X_{APS4}X_{APS6}$ masculiniser mutant. the hybrid $X_{APS4}X_{APS6}$ masculiniser mutant was isolated to be genotyped.

3.2.3. Masculiniser cross with APS4 and APS6 females to sex and genotype progeny

Crosses

APS20 *Arh-mas-1* was crossed with virgin females from APS4 and APS6 strain to determine the pattern of divisions occurring in masculinisers spermatogenesis. Masculinisers were crossed with females of APS4 strain to sex progeny resulting from the cross and with females of APS6 strain to sex and genotype progeny

resulting from the cross. Masculinisers generally are not interested in mating, and thus, masculinisers and females were left ~24 h together for the cross to happen, after the cross masculinisers were removed. Gravid females were moved to a new plate every day. Progeny of crosses with APS4 females were scored in three separate categories, (XO) males, (XX) females or hermaphrodites, and (XXX) dump. Single animals resulting from APS6 females and masculinisers cross were isolated for genotyping.

3.2.4. *A. rhodensis* APS4 and APS6 X chromosome genotyping

Single nematodes were picked into 200 µl PCR tubes, each containing 10-20 µl of 1X PCR buffer mix. Tubes containing nematodes were frozen at -80 °C. Frozen samples were thawed, and 0.5 µl of proteinase K was added. Samples were incubated at 65 °C for 60 minutes, and the enzyme was deactivated at 95 °C for 15 minutes. Then, DNA was stored at -80 °C to be used when required. *A. rhodensis* X chromosome markers were amplified by adding 2 µl of forward primer, 2 µl of reverse primers, 10 µl of PCR green master mix (Promega 2X), 4 µl of water and 2 µl of DNA. Samples were run for 30-35 cycles, with initial denaturation for 7 min at 95 °C. Cycling conditions were as following; denaturation at 94 °C for 15 s, primers annealing at 55 °C for 30 s, and elongation at 72 °C for 1 min. PCR products were digested by adding 0.5 µl of a restriction enzyme to the PCR product. Samples were incubated for 1-2 h at 37 °C. Digested products were loaded into 1.8 % agarose gel, and samples were run at 70 Volts for ~40 min. Individuals' genotype was determined from gel images by matching them with wildtype genotypes.

3.2.5. Detecting apoptotic cells using SYTO 12 staining

SYTO 12™ (ThermoFisher scientific) (4 mM in DMSO) was diluted to a working solution of 33 µM in M9 buffer. Plates were placed in a slanting horizontal position, and 1ml of the SYTO 12 solution was added on the plate such that the solution stayed on one side of the plate. The plate is kept slanted so that after staining, it was easier to recover nematodes from the solution. Nematodes to be stained by SYTO12 were transferred to the plate and left to swim in it for about 1 hour in the dark. SYTO 12 solution was checked to be sufficient, so it would not dry out after a few minutes. After staining, the plate was kept

horizontal so that the liquid would spread on the plate, and nematodes were more comfortable to pick. Nematodes were transferred to a new NGM plate and left to crawl for an hour in the dark to remove excess staining from their intestine. Nematodes were immobilised with 3mM of sodium azide, mounted on slides with agar pads, and visualised under a fluorescence microscope.

3.2.6. Immunostaining of germ cells

Gonads of 10-20 nematodes were dissected inside a sperm solution (for 100 ml; 1.8 ml of 5 M NaCl, 5 ml of 1 M KCl, 0.4 ml of 0.5 M MgCl2, 2 ml of 0.5 M CaCl2, 2.383 g of HEPES and 40 ml of 50 mM dextrose dissolved in dH2O) on a poly-L-Lysine slide. Dissected nematodes were covered with a 22x40 cm coverslip, where the entire assembly should look like a cross. The coverslip was pressed diagonally but not too hard. The slide was immediately dropped in liquid N2 flask to freeze-crack the tissues. The slide was taken out of the flask using forceps, and the coverslip was taken off. Quickly, the slide was put inside cold 100 % methanol for overnight fixation at -20 °C. The slide was removed from methanol at -20°C and washed three times for 10min in a 1x PBS buffer. Three Coplin jars were made to help with the washing step, each with 1x PBS. Then, dissected nematodes were incubated with 50 µl of blocking solution (for 10 ml; 0.05 g of BSA, 0.1 ml of 4% sodium azide and 10 µl of tween dissolved in 1x PBS) for at least 30 min at room temperature inside a humid chamber to prevent the sample from drying out. Blocking solution was removed, and dissected nematodes were incubated in 30-50 µl of the primary antibody solution, antibody diluted (1:1000) in antibody buffer (for 10 ml, 0.3 g BSA, 0.1 ml of 4% azide dissolved in 1xPBS), for 3-4 hours at room temperature or overnight at 4 °C. At the end of the incubation period, the primary antibody was washed 2x for 5 min with 1x PBS. Then, 30-50 µl of secondary antibody solution was added, antibody diluted (1:1000) in antibody buffer, and dissected nematodes were incubated in the dark for 3-4 hours. The slide was washed for 2min in 1x PBS. Excess PBS was removed, and the sample was mounted with DAPI. Coverslip was placed on the sample, sealed with nail polish, and observed under the microscope when dried. Z-stacks through the whole gonad was acquired, 10-15µm in 90-120 z-planes. Stacks were analysed using Fiji image and minimally using Adope Photoshop software analysis.

3.3. Results and Discussion

3.3.1. A sex-determination masculinising mutation (*mas-1*) was isolated from ethyl methanesulfonate (EMS) mutagenesis screen

It is still difficult to perform targeted loss-of-function of selected genes to generate mutations in *Auanema*. Therefore, I conducted a chemical mutagenesis screen to identify recessive mutations in a sex determination mutant using Ethyl methanesulfonate (EMS) (Figure 3.3) [113]. EMS is a chemical mutagen that causes random G/C to A/T transitions [114, 115]. EMS will cause other type of mutations as well as desired mutations at random. Therefore, during the mutagenesis screen it is necessary to mutate large number of animals to maximise the chance of finding the mutation of interest, and once the mutation of interest is found it is essential to backcross it with the original wildtype strain to reduce random mutations that may have potentially occurred with the isolated mutation of interest. *A. rhodensis* rapid generation time and its consistent production of hermaphrodites make it a suitable genetic model for isolation of mutants using a mutagenesis screen [69, 116]. After performing EMS mutagenesis and screening 521 F1s, a masculiniser and four dumpy mutants (short and fat) were identified in the F2 generation. I screened for F1s that produced a significant percentage of males (>20%), since F1 hermaphrodite heterozygous for the *mas-1* +/- mutation should produce ~25% of F2 masculinisers (Figure 3.3).

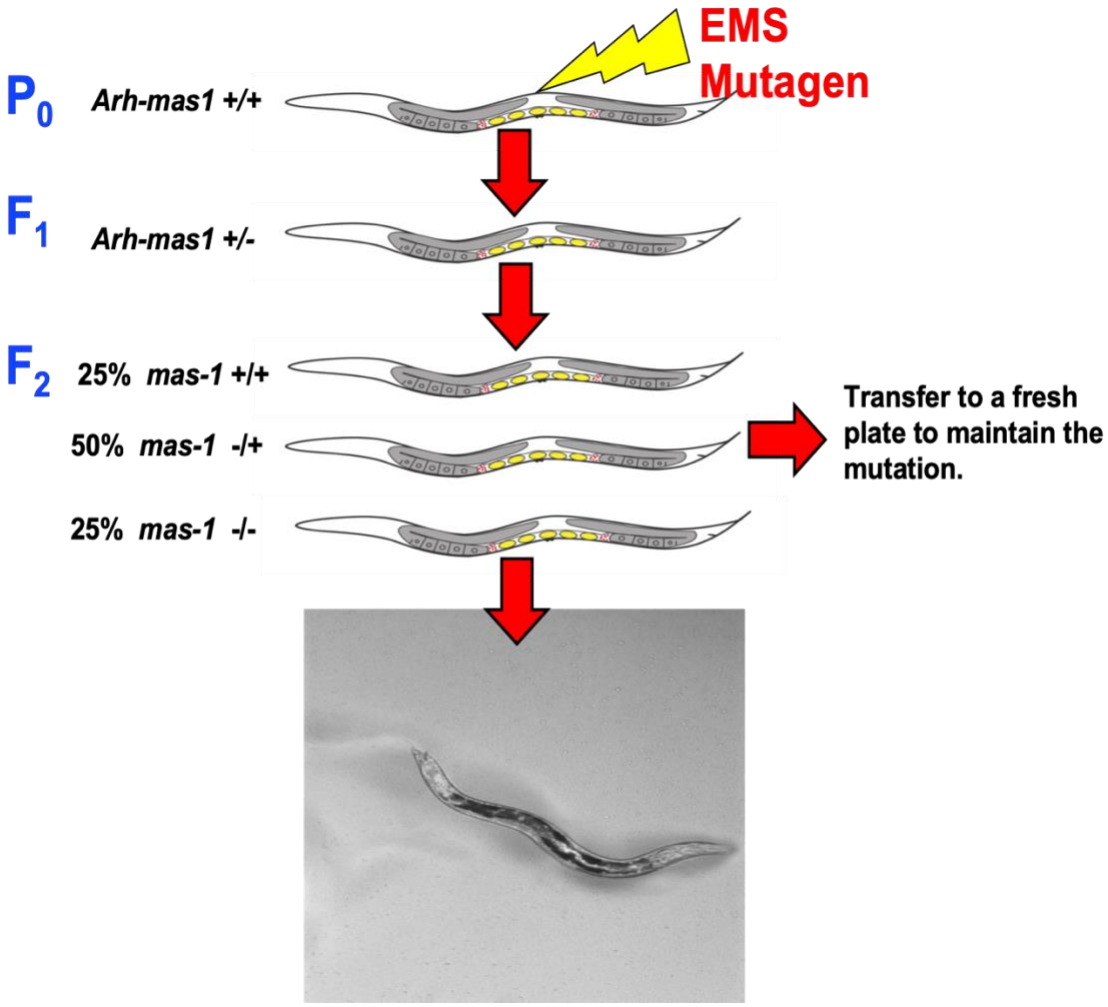

Figure 3.3: F2 screening for masculiniser mutants.
A recessive masculiniser mutation (*Arh-mas-1*) was identified in the second generation (F2) of mutagenised parental strain (P0). F2 progeny from 521 F1s were screened to identify a masculiniser phenotype. Hermaphrodites from heterozygote *Arh-mas-1* +/- plate were transferred to a fresh new plate to maintain the mutation.

Microscopic examination revealed that the the size and morphology of masculinisers and wildtype males are almost indistinguishable. As wild type males, masculinisers have a blunt tail with spicules, which are structures used for female insemination (Figure 3.4). Masculinisers were more distinguishable from wildtype males at their late adult stage, as masculinisers display dark gut morphology with irregular dark patches along their gut compared to the near transparent wildtype males (Figure 3.4A). The masculiniser phenotype itself was not thoroughly investigated in this current study. In this study, the goal was to confirm that those masculinisers are, in fact, XX pseudo-males, subsequently observe the spermatocyte division in the presence of two X chromosomes.

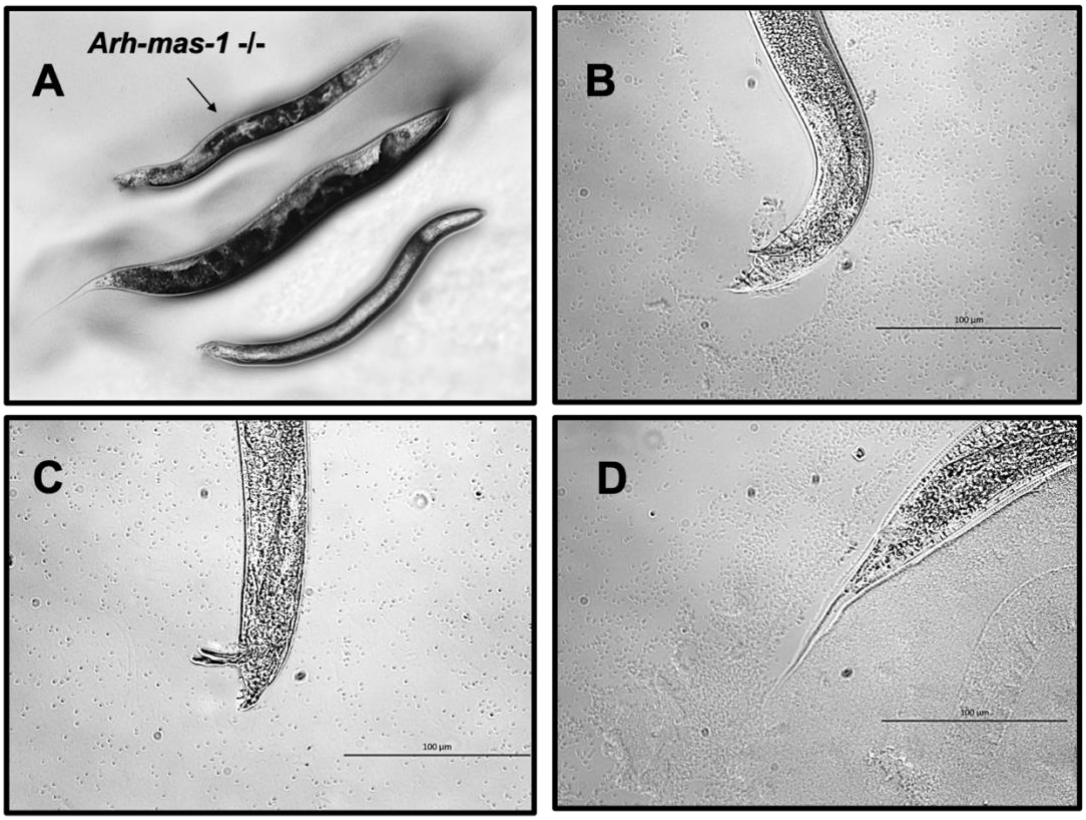

(A) *Arh-mas-1,* hermaphrodite and male, (**B)** Male tail, (**C)** *Arh-mas-1* tail and (**D)** Hermaphrodite tail

Figure 3.4: Masculiniser mutants are genotypically XX animals, but they have the morphology of a male.
(A) *Arh-mas-1* can be distinguished from wildtype males and hermaphrodites/females through body size and tail morphology **(C-D)**. WT male **(B)** and *mas-1* **(C)** have blunt tail and spicules, a structure used for inseminating XX animals. **(D)** XX hermaphrodite tail is long and thin. Despite having a blunt male tail, *Arh-mas-1* can be distinguished from wildtype males by the gut morphology as masculinisers generally appear with dark gut under the microscope **(A)**, especially during the late adult stage, compared to the near transparent wildtype male body. Bar, 100 µm.

3.3.2. Masculiniser strain backcross

3.3.2.1. Backcrossing with a polymorphicAPS6 strain using males heterozygote for the *mas-1* mutation (*mas-1* +/-)

APS4 masculiniser strain was backcrossed with the *A. rhodensis* polymorphic APS6 strain, to test whether putative masculinisers (APS4 background) contain two X chromosomes. Crossing APS4 *Arh-mas-1* +/- male with the APS6 *Arh-mas-1* +/+ wildtype female produces 50% F1 progeny (males and females/hermaphrodites) heterozygous for the *Arh-mas-1* +/- and 50% F1

progeny of all sexes that are wildtype, all the XX progeny resulting from the cross will be hybrid $X_{APS4}X_{APS6}$ heterozygous for the X chromosomes at all loci. In APS4 masculiniser plate, it is not possible to distinguish between wildtype males and males that are heterozygous for the *Arh-mas-1* +/- mutation because they are phenotypically identical. Therefore, ten P0 separate crosses were made, expecting some of those males to be heterozygous for the *Arh-mas-1* +/- mutation. From each cross, it is also not possible to distinguish between F1 *A. rhodensis* adult hermaphrodites and females that are wildtype or heterozygous for the *Arh-mas-1* mutation, therefore 100 F1 XX, 10 F1 XX per cross were isolated (Figure 3.5 B). F1 hermaphrodites that are heterozygote for the X chromosome and *Arh-mas-1* +/- will generate 25% F2 masculinisers that are $X_{APS4}X_{APS6}$ hybrid heterozygous for the X chromosome at all loci, 50% F2 heterozygous progeny (males and females/hermaphrodites) for the *Arh-mas-1* -/+, and 25% wildtype F2 progeny of all the three sexes (Figure 3.3 and 3.5). Hybrid ($X_{APS4}X_{APS6}$) masculinisers were genotyped using X chromosome markers designed along the X chromosome (Figure 3.5A) [83]. F2 masculinisers produced by F1 heterozygous hermaphrodites will be heterozygous for the X chromosome at all X chromosome loci due to the complete lack of recombination between the two X chromosomes in *A. rhodensis* hermaphrodites [83]. Whereas, F2 masculinisers resulting from F1 *Arh-mas-1* +/- females that have mated with *Arh-mas-1* +/- F1 males, were homozygous for some X chromosome markers and heterozygote for others as a result of X chromosome recombination in the female germline (Figure 1.6 and 3.5C).

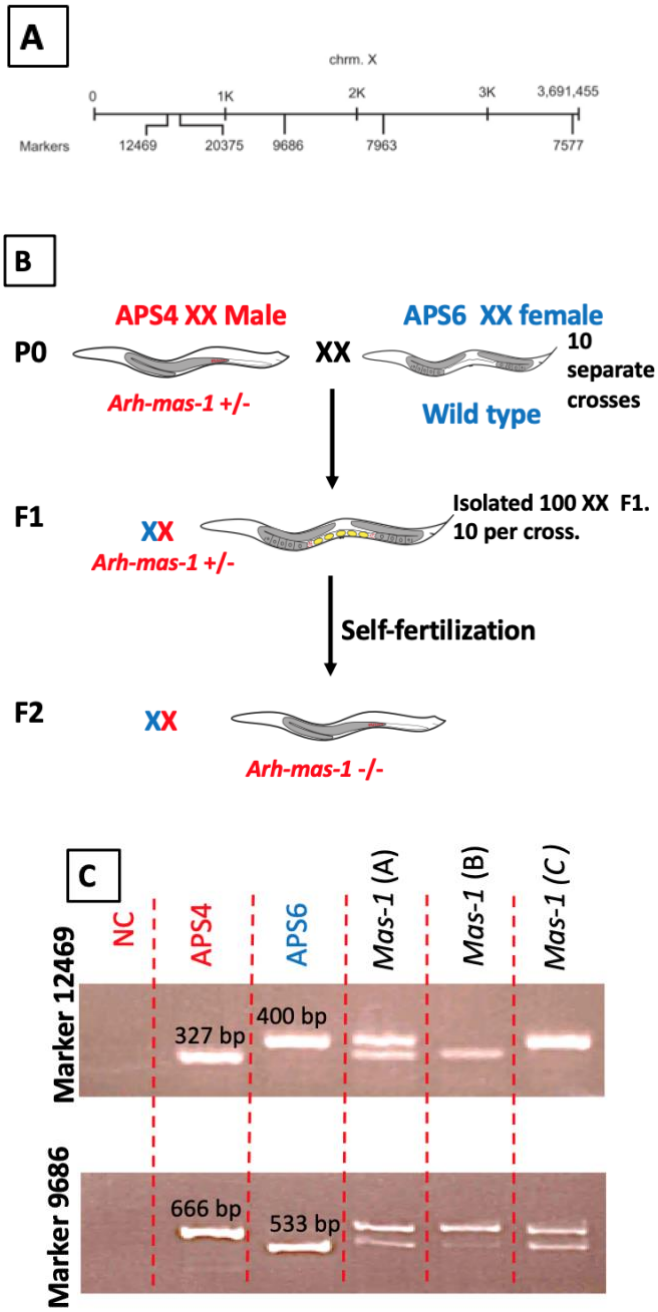

Figure 3.5: Masculiniser strain backcrossed with the polymorphic strain (APS6) to produce hybrid $X_{APS4}X_{APS6}$ masculinisers.

X chromosome markers (**A**) designed to genotype APS6 (blue) and APS4 (red) X chromosomes at different loci were used to genotype masculinisers resulting from the cross. P0 males heterozygous for the *mas-1* mutation were crossed with a wildtype APS6 female to produce F2 masculinisers that are heterozygote for the X chromosome (**B**). Genotyping (**C**) using marker (9686) illustrates that *mas-1* A, B, and C are heterozygote for the X chromosome. Whereas genotyping using marker (12469) illustrates that *mas-1* (A) is a heterozygote for the X chromosome, *mas-1* (B) has an APS6 X chromosome (at that locus), and *mas-1* (C) has APS4 X chromosome (at that locus). Genotyping results from the two different markers revealed that *mas-1* (A) was produced by a hermaphrodite were the X chromosome did not recombine. Whereas, *mas-1* (B) and *mas-1* (C) were

produced by females as the X chromosome has recombined. X chromosome markers figure (A) was adapted from [83].

3.3.2.2. Backcrossing with wildtype APS4 strain

EMS chemical mutagenesis causes genome-wide random mutations. Therefore, there could be other genes that have been mutated alongside the *mas-1* mutation. To eliminate any other potential mutations that may have been created alongside the *Arh-mas-1* mutation, the masculiniser strain was backcrossed with APS4 wildtype female. The masculiniser strain was backcrossed with *A. rhodensis* APS4 strain in two separate experiments. In the first experiment, five rounds of backcrosses were performed using males that were heterozygote for the *mas-1* mutation; however, this backcrossed strain was lost. Therefore, a second experiment was conducted after realising that masculinisers are fertile, and three rounds of backcrosses were conducted.

3.3.2.2.1. Backcrossing using mas-1 +/- males

The masculiniser strain was backcrossed with APS4 strain five times using P0 males that are heterozygote for the *Arh-mas-1* mutation. Whenever a masculiniser was identified within the F2 population from a cross between WT APS4 female and P0 *Arh-mas-1 +/-* males, male siblings were isolated for the next round of backcross (Figure 3.6A). APS4 P0 *Arh-mas-1 +/-* cross with wildtype APS4 female will produce 50% F1 (males, females and hermaphrodites) *Arh-mas-1 +/-* and 50% wildtype. F1 hermaphrodite that is *Arh-mas-1 +/-* will produce 25% F2 masculinisers, 25% F2 wildtype progeny of all the three sexes and 50% F2 *Arh-mas-1 +/-* of all sexes. F2 *Arh-mas-1 +/-* males are isolated from each cross for the next round of backcross (Figure 3.6A). Unfortunately, backcrossed strain using this method was lost because it was tough to distinguish between males and masculinisers. Masculinisers were only distinguishable from males by darker gut pigmentation later in their adult life (Figure 3.6B and C). Masculinisers lost the intensity of gut pigmentation progressively with each backcross; hence it was difficult to distinguish masculinisers from wildtype males (Figure 3.6B and E).

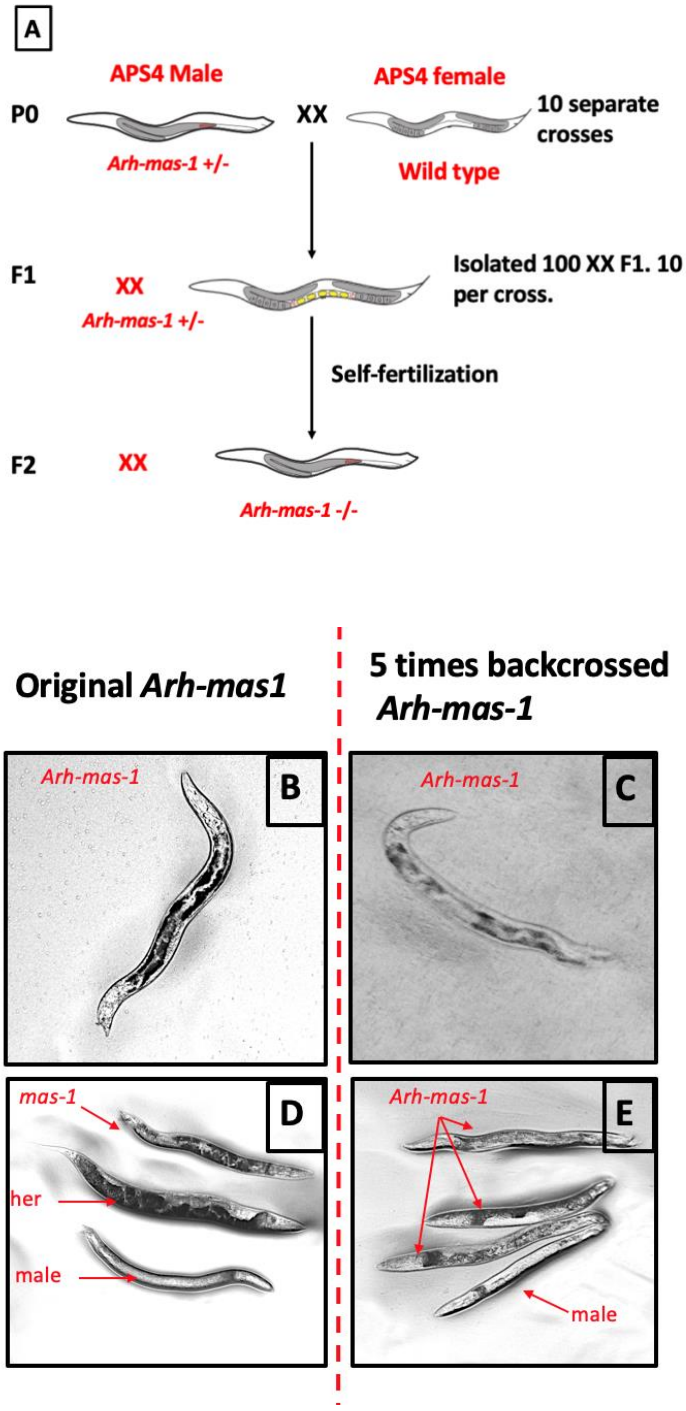

Figure 3.6: Masculiniser strain *Arh-mas-1* backcross with (APS4) female using (APS4) males heterozygote for the *mas-1* mutation.
Males heterozygote for the *mas-1* were crossed with wt APS4 female (**A**), F1 hermaphrodite progeny that are heterozygote for the *Arh-mas-1* mutation will produce F2 masculinisers. Masculinisers were isolated for the next round of backcross. Backcrossing using this scheme was repeated five times. Masculinisers recovered from EMS mutagenesis are distinguishable from wildtype males through gut morphology (**B** and **D**). After backcrossing the masculiniser strain five times with APS4 strain, masculinisers lost the intensity of the gut pigmentation, making it hard to distinguish between males and masculinisers (**C** and **E**).

3.3.2.2.2. Backcrossing using fertile *Arh-mas-1*

A second backcrossing experiment was conducted by crossing masculinisers with wildtype females. This method was conducted shortly after discovering that the masculiniser mutants recovered from the EMS mutagenesis are fertile. In each backcross, five masculinisers were crossed with wildtype APS4 females in separate crosses to produce XX F1 heterozygote for the *Arh-mas-1* mutation. P0 cross between wildtype APS4 female and masculinisers will produce F1 progeny of all sexes that are *Arh-mas-1 +/-* heterozygous. F1 *Arh-mas-1 +/-* self-fertilising hermaphrodite will produce 25% masculinisers (Figure 3.7A). 50 XX F1s (10 per cross), either self-fertile *Arh-mas-1 +/-* hermaphrodites or females that have mated with male siblings heterozygote for the *mas-1* mutation, were isolated to separate individual plates. Masculinisers recovered in the F2 generation were isolated for the next round of backcrossing (Figure 3.7A). Backcrossing using this scheme with APS4 females was conducted three times. Masculinisers strain with three times backcrosses to APS4 was named APS20 [*Arh-mas-1*(*brz-3*)].

APS20 strain was backcrossed again with polymorphic APS6 females (Figure 3.7B). Hybrid $X_{APS4}X_{APS6}$ masculinisers recovered in the F2 were subjected to genotyping using X chromosome markers (Figure 3.7A) to confirm that masculinisers recovered from the backcross strain contain two X chromosomes (Figure 3.7C). From this point onwards, APS20 [*Arh-mas-1*(*brz-3*)] strain was used for all further investigation; I will still refer to it as masculiniser or *Arh-mas-1* for the rest of the thesis.

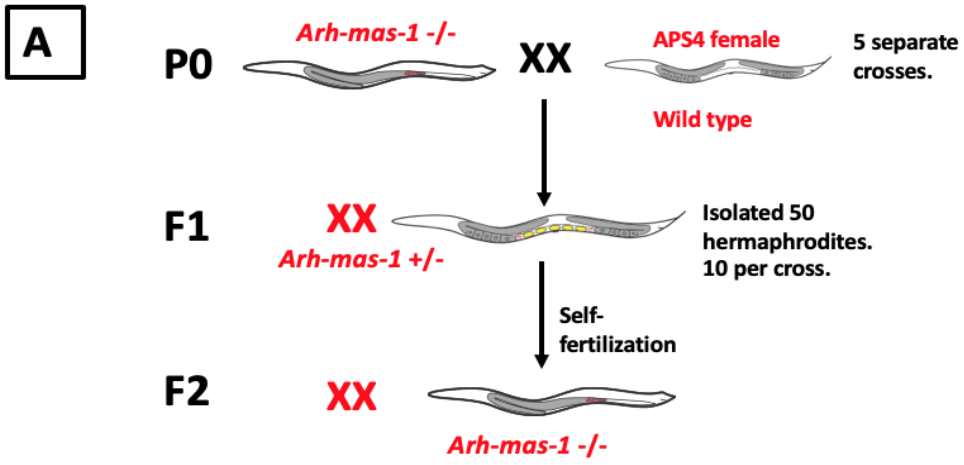

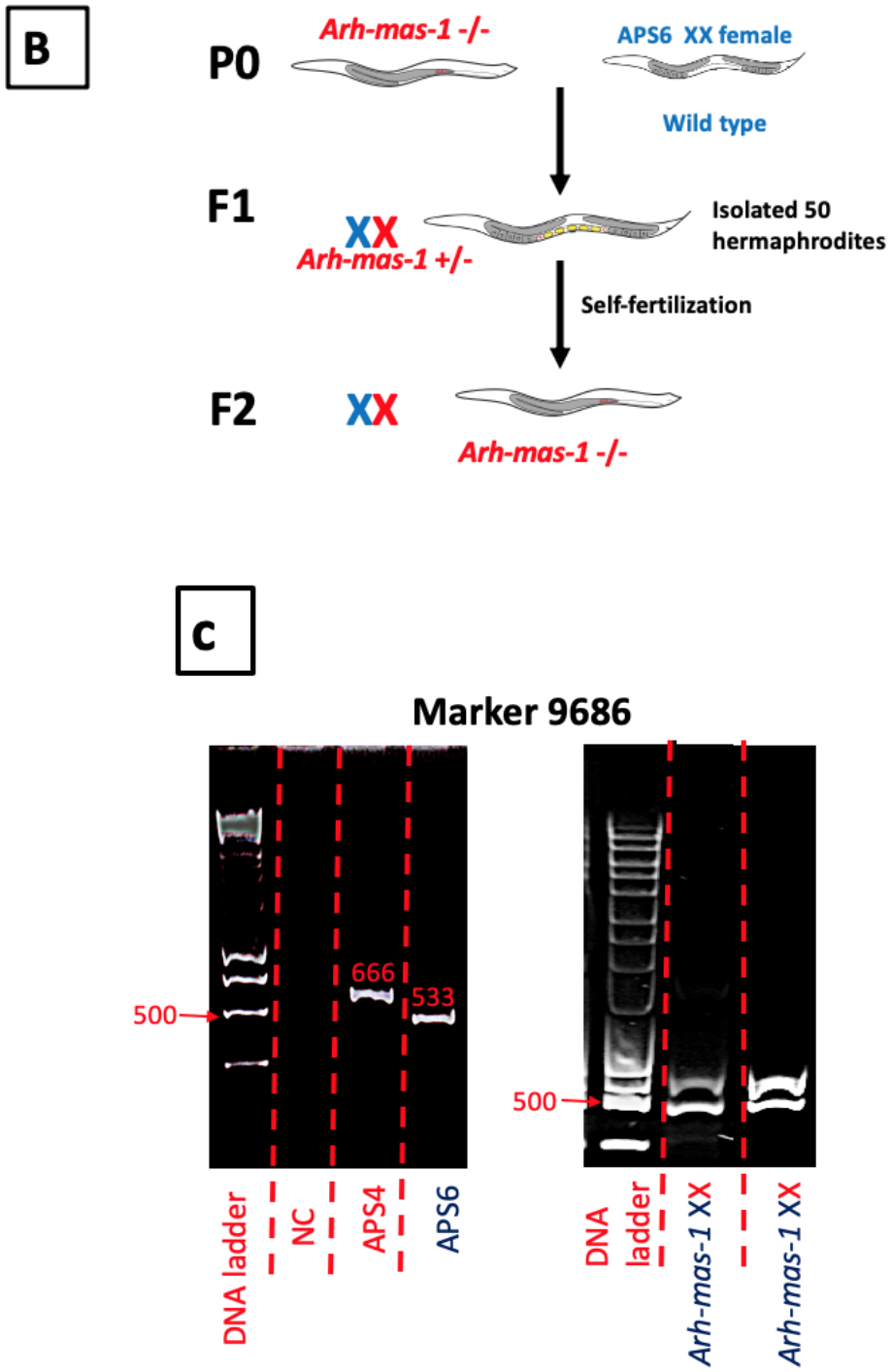

Figure 3.7: Backcrossing of masculiniser strain using fertile masculinisers. Fertile masculinisers were backcrossed with APS4 females in 5 separate crosses (**A**). Some XX F1s resulting from APS4 wildtype female and masculiniser cross will be heterozygous for the *mas-1* mutation. Masculiniser recovered from the F2 generation were isolated for the next round of backcross with APS4 females. After three rounds of backcrosses, masculinisers were crossed with polymorphic strain APS6 in order to produce $X_{APS4}X_{APS6}$ hybrid masculinisers (**B**). Hybrid masculinisers were genotyped to illustrates that they are pseudo-males diploid for the X chromosome (**C**).

3.3.3. Sexing and genotyping masculinisers progeny revealed that masculinisers produce nullo-X, X-bearing, and diplo-X sperm

The fertility of masculinisers offers the opportunity to investigate masculinisers spermatogenesis through sexing and genotyping of their F1 progeny. Sexing F1 progeny resulting from *A. rhodensis* APS4 females and APS20 masculinisers contributed to our understanding of masculinisers spermatogenesis. *A. rhodensis*, female oogenesis predominantly produce X-bearing oocytes and rarely produce nullo-X oocytes [69]. Since we know the gametes produced by *A. rhodensis* female, the sex ratio of progeny resulting from masculinisers cross with a wildtype female will reveal types of sperm produced by masculinisers. During the maintenance of the masculiniser strain, animals with (short and fat) *dpy* phenotype were observed (Figure 3.8). Animals with *dpy* phenotype isolated to separate plates showed that they are infertile with a very short life span compared to other *A. rhodensis dpy* mutants. The presence of animals with *dpy* phenotype in a plate heterozygote for the masculiniser mutation could be attributed to the occurrence of a *dpy* mutation alongside the masculinisers mutation during EMS mutagenesis. However, the presence of *dpy* mutation alongside the *mas-1* mutation can be ruled out for the following reasons; masculinisers phenotype was only selected for when maintaining the mutation, there was no presence of *dpy* males only *dpy* hermaphrodites/females, masculinisers strain was backcrossed with the wildtype strain to eliminate mutations that may have happened alongside the *Arh-mas-1*, and the identified short and fat mutants are only produced by female siblings isolated from *Arh-mas-1* heterozygote plates. Since they are only produced by females, I hypothesised that masculinisers produce viable diplo-X sperm, as in hermaphrodite; and their crosses with female siblings produce short and fat triploid-X hermaphrodites/females. It has been identified that 3X hermaphrodites in *c. elegans* are generally shorter and infertile compared to the 2X hermaphrodites [117, 118].

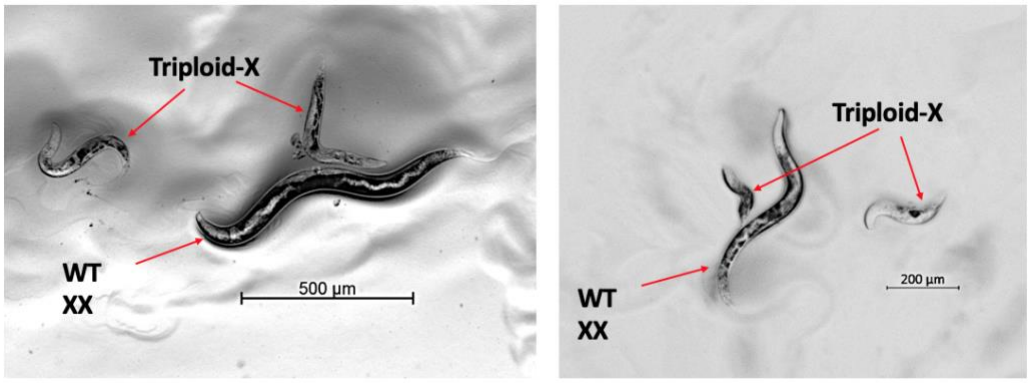

Figure 3.8: Short and fat triploid-X animals compared to wildtype XX animals.
Wildtype Females cross with masculinisers produced animals that are considerably short, and fat compared to wildtype animals. Those short and fat individuals are believed to be triploid-X resulted from masculinisers ability to produce functional diplo-X sperm.

To predict the pattern of spermatocytes divisions in masculinisers, they were crossed with WT APS4 females in 23 separate crosses and produced a total progeny of (3135). Total brood was scored in three categories XO males, XX females/hermaphrodites, and triploid-X females/hermaphrodites. The overall compositions of F1 progeny resulting from masculinisers cross with APS4 females differ. Masculinisers crosses produced considerably more hermaphrodites/females (75%) than males (23%) (Wilcoxon test = 479, p-value <0.001), as well as more males than triploid-X individuals (1 %) (Wilcoxon test = 520, p-value <0.001) (Table 3.1) (Figure 3.9). Considering that *A. rhodensis* females predominantly produce X-bearing oocytes, we can conclude that masculinisers generally produce X-bearing sperm and rarely produce diplo-X sperm. However, the percentage of males produced from masculinisers crosses (23%) is significantly higher than wildtype crosses (1-2%). The high percentage of males produced from masculinisers outcross suggests that masculinisers might be producing functional nullo-X sperm, which challenges the primary hypothesis. In the following experiments, the production of functional nullo-X sperm by masculinisers will be investigated. Since males only contain a single X chromosome using molecular markers for the X, it will be possible to determine the strain of which the nullo-X gamete belongs.

Table 3.1: Count of progeny resulting from wt APS4 female cross with masculinisers from 23 separate crosses.
Progeny were sexed in three categories; (XO) Males, XX Her/Fem, and short/fat (triploid-X).

	Males (XO)	Hermaphrodites/ Female (XX)	Triploid-X (XXX)
Total (3135)	733	2359	43
Percentage %	23.38	75.25	1.37
Mean	31.86	102.56	1.86
SD	23.95	60.39	3.02

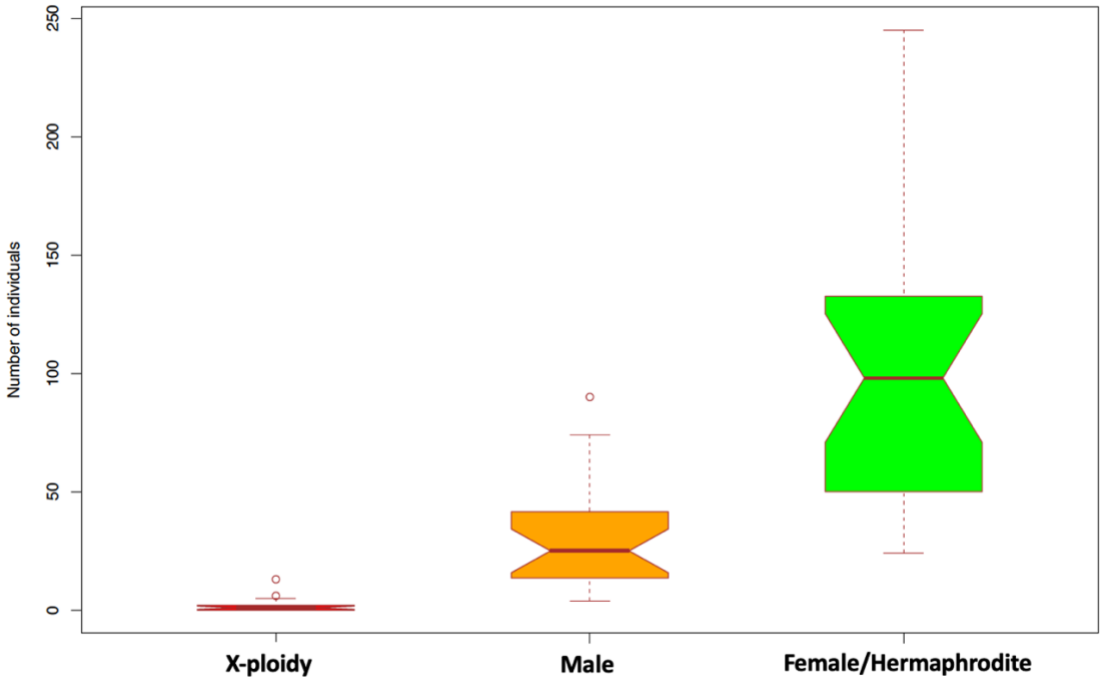

Figure 3.9: Boxplot of F1 progeny resulting from APS4 females cross with masculinisers from 23 separate crosses.
Masculinisers generally produce XX (Females and hermaphrodites), suggesting its predominant production of X-bearing sperm. Masculinisers low production of triploid-X animals suggests its rare production of diplo-X sperm. Male progeny is significantly higher than wildtype crosses suggesting masculinisers might produce viable nullo-X sperm.

Progeny resulting from masculinisers crosses with APS6 females were genotyped to determine the type of sperm produced by masculinisers spermatogenesis. *A. rhodensis* X chromosome markers (Figure 3.5A) were used to determine the origin of gametes constituting F1 progeny resulting from the crosses. Since males only contain a single X chromosome, if masculinisers do not produce nullo-X

sperm F1 male progeny expected to inherit the X chromosome from (APS4) masculinisers and the nullo-X oocyte from (APS6) females. A total of 90 F1s were collected from different separate crosses between APS6 females and (APS4) masculinisers; divided into 57 males and 33 females (Table. 3.2). All of the genotyped (n= 33) XX progeny were heterozygous for the X chromosome marker, illustrating the production of viable X-bearing sperm by masculinisers (Figure 3.10). Thirteen of the genotyped males inherited the X chromosome from masculinisers (APS4) (Figure 3.10), indicating that XX masculinisers produce 1X-bearing sperm. However, 44 out of 57 males inherited the X chromosome from the APS6 mother, indicating the production of functional nullo-X sperm by masculinisers (Figure 3.10). Production of nullo-X sperm would challenge our initial hypothesis unless the nullo-X cell inherited sperm components in the absence of X chromosomes from a dividing spermatocyte. However, before outlining conclusions, investigating masculinisers spermatogenesis by immunostaining is crucial to observe the pattern of spermatocyte division, mainly how those nullo-X and diplo-X sperm are formed.

Table 3.2: Genotyping of masculinisers progeny from a cross with the polymorphic strain (APS6).

	APS4	APS6	Total
XO Males	13	44	57
XX Her/Fem	All heterozygote		33

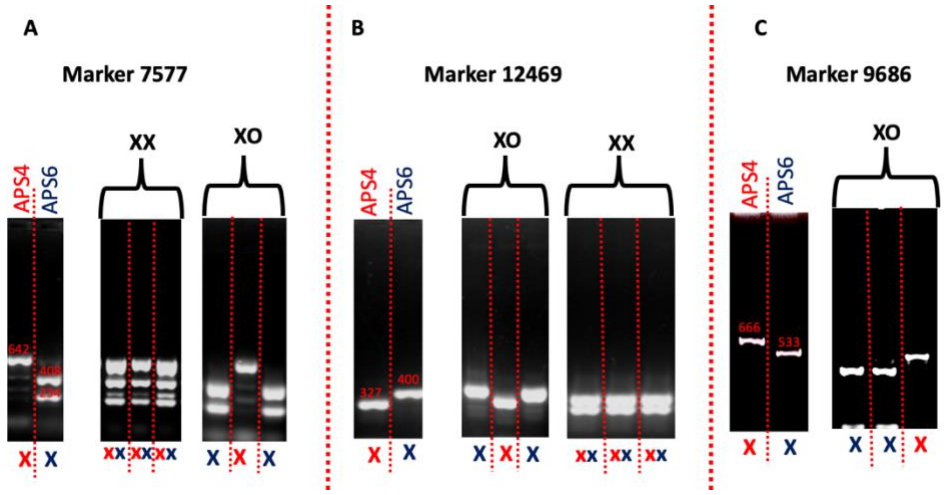

Figure 3.10: Genotyping of masculinisers progeny.
The same individuals were genotyped in A and B using different markers for the X chromosome. XX progeny in A and B were heterozygous for the X

chromosome marker, whereas XO males were homozygous for the X chromosome markers, and some of those males inherited the nullo-X from the *Arh-mas-1* and the X from APS6 mother. More males were genotyped in C to ensure that *Arh-mas-1* produces functional nullo-X sperm.

3.3.4. Syto-12 staining indicates apoptosis in masculinisers germline

The asymmetric division of the secondary spermatocyte in wildtype males and hermaphrodite spermatogenesis produces only one functional sperm and a residual body that undergoes apoptosis. Sexing and genotyping masculinisers progeny indicates that the XX spermatocyte in masculinisers predominantly produces 1X-bearing sperm; in rare events, XX spermatocyte divides asymmetrically producing diplo-X sperm, leading to the development of short and fat X-polyploid, and unexpectedly masculinisers produce functional nulo-X sperm. Since there is a production of functional nullo-X sperm, it is not yet clear if there would be apoptosis in the masculinisers' germline. Masculinisers were incubated with SYTO 12 to be able to visualise apoptotic cells within masculinisers germline. SYTO-12 is retained exclusively inside cells undergoing apoptosis, which in turn makes it easy to visualise apoptosis in the germline of live animals [119]. SYTO-12 staining reveals that there are cells undergoing apoptosis in masculinisers germline (Figure 3.11).

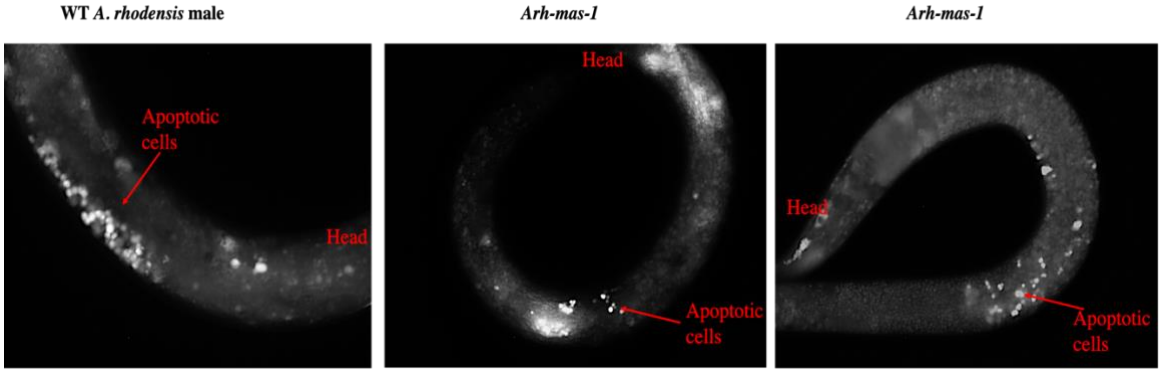

Figure 3.11: Apoptosis in the germline of masculinisers and wt *A.rhodensis* male.
Apoptotic cells in the masculinisers and wt male germline are labeled in red.

Production of functional nullo-X sperm challenges our hypothesis that the X chromosome is a polarising signal if the nullo-X sperm are formed from an asymmetric division in the presence of X chromosomes. However, it is not clear from the apoptotic marker staining if those cells undergoing apoptosis are nullo-X cells resulting from asymmetric segregation of duplo-X chromosomes to one side

of the dividing spermatocyte. Another reason for the presence of apoptotic cells could be the production of a central residual body where unessential cellular components for sperm function are discarded. Immunostaining of MSP and other essential sperm components will help us determine the exact division scenarios during masculinisers spermatogenesis. With immunostaining, it will be evident if the nullo-X sperm are produced during the event of asymmetric segregation of X chromosomes.

3.3.5. MSP in XX masculinisers anaphase II either segregate equally or segregate exclusively to one pole with more significant DNA mass

Sexing and genotyping progeny resulting from wildtype *A. rhodensis* female cross with masculinisers predicted specific patterns of masculinisers spermatogenesis. Sexing and genotyping *Arh-mas-1* progeny indicates that masculinisers predominantly produced X-bearing sperm, and in rare instances, produce diplo-X sperm and nullo-X sperm. In the first anaphase of *Arh-mas-1* XX primary spermatocyte meiosis division, MSP and tubulin segregate equally to both secondary spermatocytes (Figure 3.12). In some instances of anaphase I chromatin mass does not segregate equally; as a result, one secondary spermatocyte inherits more significant DNA mass potentially due to the unequal segregation of the unpaired X chromosomes in anaphase I, however, no lagging-X was observed. In the second anaphase, MSP either segregates symmetrically to both daughter cells resulting in the formation of two spermatids or segregate exclusively asymmetric to the daughter cell with the more significant DNA mass. In contrast, the other daughter cell with small DNA mass inherits tubulin and become a residual body with DNA (Figure 3.12).

Unequal distribution of DNA after the second anaphase is attributed to the unequal segregation of X chromosomes. Different variations of the lagging-X chromosome were observed in the second anaphase, including 1x, 2X, 3X, and 4X lagging-X chromosomes. In addition to variation in numbers of lagging-X chromosomes, a variation in the DNA mass of those lagging-X was observed determined by DAPI surface area. The difference in the mass of the lagging-X chromosomes suggests that the nature of the lagging-X can be either a chromosome from a single chromatid (small DAPI surface area) or a chromosome

from two sister chromatids (big DAPI surface area). The nature of the observed lagging-X chromosome can be determined from the size of the DAPI surface area. The variation and the number of lagging-X chromosomes observed in anaphase II depends on the segregation pattern of X chromosomes in anaphase I. Segregation of X chromosomes in anaphase I has multiple possible patterns depending on if X chromosome sister chromatids split equally or if X chromosome sister chromatids do not split. Patterns of X chromosome segregation in the first meiotic division determines the number and the structure of X chromosomes inherited in each secondary spermatocyte. As a result, multiple segregation patterns of X chromosomes are also expected in anaphase II; thus, variation in the number of lagging-X chromosomes are observed.

When a 1x lagging-X chromosome is observed, it can be either a chromosome from a single chromatid (small DNA mass) or an X chromosome from two sister chromatids (big DNA mass). When a 1x lagging-X chromosome is observed, it is always asymmetric division with MSP segregating to the side inheriting the lagging-X chromosomes resulting in the formation of an X-bearing sperm or duplo-X sperm, while tubulin segregates to the other cell that undertakes the role of a residual body with DNA.

When 2X lagging-X chromosomes were observed, they either segregate equally with the MSP or asymmetrically together with the MSP to only one cell, while the nullo-X cell inherits tubulin. X chromosomes during the 2X lagging-X chromosome can be either a chromosome from a single chromatid (small DAPI area) or a chromosome from two sister chromatids (bigger DAPI area).

In the events when 3X lagging-X chromosomes were observed, MSP segregation was symmetric to both daughter cells. 2 X chromosomes lag from the nucleus of one cell while one X chromosome lags from the nucleus of the other cell. In some divisions, all 3-lagging chromosomes were from a single chromatid, while in other divisions, two X chromosomes were from single chromatids, and one was from two sister chromatids as identified by DAPI surface area.

4X lagging chromosomes were also observed in anaphase II, suggesting unequal segregation of X chromosomes in anaphase I. Where X chromosomes in anaphase I segregate exclusively to one secondary spermatocyte resulting in a secondary spermatocyte with all the Xs and a secondary spermatocyte without X chromosomes. This unequal segregation of X chromosomes is represented by the unequal segregation of DNA masses observed in anaphase I. Observed 4X lagging-X chromosomes in anaphase II explains the formation of nullo-X sperm by *Arh-mas-1*, where nullo-X sperm originates from symmetrically dividing secondary spermatocyte without X chromosomes. This is the only observation that can explain the origin of nullo-X sperm, since, in the event of asymmetric segregation, MSP segregate to the cell with a larger DNA mass that has inherited X chromosomes and the other cell with small DNA mass (nullo-X) inherits tubulin and takes the role of a residual body. Sometimes during the event of symmetric segregation of sperm components, a formation of a central residual body was observed where actin was disposed of in a central region (Figure 3.12). However, it is not clear if those cells separate and become functional sperm.

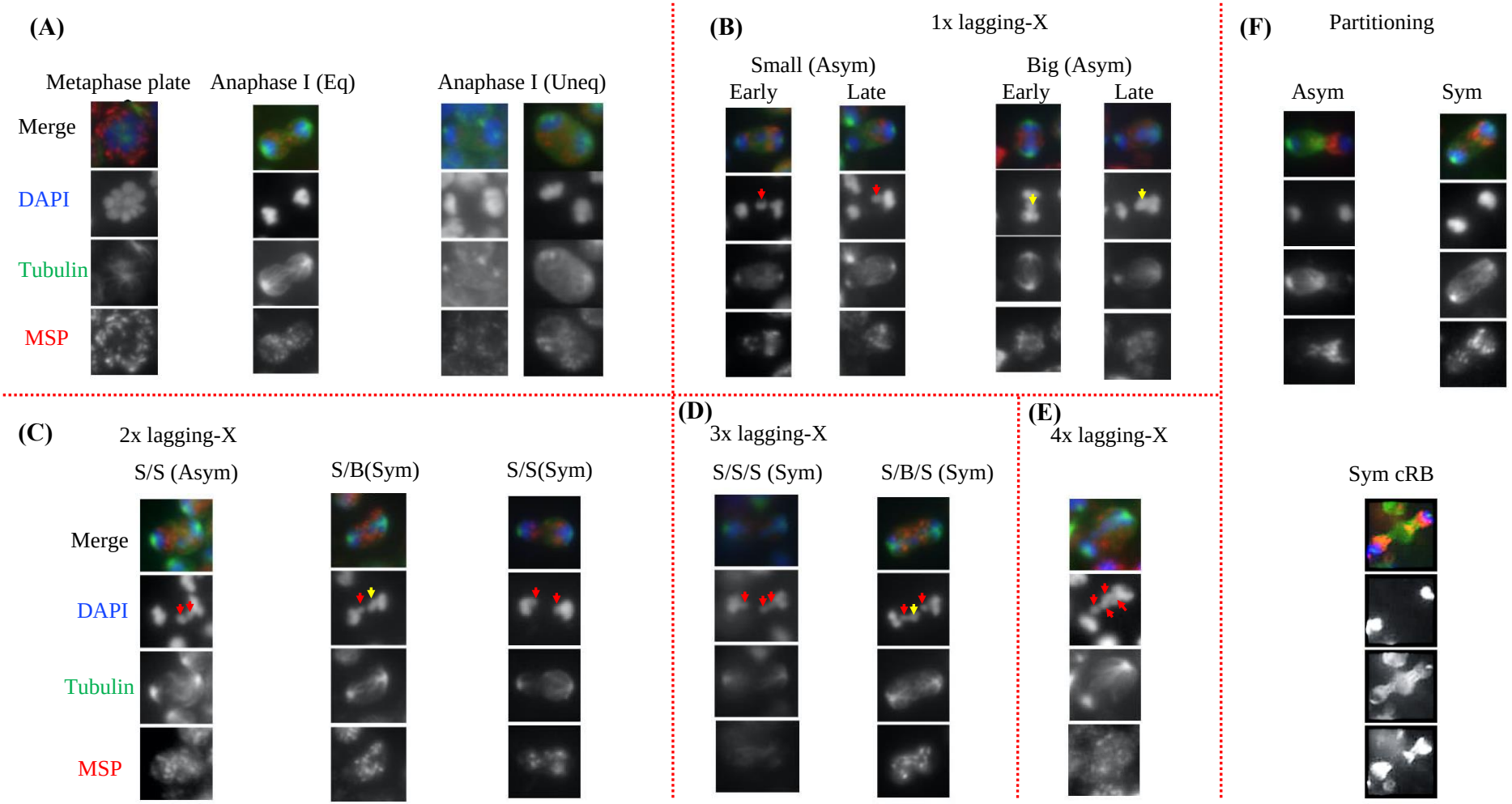

Abbreviations; (Eq) equal, (Uneq) unequal, (S) small DAPI surface area, (B) big DAPI surface area, (Sym) symmetric, (Asym) asymmetric and (cRB) central residual body

Figure 3.12: Anaphase II of *Arh-mas-1* spermatogenesis, MSP either segregates symmetrically to both sperms or exclusively to the cell with larger DNA mass.

(A) Immunostaining using MSP and tubulin antibodies in *Arh-mas-1* primary spermatocyte meiosis during metaphase I and anaphase I. DAPI staining in masculinisers metaphase I indicates that *Arh-mas-1* primary spermatocyte contains eight chromosomes (6 autosomes and 2 X chromosomes). MSP and tubulin of anaphase I of *Arh-mas-1* primary spermatocyte meiosis always segregate symmetrically to both secondary spermatocytes. However, in some events, unequal distribution of DNA was also observed (Uneq) manifested by the large size of the DAPI surface area of one secondary nucleus compared to the other. This unequal distribution of DNA is attributed to the unequal segregation of X chromosomes during anaphase I. **(B)** During anaphase II of *Arh-mas-1* spermatogenesis 1x lagging X chromosome was observed. In the event when a 1x lagging X chromosome was observed, MSP segregates asymmetrically with the cell inheriting the lagging-X. 1x lagging-X chromosome can be either a small DAPI surface area (red arrow) or a big DAPI surface area (yellow arrow). The size of the DAPI surface area suggests that the lagging chromosome is a single chromatid (small surface area) or chromosomes of sister chromatids (big surface area). **(C)** 2X lagging-X chromosomes were also observed in the second anaphase of *Arh-mas-1* spermatogenesis. Different division scenarios were observed in the occasion of 2X lagging-X chromosomes. 2 small DAPI (s/s) (red arrow) X chromosomes of a single chromatid segregating asymmetrically (S/S, Asm) with the MSP exclusively to one cell. Both lagging-X chromosomes (S/B) segregate equally with the MSP (S/B, Sym), where one X chromosome is of sister chromatids (yellow arrow). And, symmetric distribution of MSP (S/S, Sym) with equal segregation of X chromosomes (single chromatids). **(D)** when 3X lagging-X chromosomes observed MSP distribution in anaphase II was symmetric. Three small DAPI signal of X chromosomes from single chromatids (red arrow) segregate in a way where two chromosomes segregate to one cell, and one chromosome segregate to the other, while MSP segregates symmetrically (s/s/s, Sym). In other scenarios (S/B/S. Sym), one of the two X chromosomes moving together to one cell is from two sister chromatids with a bigger DAPI signal (yellow arrow). **(D)** 4X lagging-X chromosomes during the second anaphase of *Arh-mas-1* spermatogenesis suggest unequal distribution of X chromosomes in anaphase I, where all X chromosomes segregate to only one secondary spermatocyte. **(F)** In anaphase II, partitioning MSP either segregate asymmetrically with the cell inheriting lagging-X chromosomes (big DAPI surface area) or distribute symmetrically to both spermatids. In the event of asymmetric segregation (Asym), MSP segregates to the future sperm, while tubulin segregates to the cell with a smaller DAPI surface area (nullo-X cell). However, in the event of symmetric segregation (Sym), both MSP and tubulin segregate symmetrically to both spermatids. There are cases when tubulin in symmetric segregation (Sym, CRB) was discarded in a central region, suggesting the formation of a residual body. However, it is not clear if those sperms segregate fully and become functional sperm.

3.3.6. Staining using mitochondria antibody (ATPB) revealed that mitochondria either segregate equally or asymmetrically to the cell with more DNA

Mitochondria during *Arh-mas-1* spermatocytes meiosis were labeled using antibodies against mitochondrial ATP synthase beta subunit (ATPB) to track the pattern of mitochondria segregation [120, 121]. In the first anaphase of *Arh-mas-1* male spermatogenesis mitochondria segregated symmetrically to both daughter secondary spermatocytes. However, during the second anaphase, mitochondria either segregated in a unipolar or bipolar pattern. In the event of unipolar segregation, mitochondria segregate with the cell that has more DNA mass, the cell that inherited lagging-X chromosome, meanwhile, the cell with smaller DNA mass, nullo-X cell, does not inherit any mitochondria and take the role of a residual body with DNA (Figure 3.13).

During the second anaphase, X chromosomes lag in 1X, 2X, or 3X variations similar to the variations observed in MSP/tubulin antibody staining. In the 1X variation, X chromosome lags from one of the two dividing nuclei. Later, mitochondria segregate exclusively to the cell with the lagging-X (more significant DNA mass), and the sister cell with smaller DNA mass behaves like a residual body with DNA. In the 2X variation, lagging X either segregate symmetrically to both cells resulting in bipolar segregation of mitochondria to both future cells or sometimes both lagging X chromosomes segregate together, resulting in unipolar segregation of mitochondria to only the cell inheriting both lagging-X chromosomes and the other cell becomes a residual body with DNA. In the 3X variation, mitochondria segregate symmetrically to both daughter cells, where two X chromosome lag from one dividing nucleus and one X chromosome lags from the other nucleus (Figure 3.13).

Immunostaining analysis using antibodies against mitochondrial (ATPB), MSP, and tubulin combined with DAPI staining of chromosomes illustrated that masculinisers pseudo-males either produce single X-bearing sperm, duplo-X sperms, nullo-X sperms and sperms with X chromosome polyploidy (Figure 3.13).

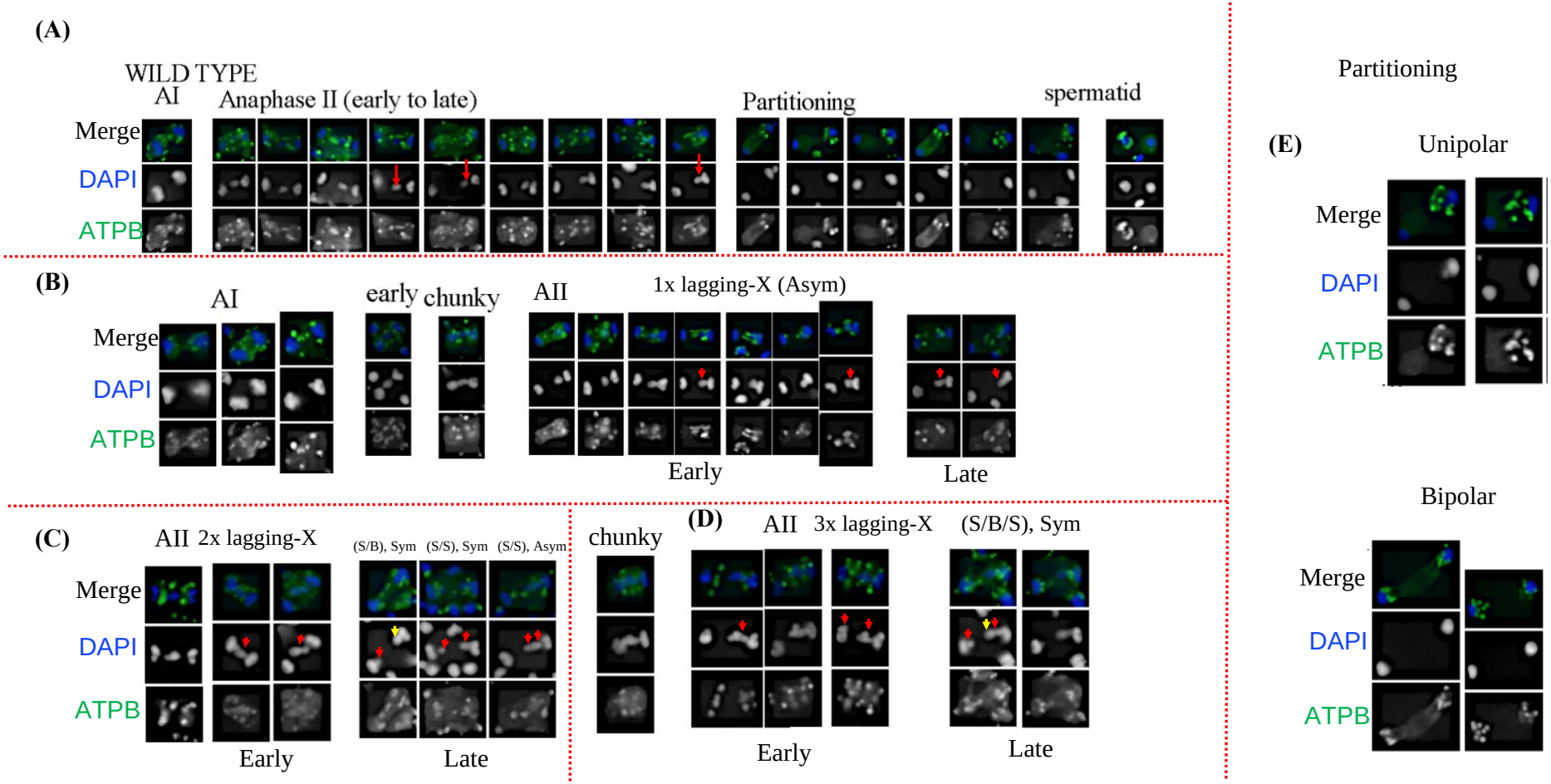

Abbreviations; (AI) first anaphase, (AII) second anaphase, (S) small DAPI surface area, (B) big DAPI surface area, (Sym) symmetric, (Asym) asymmetric and (Chunky) lagging-X is observed but no segregation of mitochondria yet.

Figure 3.13: Mitochondria in masculinisers male anaphase II segregate either symmetrically or asymmetrically to the cell with the more significant DNA mass.

(A) Mitochondria stained with antibody against ATP synthase beta subunit (ATPB) (green) and DNA staining using (DAPI) (blue) in *A. rhodensis* wild type male spermatogenesis. The single unpaired X chromosomes lag (red arrow) during the second anaphase. Mitochondria segregate exclusively to the cell that inherits the X chromosome (bigger DNA mass), resulting in the production of X-bearing spermatid and a residual body with DNA. **(B)** In *Arh-mas-1* pseudo-male spermatogenesis, mitochondria during anaphase I segregate symmetrically to both secondary spermatocytes. However, in the second anaphase, mitochondria segregate exclusively to one daughter cell. A lagging-X chromosome is observed (red arrow) during the second anaphase, and mitochondria segregate with the lagging-X chromosome. **(C)** 2X lagging-X chromosomes are also observed in masculinisers second anaphase. 2X lagging-X chromosomes either segregate equally to both daughter cells with mitochondria segregating symmetrically (S/B, Sym) (S/S, Sym), or both X chromosomes segregate together to one cell with mitochondria segregating asymmetrically with the X (S/S, Asym). The structure of lagging-X chromosomes is determined from the surface area of the DAPI signal, the small surface area represents a chromosome of a single chromatid (red arrow), and a large surface area represents a chromosome of two sister chromatids (yellow arrow). **(D)** 3X lagging-X chromosomes are also observed in *Arh-mas-1* male anaphase II. Where, 2X lagging-X chromosomes segregate to one daughter cell, while 1x lagging-X chromosome segregates to the second daughter cell. Mitochondria segregate symmetrically to both daughter cells in the event of 3X lagging-X chromosomes. Overall, mitochondria in *Arh-mas-1* spermatogenesis either segregate symmetrically to both spermatids **(E)** or asymmetrically to the daughter cell with larger DNA mass because of X chromosomes inheritance.

3.4. Conclusion

Masculinisers recovered from EMS mutagenesis are genetically XX individuals; however, they have the morphology of a male. Masculinisers can be distinguished from wildtype males during the late adult stage by dark gut pigmentation (Figure 3.4). In this study, the *Arh-mas-1* phenotype itself was not thoroughly investigated since the aim of the study is to determine if the X chromosome is a polarising signal during XX spermatocyte spermatogenesis. Nile red was used to investigate those dark patches as potential fat storage, but no clear difference was shown between wildtype males and masculinisers [122, 123]. Another reason for the presence of dark patches could be the production of vitellogenin, a precursor for yolk proteins; however, masculinisers were not tested for the production of vitellogenin proteins. Production of vitellogenin protein can be investigated directly by amplifying *vitelogenin*-1(*vit-1*) RNA by standard PCR from masculinisers cDNA [124, 125].

Sexing and genotyping of masculinisers progeny indicates that *Arh-mas-1* generally produces X-bearing oocytes and a low percentage of nullo-X sperms. Genotyping results did not illustrate the production of diplo-X sperm by masculinisers as we expected to observe XX animals with only APS4 marker (Figure 3.10). All genotyped XX *Arh-mas-1* progeny were heterozygote, no APS4 homozygous for the X were observed probably due to the small sample size of genotyped XX individuals. So far, there is no genetic evidence illustrating the production of diplo-X sperm by masculinisers apart from the short and fat triploid-X animals recovered from masculinisers cross with APS4 females. I tried to karyotype those triploid-X animals using single animal karyotyping by quantitative RT-PCR of X-linked *XOL-1* genes [126, 127]. Since males contain a single X chromosome and females/hermaphrodites contains two X chromosomes they will be a good control to determine that the short and fat individuals are triploid-X individuals, as the average cycle threshold (Ct) value expected to double for XX individuals from the value of males and triple for triploid-X individuals. However, it was hard to obtain conclusive results due to the small amount of DNA contained in a single animal. Production of diplo-X sperms was evident in immunostaining data, wherein *Arh-mas-1* anaphase II 2X lagging-X

chromosomes observed to segregate exclusively with mitochondria and MSP to one daughter cell.

During spermatogenesis of *Arh-mas-1* male, MSP and mitochondria in anaphase II either segregate symmetrically or asymmetrically to the cell that inherits X chromosomes. In the event of asymmetric segregation, mitochondria and MSP segregate to the cell with the bigger DNA mass due to its inheritance of X chromosomes. Different patterns of lagging-X chromosomes observed in *Arh-mas-1* anaphase II including, 1X, 2X, 3X, and 4X lagging-X chromosomes (Figure 3.12) (Figure 3.13). The pattern of lagging-X chromosomes observed in the second anaphase is dependent on the way unpaired X chromosomes segregate in the first anaphase (Figure 3.14). Sperm components in the first meiotic division segregate symmetrically irrespective of the X chromosomes segregation, as in all other examples of *A. rhodensis* spermatogenesis. Segregation of the X chromosome in the first anaphase does not follow a single uniform pattern. In the first anaphase unpaired X chromosomes may split and segregate equally, or segregate to both poles as a whole without splitting. They may all segregate together to only one secondary spermatocyte, or one X segregates exclusively to one cell and the other splits to segregate equally to both cells, whereby one secondary spermatocyte will inherit one X chromosome, and the other will inherit 3 X chromosomes (Figure 3.14). Unequal segregation of X chromosomes in the first anaphase is manifested by the difference in surface area of DAPI staining between secondary spermatocytes nuclei (Figure 3.12). Multiple patterns of X chromosome segregations are also expected in anaphase II depending on the number and structure of X chromosomes inherited from the first meiotic division (Figure 3.14).

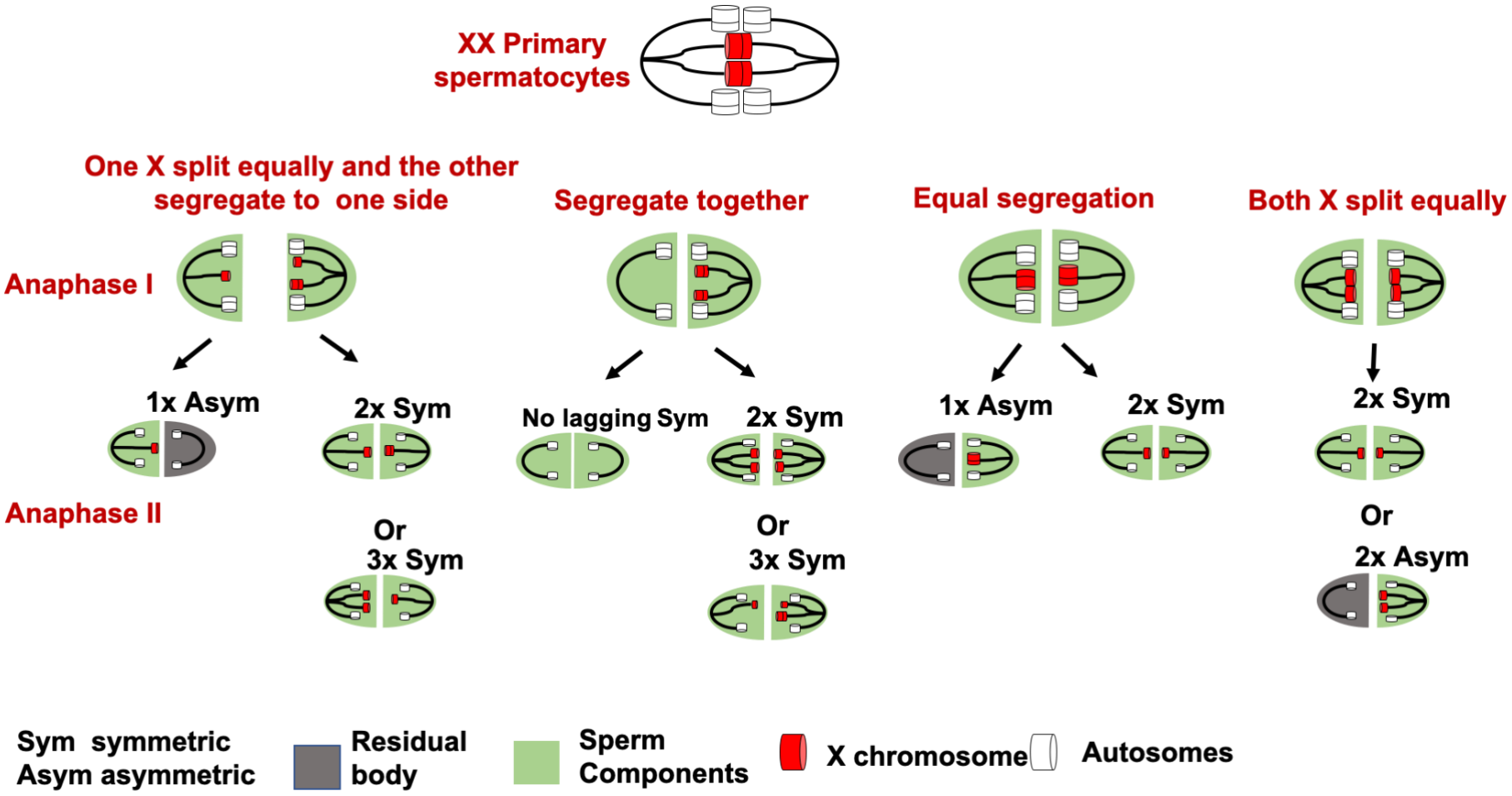
XX Primary spermatocytes
One X split equally and the other segregate to one side
Segregate together
Equal segregation
Both X split equally
Anaphase I
1x Asym
2x Sym
Anaphase II
Or
3x Sym
No lagging Sym
2x Sym
Or
3x Sym
1x Asym
2x Sym
2x Sym
Or
2x Asym
Sym symmetric
Asym asymmetric
Residual body
Sperm Components
X chromosome
Autosomes

Figure 3.14: Expected patterns of X chromosome segregation during masculinisers spermatogenesis.
In the first anaphase, unpaired X chromosomes may split and segregate equally, or segregate equally without splitting. They may segregate together to only one secondary spermatocyte, or one X segregates exclusively to one cell and the other splits to segregate equally to both cells, whereby one secondary spermatocyte will inherit one X chromosome, and the other will inherit 3 X chromosomes. According to the number and the structure of X chromosomes inherited in each secondary spermatocyte, different scenarios of X chromosomes segregation patterns are expected.

Genetics and cytological studies revealed that masculinisers produce X-bearing, duplo-X, and nullo-X sperms. Anaphase II in *Arh-mas-1* spermatogenesis exhibits different segregation patterns than expected, depending on the number and structure of X chromosomes inherited from the first meiosis. X chromosomes either segregate exclusively to one spermatid with sperm components or segregate to both spermatids, while sperm components segregate equally (Figure 3.15). In anaphase II, 4X lagging-X chromosomes were observed, suggesting unequal segregation of X chromosomes in anaphase I, where X chromosomes segregate to only one secondary spermatocyte. Nullo-X sperm is expected to originate from symmetrically dividing secondary spermatocyte without X chromosomes. Further research is required to determine the exact pattern of X chromosome segregation as multiple segregation patterns are expected. Future research will include the use of fluorescent in situ hybridisation (FISH) against the X chromosomes to track the pattern of its segregation during spermatogenesis. However, irrespective of the pattern of X chromosome segregation, this study concludes that the X chromosome is a polarising signal in *Arh-mas-1* spermatogenesis since in the event of asymmetric segregation sperm components segregate with the lagging-X chromosomes to the spermatid with the larger DNA mass. At the same time, the other sister nullo-X cell behaves as a residual and inherits tubulin (Figure 3.15).

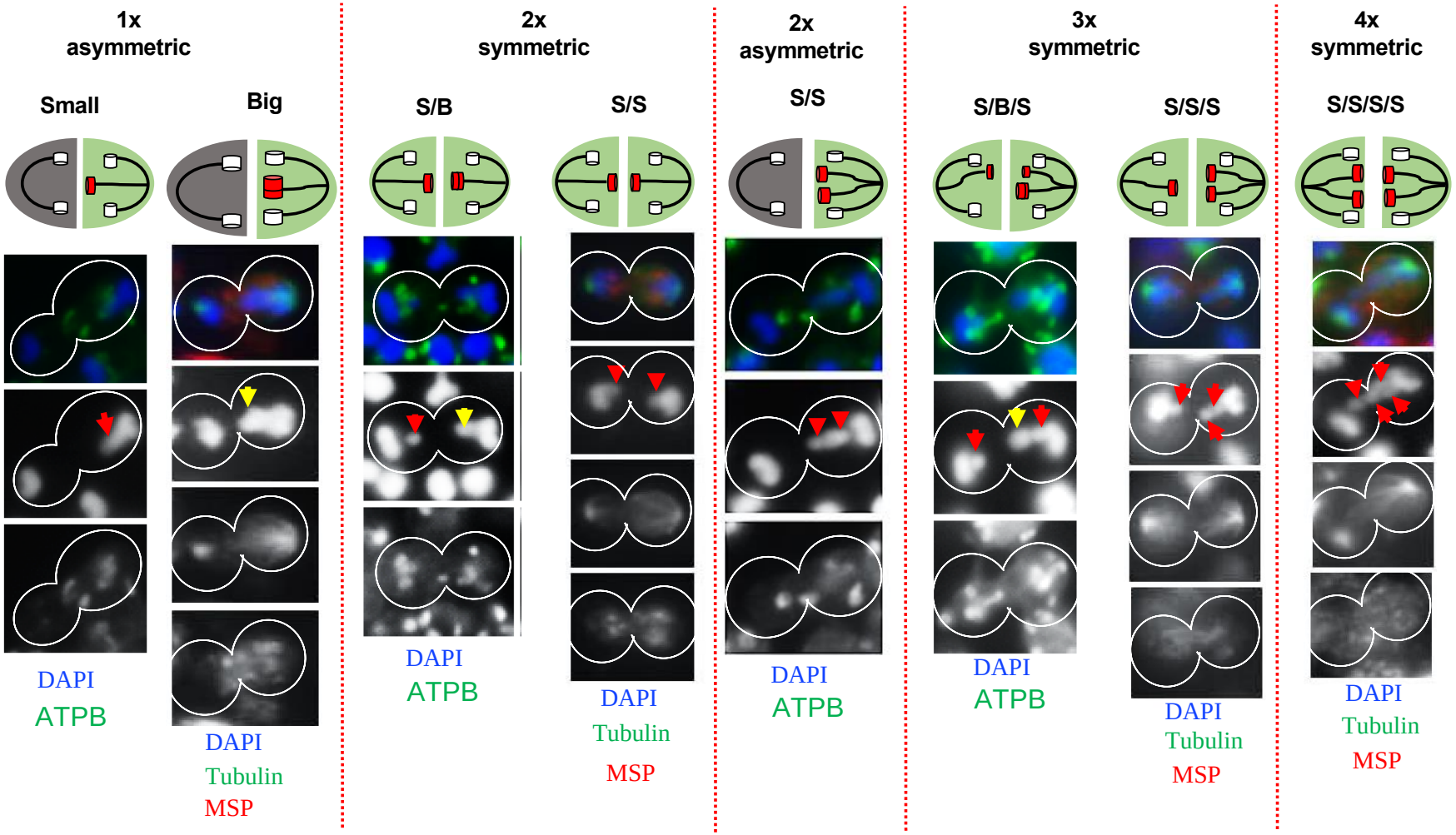
1x
asymmetric
Small
Big
DAPI
ATPB
DAPI
Tubulin
MSP
2x
symmetric
S/B
S/S
DAPI
ATPB
DAPI
Tubulin
MSP
2x
asymmetric
S/S
DAPI
ATPB
3x
symmetric
S/B/S
S/S/S
DAPI
ATPB
DAPI
Tubulin
MSP
4x
symmetric
S/S/S/S
DAPI
Tubulin
MSP

Figure 3.15: Variations of lagging-X chromosomes segregation in anaphase II of *Arh-mas-1* spermatogenesis.
Multiple patterns of lagging-X chromosomes segregation observed during masculinisers spermatogenesis. Numbers and patterns of lagging-X chromosomes in anaphase II depends on the numbers and structure of X chromosomes inherited in each secondary spermatocyte. In the event of asymmetric division, sperm components segregate with the lagging-X chromosomes to the spermatid with the more significant DAPI surface area. Red arrow indicates a lagging-X chromosome from a single chromatid because of its smaller DAPI surface area, while the yellow arrow indicates a lagging-X chromosome from two sister chromatids with a bigger DNA mass represented by DAPI surface area.

Chapter 4

Identifying genomic region regulating X chromosome and sperm components segregation in *A. freiburgensis*.

Summary:

This chapter reports the mapping of 4 QTLs on the X chromosome in *A. freiburgensis* that are associated with an asymmetric cell division. During this process, the X chromosome acts as a cue to polarise the cytoploplasm of the dividing cell. To identify the underlying QTLs, I generated Recombinant Inbred Advanced Intercross Lines (RIAILs). Hybrid *A. freiburgensis* strains from two polymorphic strains resulted in a new transgressive phenotype in some RIAILs, in which they produced a high number of males. The DNA from each RIAIL was extracted and pooled into two bulks, one with normal proportion of males (<20%) and other with high number of males (>20%). Bulk segregant analysis BSA identified the underlying QTLs located on the X chromosome.

4.1. Introduction:

4.1.1. Recombinant inbred lines (RILs) are a powerful tool for genetic mapping

Correlating phenotypes with genotypes is the basis of genetics. Mapping allelic variants associated with traits is achieved through the generation of recombinant inbred lines (RILs). Recombinant inbred lines (RILs) are created by crossing two polymorphic strains, followed by sibling mating or selfing for several generations [128-130]. At the end of the breeding scheme, each RIL genome will be a mosaic shuffle of parental strains genome due to meiotic recombination [131]. Recombinant lines inbred to isogeny are homozygous at all loci and can be maintained separately [131]. Genetic mapping using recombinant inbred lines has

many advantages: 1) From the same set of genomes, multiple different phenotypes can be obtained. 2) RILs and parents' genome genotyping is carried out against the same reference. 3) Sufficient mapping resolution can be obtained from RILs, since meiotic recombination in RILs generates more significant haplotype breakpoints than those taking place in any single meiosis [128]. Genetically distinct RILs either exhibit quantitatively varying phenotypes derived from parental strains or in rare cases a new extreme phenotype (transgression) may form, due to shuffling of a linked group of polygenes, as a result of RILs genome dense breakpoints introduced through recombination [131, 132]. Polygenes are a group of genes that interact together in an epistatic interaction to influence a phenotypic trait, examples of polygenetic inheritance in human includes skin colour, height, weight and eye colour [133]. When a group of a linked polygenes are disrupted and shuffled due to RILs genome dense breakpoints, a new transgressive phenotype appears in some of the RILs that is not in the original parents used to establish the lines [133]

RILs phenotype can be mapped to their causative loci, referred to as quantitative trait loci (QTL). The mapping of a QTL depends on genotyped markers being located near the causative loci [131]. Genotyped markers and underlying QTL have to be in a linkage disequilibrium (LD) showing a non-random association with the underlying phenotype [131, 134]. Increasing RILs genome breakpoints by meiotic recombination increases the chance of genotyping a marker near the underlying QTL [133]. There are two techniques predominantly used to increase the number of meiotic recombination. The first technique simply increases the amount of derived F2 individuals, each with unique recombination [135]. In the second approach the number of meiosis is increased per individual to increase mapping resolution [135]. The number of haplotype breakpoints can be accumulated by allowing sibling mating in the F2 progeny of two polymorphic parents and promoting lines intercross for successive generations before selfing [136]. This advanced form of highly recombinant inbred lines is called Recombinant Inbred Advanced Intercross Lines (RIAIL) (Figure 4.1 and 4.2)[135].

4.1.2. *A. freiburgensis* Recombinant Inbred Advanced Intercross Lines (RIAILs) design and construction

A. freiburgensis, as *c. elegans*, exhibits certain features that render it a good model for the construction of recombinant inbred lines [137]. It is free-living species, produces plenty of progeny, and has a short life cycle [69]. *A. freiburgensis* reproduces in two ways: by hermaphrodite self-fertilisation, and males outcrossing with females or hermaphrodites. By mating males with females, recombination events are generated and can be brought to homozygosity by letting the hermaphrodites to inbreed by self-fertilisation. *c. elegans* chromosome undergoes a single recombination event per meiosis [138-140]. Assuming *A. freiburgensis* is similar, recombinant inbred lines (RILs) derived from F2 progeny of polymorphic parents will contain few recombinant breakpoints per chromosome, making it challenging to introduce haplotype breakpoints near the underlying QTL.Moreover, the X chromosome of closely related *A. rhodensis* species does not recombine in hermaphrodites [15]. Therefore there is a high chance it also does not recombine in *A. freiburgensis* hermaphrodites [83]. Inbreeding *A. freiburgensis* recombinant lines from the F2 generation by hermaphrodite selfing will have a significant flaw, because the X chromosome might not contain any haplotype breakpoints. Hybrid RILs derived from polymorphic strains were heterozygous for all X chromosome markers, indicating that the X chromosome does not recombine in *A. rhodensis* hermaphrodites [83].

RIAILs were generated using two *A. freiburgensis* polymorphic strains. We used *A. freiburgensis* instead of *A. rhodensis* because in preliminary studies we did not manage to generate *A. rhodensis* RILs with a transgressive phenotype (lines with high production of males). However, RILs generated in *A. freiburgensis* resulted in lines that have a high proportion of males (Adams, S. personal communication). These RILs were derived from *A. freiburgensis* APS14 and APS7 strains, which were crossed in both directions. F1 hermaphrodites resulting from both crosses were isolated to produce F2 hermaphrodites. Then, F2 hermaphrodites were used to establish the lines by single nematode descent (SWD). 5 lines from a total of 30 F2-derived RILs (approx. 16.6%) produced a high number of males. Moreover, males from those lines also produced a high

number of males after an outcross. Therefore, to improve the genetic map in *A. freiburgensis*, lines from the F2 were crossed for successive generations before being inbred by selfing to produce Recombinant Inbred Advanced Intercross Lines (RIAILs).

Initially, *A. freiburgensis* APS14 female was crossed with APS7 male to establish the recombinant lines. The Breeding design involved an inbreeding avoidance (IA-RIAILs) crossing scheme from F2 to the F7 generation to avoid consanguineous mating [141, 142]. Every two lines derived from unique F2 recombination were only crossed once during the crossing scheme to maximise meiosis breakpoints (Figure 4.1) [135, 141]. Then, hermaphrodite selfing by SWD for ten generations brought all introduced haplotype breakpoints during the crossing scheme into homozygosity (Figure 4.1).

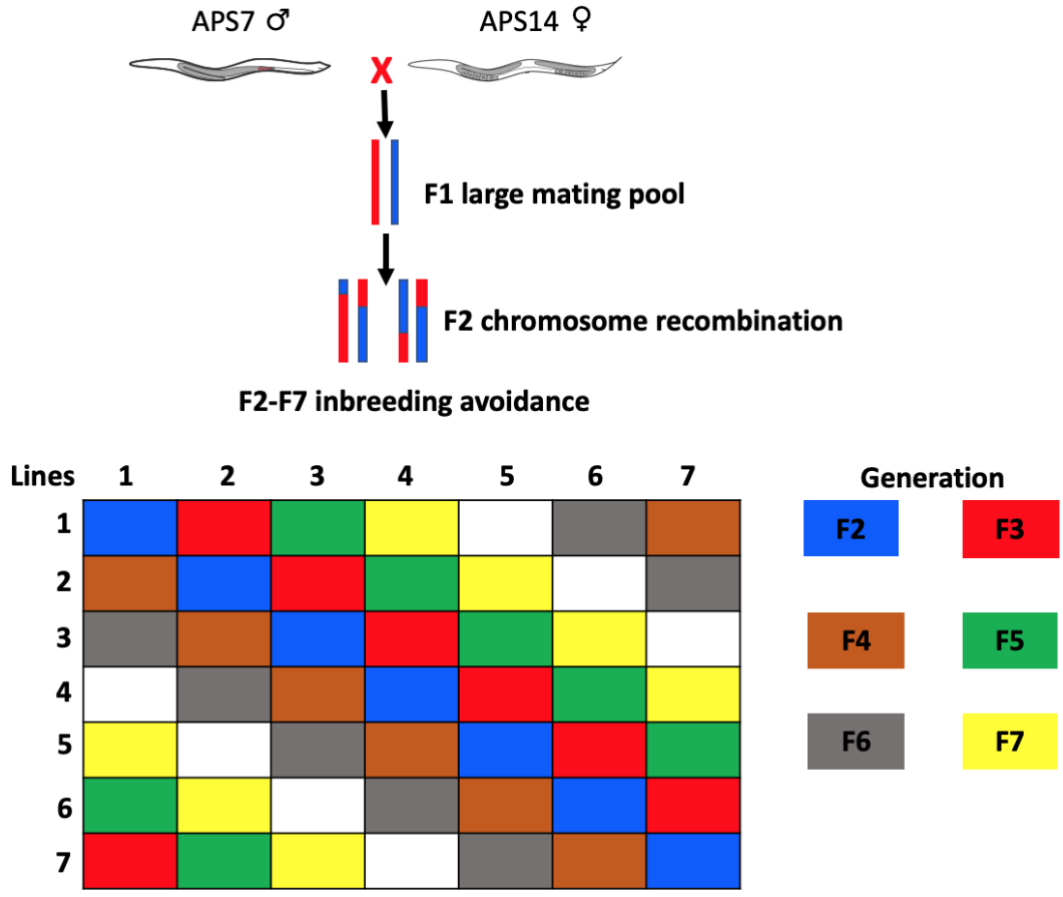

Figure 4.1: Inbreeding avoidance recombinant inbred advanced intercross lines (IA-RIAILs) designed for *A. freiburgensis*.
IA-RIAILs were designed in a way to maximise haplotype breakpoints and to avoid consanguineous mating. Every two lines were only crossed once during the 7th generation crossing scheme. A colored grid was made to ensure lines inbreeding avoidance. Each color corresponds to a generation from F2 to F7.

A. freiburgensis RIAILs were constructed to determine if a group of linked polygenes mosaic shuffling from two different parental genomes will give rise to a new extreme phenotype (transgression). Generation of genetic variations via independent assortments of entire chromosomes and meiotic recombination are a driving force for speciation, adaptation, and selection [143, 144]. Meiotic recombination enables the creation of unique haplotypes through crossovers and gene conversion at many sites along the chromosome [145]. However, the distribution of meiotic recombination across the genome is not consistent in many organisms [108, 144, 146]. As a result, over an evolutionary period, favourable polygenes are maintained on genomic regions with a low rate of recombination [144]. Epistatic interactions between loci within species maintain genetic variations, and disruption of this epistasis leads to the development of an extreme phenotype [147]. A group of polygenes epistatic interactions across different loci can be shuffled by the accumulation of meiotic recombination leading to the development of a novel phenotype or transgression [132, 147]. The generation of extreme phenotype from segregating hybrid population is defined as transgressive segregation [148]. This segregation is a fundamental mechanism through which novel adaptive phenotype develops, and speciation thought to arise [148].

Generation of IA-RIAILs will increase recombination between homologs chromosomes from two *A. freiburgensis* strains with different genetic backgrounds; as a result, crossovers will accumulate over a relatively short period. I expected that producing *A. freiburgensis* RIAILs by mixing two strains (APS14 and APS7) from different genetic backgrounds will give rise to lines where males produce a high number of males after an outcross. In wildtype *A. freiburgensis* male, I expect that asymmetric segregation of cytoplasmic components exclusively with the X chromosome in anaphase II to produce only X-bearing sperm is maintained via an epistatic interaction between a group of linked polygenes. Therefore, I hypothesise that the mosaic shuffle from the two different parental genomes in RIAILs, will disrupt the epistatic interaction that maintenance asymmetric segregation, leading to the production of a high number of males in some RIAILs. Spermatogenesis in males from those RIAILs are

capable of producing a functional nullo-X sperm, resulting in the production of a high number of males after an outcross.

The novelty of *A. freiburgensis* as a model system enables the identification of the type of divisions occurring in males' germline through broad count after an outcross with a wt female. Indeed, 65% of the 110 generated RIAILs produced a high number of males (Figure 4.3). Males from lines producing a high number of males also produced a high number of males when crossed with a wildtype female, indicating their ability to create a functional nullo-X sperm. Genotyping of RIAILs will enable correlating observed phenotypes with the underlying candidate trait loci (QTLs) responsible for the observed phenotype.

4.1.4. Bulk Segregant Analysis (BSA) is an elegant strategy to identify QTLs linked to a phenotype of interest

Bulk segregant analysis (BSA) is a simplified alternative to the conventional QTL mapping used to identify molecular markers closely associated with genes [133, 149-153]. After assessing the degree of expression of a phenotype of interest in a segregating population, individuals with extreme contrasting phenotypes bulked into two groups. DNA from individuals constituting each contrasting bulk is extracted separately, then pooled equally into a DNA sample corresponding to each bulk [151-154]. The fast development of Next Generation Sequencing (NGS) – NGS-BSA based strategies accelerated the process of identifying quantitative genes in plants [149, 151, 152, 155]. NGS-BSA based approach has also been used successfully to identify complex traits in *c. elegans* [133, 156, 157]. In the BSA approach, QTLs are generally identified by comparing allele frequencies between the two genotyped bulks [133, 150]. BSA-QTL analysis of *A. freiburgensis* RIAILs identified 4 QTLs located on the X chromosome that are in involved in X chromosome segregation and subsequent spatial localisation of sperm components. QTLs were identified using two methods; QTL-seq approach and The G' approach.

QTL-seq

Takagi et al. (2013) developed a pipeline to identify quantitative trait loci in rice [150]. Takagi et al. (2013) suggests that in each bulk equal contribution of both

parental genomes is expected in most of the genomic regions in a 1:1 ratio. However, unequal representation of genome from both parents will indicate genomic regions containing QTLs for the contrasting phenotype. The contribution of genomic reads from both parents in each bulk can be estimated through discriminating short reads corresponding to each parent through single nucleotide polymorphism (SNPs). Sequenced short reads from each bulk are aligned against a reference genome of one of the two parents. Subsequently, the number of reads containing SNPs (alternate allele) was counted from the total number of reads, and their ratio was determined. The ratio of those SNPs containing reads from the total number of reads at a specific genomic position is defined as SNP-Index.

SNP-Index = alternate allele depth / total read depth

At a specific genomic region, SNP-index of 0 indicates that reads at that position are from the parent that was used as a reference genome for genotyping contrasting bulks. SNP-Index of 1 indicates that all the reads are from the other parent. A SNP index of 0.5 indicates an equal contribution of reads from both parents. In practice, a SNP index is calculated for all the SNPs detected in each genotyped bulk. The relationship between SNP-Index and SNP position is represented in a graphic plot. To simplify the visualisation a sliding window analysis is applied by averaging SNP-indices of a number of SNPs located within a determined genomic interval (tricubed-smoothed SNP-index). The graphs for both contrasting phenotypes are expected to be similar across genomic regions that are not contributing to the difference of phenotype between the two bulks. However, in the genomic areas harbouring QTL underlying the contrasting phenotype unequal representation of the parental genome will be observed in both bulks. Therefore, graphs from both bulks with contrasting phenotypes are combined to determine the QTL region by subtracting SNP-index values at each SNP position of one bulk from the other to produce a delta-SNP graph. In this graph, Delta-SNP index of 0 represents equal contribution of genomic reads from both parents (e.g., A and B), delta-SNP index of 1 represents that bulked DNA on that genomic location is derived from parent A, and delta-SNP of -1 indicates that reads are contributed from only parent B [150].

G' analysis

An alternative approach developed by Magwene et al. (2011), based on G-statistic, was conducted to identify QTLs associated with the asymmetric segregation of X chromosome and spatial localization of sperm components. After the preparation of DNA pools from contrasting bulks, SNPs from both bulks were genotyped at each position with an average coverage of C. The data for each SNP can be summarized in a 2X2 table (Table 4.1). A_1 is the allele from parent used as a reference genome, A_0 is the corresponding allele from the other parent, and n_i represents the count of both parents allele after genotyping each bulk.

Table 4.1: Coverage at an individual SNP.

	High bulk	**Low Bulk**	**Total**
A_1	n_1	n_2	$n_1 + n_2$
A_0	n_3	n_4	$n_3 + n_4$
Total	$n_1 + n_3$	$n_2 + n_4$	

In most genomic regions that do not affect the contrasting phenotype observed allele frequency for A_0 in the high bulk $P_1 = n_3 / (n_1 + n_3)$ will be equal to observed allele frequency for A_0 in low bulk $P_2 = n_4 / (n_2 + n_4)$. However, in genomic regions harbouring QTLs that affect the phenotype $P_1 > P_2$, where an allele from one parent will be overrepresented in that region. The following equation characterises G-statistic at each SNP:

$$G = 2 \times \sum n_i \times ln(\frac{observed\ (ni)}{expected\ (ni)})$$

For each SNP, n_i from i = 1 to 4 correspond to the reference and alternative allele depth for each bulk and *observed (ni)* correspond to the allele depth as reported for each SNP.

$$E(x)\ (n_1) = \frac{(n1 + n2)*(n1+n3)}{(n1+n2+n3+n4)}$$

$$E(x)\ (n_2) = \frac{(n2 + n1)*(n2+n4)}{(n1+n2+n3+n4)}$$

$$E(x)\ (n_3) = \frac{(n3+n1)*(n3+n4)}{(n1+n2+n3+n4)}$$

$$E(x)\ (n_4) = \frac{(n4+n2)*(n4+n2)}{(n1+n2+n3+n4)}$$

G value for each SNP is calculated from expected values with the notion that alleles read depth is equal in both bulks. The null hypothesis is that the investigated SNP is not associated with a QTL region. Moreover, if we hypothesise an equal average sequencing coverage of both bulks, then $E(n_1)=E(n_2)=E(n_3)=E(n_4)=C/2$. If sequencing coverage of both bulks at a particular SNP is not equal, the allele from one parent is over-represented, then the null hypothesis will be rejected, and that SNP might be significant for the underlying QTL. To help simplify the visualisation of G value on a graph across the entire genome, G' A smoothed version of G value is calculated by averaging G values of neighbouring SNPs depending on the suggested window size. From the null distribution of the G' that assumes no QTL, p-values can be estimated. Mean and variance of the G' null distribution is estimated, then p-values are calculated.

A. freiburgensis RIAILs construction and subsequent BSA analysis led to the discovery of 4 QTLs located on the X chromosome associated with X chromosome segregation and cytoplasm spatial localization in *A. freiburgensis* male spermatogenesis. In this chapter, First, I will outline the results of RIAILs construction and phenotype characterization of RIAILs. Then, I will present the BSA analysis and QTLs located on the X chromosome associated with the observed transgressive phenotype. Finally, I will discuss genes within identified QTLs that might have a direct role in X chromosome co-segregation with sperm components.

4.2. Materials and Methods

4.2.1. Producing *A. freiburgensis* Recombinant Inbred Advanced Intercross Lines (RIAILs)

Recombinant inbred advanced intercrosses lines (RIAILs) were generated in *A. freiburgensis* by crossing APS7 male with polymorphic strain APS14 female. Hybrid F1s progeny resulting from the cross was left to mate in a large mating pool. F1 self-producing hermaphrodites and females, each have mated with one or more males, were isolated to a separate plate each to establish 110 lines. 3-5 F2 females were picked from each line and crossed with two males from a different line, in an inbreeding avoidance scheme. Inter-crosses between lines from F2 to F7 was established in a way where every two lines were only crossed once to maximise haplotype breakpoints. After seven generations of crosses, lines were inbred by single worm descent for ten generations to bring all the alleles into homozygosity at all loci. Once the 17th generation was reached, lines were maintained by scooping mixed animals from a crowded plate to a fresh new plate once a month, at this point each line is homozygous at each locus.

4.2.2. Freezing *A. freiburgensis* Recombinant Inbred Advanced Inter-crosses Lines

The freezing protocol explained in section 2.2.8. Lines were frozen in liquid nitrogen to be recovered if lost in the future. Each line was frozen in triplicate tubes. Tubes were then placed inside a styrofoam box and put inside -80 incubator, left overnight to help freezing nematodes slowly. Then tubes were moved to the final liquid nitrogen storage.

4.2.3. Crossing males from *A. freiburgensis* Recombinant Inbred Advanced Intercross Lines (RIAILs) with wild type females

In each cross, a male from each line was crossed with a wild type APS7 female for ~24h. After the cross, males were isolated and incinerated. The gravid female was moved to a new plate every day until they stopped laying eggs, in order to synchronize the growth of the F1 progeny. Ratios of male to female progeny were scored for each cross.

4.2.4. DNA Extraction from *A. freiburgensis* Recombinant Inbred Advanced Inter-crosses Lines (RIAILs)

Washing plates

Nematodes were harvested from non-starved plates right after the bacteria has been consumed with M9 or water from five 10 cm plates for each line. Nematodes from all stages were washed and collected in a 50ml conical tube. Nematodes were washed two times, then mixed gently for 1 hour on a roller to introduce starvation. Starving nematodes will help clean them from bacteria that reside in their gut. Then, nematodes were washed 2-3 times with water. After each wash, nematodes were let to settle to the bottom of the tube rather than centrifuging. Nematodes are generally heavier than bacteria so that they will settle at the bottom of the tube faster. The supernatant containing bacteria was discarded after each wash. Nematodes were pelleted by centrifuging to maximum speed, and excess water was removed. Pellet was separated into two 1.5 ml Eppendorf or more depending on the size of the pellet. 500 µl of lab-made lysis buffer was added. Lab-made lysis buffer contains; 100 mM Tris (pH 8.5), 100 mM NaCl, 50 mM EDTA, 1% SDS and 1% beta-Mercaptoethanol added fresh to the lysis mix before each extraction. Tubes were then frozen in -80 overnight.

RIAILs DNA extraction

The frozen pellet was allowed to thaw at room temperature then frozen again instantly using liquid nitrogen or dry ice. This repeated cycle of thawing and freezing was repeated three times to allow the physical break of nematodes cuticle. 2.5 µl of proteinase K (20mg/ml) was added to each tube. Tubes were incubated at 65 °C for 3-4 hours. Tubes were centrifuged at maximum speed for 5 minutes to pellet protein and large debris at the bottom of the tube. The supernatant containing DNA was moved to a fresh new tube. Tubes were cooled by incubating on ice for 5 minutes. Then 170 µl of protein precipitation solution from Gentra Puregene Core kit A provided by Qiagen was added. Tubes were inverted 50 times and incubated on ice for 10 minutes. Tubes were centrifuged at maximum speed for 2 minutes, then incubated on the ice again for 10 minutes, and the centrifuging step was repeated. The supernatant was moved to a fresh new

tube, being careful not to disrupt the pellet. Tubes were then centrifuged again to pellet any carried over protein, and the supernatant was moved to a fresh tube.

Alcohol precipitation

500µl of isopropanol and 100 µl (1/10) volume of 3M NaAC was added. Tubes were inverted 50 times to mix and incubated in ice for 15 minutes. Then centrifuged at maximum speed for 10 minutes to pellet the nucleic acid. The supernatant was discarded, and the nucleic acid pellet was washed in 400µl of 70% ethanol. Tubes were centrifuged at maximum speed for 5 minutes, and the supernatant was discarded. The nucleic acid pellet was left to dry at room temperature. 100 µl of 10 mM Tris-HCl (pH 8.0) added to dissolve the DNA pellet at 4C overnight.

RNase treatment

0.5 µl of RNase was added to each tube and incubated in a heat block at 37 C with shaking (700 rpm) for 1 hour. RNA from samples was cleaned using Zymo research genomic DNA, and a concentrator kit. For 100 µl of DNA, 4000 µl of chip DNA binding buffer was added. A mixture of DNA and chip DNA binding buffer was added to the spin column. Spin columns were centrifuged for 30 s and flow-through was discarded. 200µl of DNA wash buffer was added to the column and centrifuged for 1 minute. The wash step was repeated. Finally, 100 µl of 10 mM Tris-HCl (pH 8.0) added to elute DNA. Spin columns were incubated for 3 minutes at room temperature before centrifuging for one minute. Finally, the quality of the DNA was examined by running 1 µl of DNA on 1.8 % agarose gel, and concentration was measured using Qubit fluorometer.

4.2.5. Pooling DNA from lines with similar phenotypes into different pools

Genome from the APS14 maternal strain and four DNA Pools were prepared, two pools were from lines producing a high number of males (H-Pools) and two pools from lines producing a low number of males (L-Pools). DNA in each pool was created by mixing equal concentration of DNA from 10 lines with the same phenotype. A volume containing 150 ng of DNA from each line was pipetted into the DNA pool to make up a total of 1.5 µg of DNA in each pool. The quality of

DNA was examined by running 1 µl of DNA on 1.8 % agarose gel, and concentration was measured using Qubit fluorometer.

4.2.6. DNA sequencing

Five DNA samples; 2 H-pools, 2 L-pools, and DNA from APS14 maternal strain, were sequenced. Sequencing libraries were generated using TruSeq DNA nano gel free at the GenePool facility at the University of Edinburgh. The four Pooled DNA samples plus a DNA sample for the APS14 strain were sequenced using the Illumina HiSeq platform to generate 150-bp paired-end reads, with an insert size estimation of 350 bp.

4.2.7. Sequences pre-processing and variant calling

First of all, the quality of the reads was assessed using the FastQC software to have an overview of the reads' quality, contamination, and GC content [158]. From this overview, it was possible to determine the overall quality of the samples, and the overall GC content are reasonably good. Low-quality regions of the reads were trimmed using trimmomatic software (version 0.36) [159]. Paired-end reads were reported in phred33 quality score, and reads were cleaned depending on the following criteria: (1) ILLUMINACLIP, TruSeq3-PE.fa:2:30:10, to cut adapters and other Illumina-specific sequences from the reads. (2) LEADING:3 to cut bases off the start of the read that is below a threshold quality. (3) TRAILING:3 to cut off bases at the end of the reads that are below the threshold quality. (4) SLIDINGWINDOW:4:15 a sliding window trimming, to cut once the average quality within the window falls below the threshold. (5) MINLEN:36 drop the read if it is below a minimum length of 36 base pairs.

The quality of reads was reexamined after cleaning using FastQC software. Then, BWA program was used to align short reads from each pool separately to the APS7, paternal strain, reference genome [160-162]. Alignment files in sam format were converted to bam files using samtools “view” command [160]. Initially, the analysis was conducted using four pools, two H-pool, and two L-pool; this resulted in four comparisons; each reported different numbers of quantitative trait loci (QTLs) [163]. Therefore, both bam files from the H-pools and the L-pools were merged to produce a single bam called Low Bulk (LB) and

High Bulk (HB) respectively, in order to make the analysis more robust and reduce the number of (QTLs), to only the (QTLs) that are shared between the four comparisons.

Bam files were sorted using samtools software command “sort” [160]. Sorted bam files of all pool samples and APS14 parental strain were subjected to variant calling analysis using GATK (Genomic Analysis Toolkit) to call SNPs and small indels [164]. SNPs and small indels across samples and APS14 parental strain were called using GATK “Haplotypecaller" command to produce separate variant calling files (VCF) for each sample [165]. Individual variant calling files (VCF) were merged into one file using GATK "GenotypeGVCFs” command. Joint genotyping using “GenotypeGVCFs" combined all SNPs and indels records from all samples to produce correct genotype likelihood outputting a single combined variant calling file (VCF) [166, 167]. The joint variant calling file (VCF) was converted to a table using "Variant To Table" command provided by the GATK software [168, 169].

4.2.8. Bulk segregate analysis (BSA) and quantitative trait loci (QTLs) identification

Quantitative trait loci responsible for the production of a high number of males were identified with the help of R-package "QTLseqr” [163]. Data from the table produced using GATK "Variant To Table" tool was loaded into R. Imported data were assigned new names, H-pool and L-pool were called high-bulk and low-bulk, respectively. Importing the SNP data into R using "QTLseqr" import function performs primary calculations to identify reference allele frequency, SNP-index per bulk and Δ (SNP-index):

Reference allele frequency = (Ref allele depth$_{HighBulk}$ + Ref allele depth$_{LowBulk}$) / total read depth for both bulks.

SNP-index$_{\text{per bulk}}$ = Alternate allele depth/ total read depth

Δ(SNP-index) = SNP-index$_{HighBulk}$ − SNP-index$_{LowBulk}$

After loading the data into R, the data were cleaned up by filtering out low confidence SNPs. In order to determine filtering threshold, quality of the SNPs were analysed by generating a histogram plot for the following data: (1) depth of the reads of both high-bulk and low-bulk, (2) reference sequence frequency, (3) SNPindex of high bulk and low bulk were evaluated separately.

High quality SNPs were selected and filtered from the data depending on the following parameters: 1) SNPs with reference allele frequency (0.2 <= reference allele frequency <= 0.8), 2) total sample read depth (500 >= total read depth >= 1750), 3) Depth difference between bulks <= 100, 4) filtering by read depth per sample >=40, 5) Filtering by genotype quality >=99.

QTLseq analysis

QTLseq analysis developed by Takagi et al. (2013)[150] for NGS-BSA was used to calculate the allele frequency difference, Δ (SNP-index), from the alleles depth at individual SNP. The method relies on calculating the delta-SNP-index at each SNP between high-bulk and low-bulk, to identify candidate regions, where delta-SNP-index in that region differs from the expected delta-SNP-index of 0. The analysis was conducted using "QTLseq" R package [163] were the following calculations were performed:

1- a sliding window size was set to 1Mbp, and the number of SNPs was counted in that window.

2- Within each sliding window, a tricube-smoothed delta-SNP-index was calculated by constant local regression.

3- For each sliding window, tricube-smoothed depth was calculated, and for each SNP position, the minimum read depth was calculated.

4- A simulation was preformed were the delta-SNP-index per bulk was calculated and simulated over 1000 replications based on RILs F2 population with a bulk size of 20. Confidence intervals were estimated using the quantile from the simulation.

5- At each SNP, the confidence intervals were matched with the corresponding window depth.

G' analysis

An alternative approach developed by Magwene eta al (2011) was used to identify significant QTLs from BSA [154]. Once the analysis was performed using the "QTLseq" R Package, the following steps were undertaken.

1- G statistic was calculated genome-wide, and a tricube-smoothed G statistic (G') was predicted in each sliding window.

2- P values were estimated, Benjamini-Hochberg adjusted p-values, and negative log10- were calculated [170].

Graphs were plotted using functions provided by the "QTLseqr" R package, apart from the SNPindex and deltaSNPindex figures were produced using "ggplot2" R package from the imported SNPs data using "QTLseqr" package.

4.2.9. Synteny analysis and identification of scaffolds constituting *A. freiburgensis* X chromosome

In order to determine which *A. freiburgensis* APS7 scaffolds represent the X-chromosome. *A. rhodensis* linkage groups were aligned with *c. elegans* genome, *A. freiburgensis* (APS7) scaffolds were aligned with *c. elegans* genome, and *A. freiburgensis* (APS7) scaffolds were aligned against *A. rhodensis* linkage groups (LGs). Alignment between the three species enabled visualisation of macro-synteny between the three strains and determined APS7 scaffolds that align with the X chromosome. The whole-genome alignment was generated using PROmer program part of MUMmer package (version 3.23) [171]. PRomer is a rapid whole genome alignment that uses the six-frame translation of both input sequences to generate alignments [172, 173]. The alignment file produced by PRomer was used to produce macro-synteny between the three species using Circos plot version (0.69-6) [174]. Circos plots were generated for each of the alignment, *A. rhodensis* vs. *c. elegans*, *A. freiburgensis* vs. *c. elegans*, and *A. freiburgensis* vs. *A. rhodensis*. Moreover, Circos plots were produced for the *c. elegans* X chromosome and *A. rhodensis* (LG5) to identify scaffolds form *A. freiburgensis* APS7 genome that represents the X chromosome.

4.2.10. Variants calling analysis *A. freiburgensis* strains, filtering variants and predicting their effect on the genome

Variant calling for APS14 was carried out using GATK best practice, as explained in 4.2.7. Called variants between APS7 paternal strain and APS14 maternal strain were subjected to filtration only to keep true and homozygous variants. Initially, variants were filtered according to the default values described in GATK tutorial as follows; Quality depth (QD < 0.2), Fisher strand (FS > 60), RMSMapping Quality (MQ < 40), Mapping Quality RankSum Test (MQRankSum < -12.5), Read Position RankSum Test (ReadPosRankSum < -8.0), and Strand Odds Ratio (SOR > 3.0). After variants were filtered based on depth and genotype quality using bcftools program [175]. Only variants with a depth coverage (DP) > 100, variants with genotype quality (GQ) >= 99, and quality score on Phred-scale (QUAL) >= 50. When filtering using bcftools, only homozygous variants were considered, and heterozygous variants were excluded. The effect of APS14 variants called on the genome was predicted using SnpEff (version 4.3T) [176]. APS7 *A. freiburgensis* was configured and built as a new genome into SnpEff database manually, as it was not part of the already built database for different research species. After the database was run, the analysis was run to predict the effect of the variants. A new variant calling file was outputted with an extra column illustrating the effect of each SNP.

4.2.11. Gene Ontology (GO) analysis of identified QTLs

Genome annotation produced using MAKER by a collaborator Dr. Jun Kim (personal communication), revealed that there are hundreds of cDNAs within candidate regions identified from the BSA analysis. Annotation, as well as the genome for APS7, was visualised using Geneious® (version 10.2.2). In order to narrow down the number of cDNAs within each QTL to only candidate transcripts, only transcripts with effects were extracted from the variant calling file produced by SnpEff analysis. SnpSift program part of SnpEff package was used to filter variants calling files produced by SnpEff. First of all, SNPs located within the identified QTLs were extracted using SnpSift. Out of all the SNPs within each QTL, only SNPs causing missense variants were considered. Then SNPs and transcripts IDs were extracted into a table using SnpSift “extractFields” command. A set of sed and Awk commands were used to extract IDs of

transcripts with missense mutations in each QTL. Samtools was used to extract the full-length sequence of those transcripts from the APS7 transcriptomic file. The identity of transcripts within each QTL was identified using the interactive software blast2go (version 5.2.5). Transcripts were blasted using the public NCBI blast service, with the option (blastX-fast) against the RefSeq-protein database, taxonomy was filtered to nematodes only, blast expectation value was set to 1.0E-5 and number of the blast hit was set to 5. Functional labels (Go terms) of proteins were obtained through GO mapping. Proteins associated with hits from the blast result were mapped against curated gene ontology associated proteins.

4.2.12. Genome assembly of *A. freiburgensis* mitochondria and designing of a molecular marker for mitochondria, non-muscle myosin, and myosinXVIII

APS7 mitochondrion genome was assembled by Sophie Tandonnet (Personal communication). APS4 mitochondrion genome was used as a blast query to identify contigs within the APS7 genome aligning belonging to the mitochondrion. Contigs from the APS7 genome belonging to the mitochondrion genome were extracted into a fasta file. APS7 mitochondrial contigs were assembled against APS4 mitochondrion reference using Geneious software. Variants from the APS14 variant file were loaded into Geneious. SNP between APS14 and APS7 mitochondrion that is also a restriction enzyme cut site was used to design a genetic marker. Primers were designed around the restriction enzyme cut site. Restriction enzyme will digest amplified fragment from APS7 mitochondrion but not the same amplicon from APS14 mitochondrion due to the presence of a SNP. *A. freiburgensis* mitochondria genetic marker was used to genotype mitochondria in RIAILs and identify their strain of origin. Online tool GeSeq was used to annotate the APS7 mitochondrial genome and produce a schematic map of APS7 mitochondria [177].

Genetic markers were designed for non-muscle myosin and myosin XVIII. The strain of origin of both myosins was investigated in 40 RIAILs, 20 HM, and 20 LM. Genetic markers were used to identify a direct role between non-muscle myosin, myosin XIII, and the asymmetric segregation of mitochondria during in *A. freiburgensis* male spermatogenesis.

4.3. Results

4.3.1. Generation of Recombinant inbred Advanced Inter-crosses Lines (RIAILs) in *A. freiburgensis* resulted in a transgressive phenotype: lines produce a high percentage of males

110 Recombinant inbred Advance inter-cross lines (RIAILs) were produced by crossing two polymorphic strains of *A. freiburgensis*, APS14, and APS7. The breeding scheme consisted of 7 generations of crosses, by crossing avoidance scheme between lines to increase haplotype breakpoints [138]. Followed by repeated selfing of all lines for ten generations to bring all of the alleles to homozygosity (Figure 4.2). After inbreeding RIAILs, 65% of the lines were associated with the production of a high number of males, a phenotype that is not present in any of the parental strains.

While maintaining (RIAILs), it was obvious to differentiate between lines that produce a high proportion of males (HM) and line that produce a low proportion of males (LM). Lines that produce a high number of males have slow population growth and take longer for the population to crowd, whereas lines with a low percentage of males reproduce faster, causing plates to crowd quicker. More than half of the RIAILs produced a high number of males (Figure 4.3). However, it was unclear if those males also produce a high number of male progeny after an outcross with wt females. Therefore, males from RIAILs were crossed with a wt APS7 female to determine if males from HM lines produce viable nullo-X sperm (Figure 4.4).

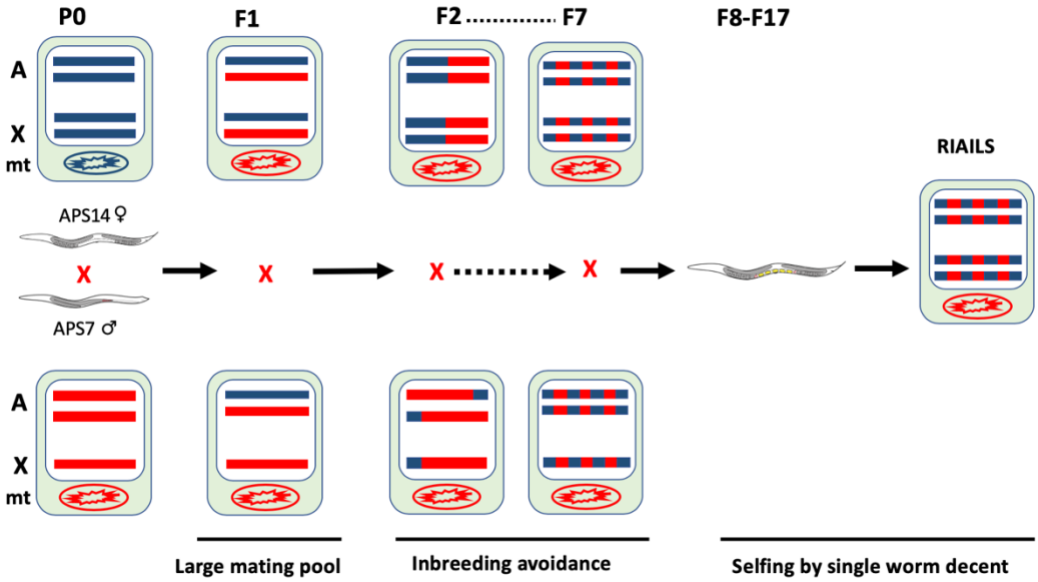

Figure 4.2: Recombinant inbred Advanced inter-crosses lines (RIAILs) produced by crossing two *A. freiburgenesis* polymorphic strains.
APS14 female was crossed with APS7 male. F1s resulting from the cross were let to mate in a large mating pool. Hermaphrodites and females that have mated with male siblings were isolated to 110 individual plates to produce F2s, each with unique recombination. From F2 to the F7 generation, lines were inter-crossed to increase haplotype breakpoints. Then, lines were selfied by single nematode descent (SWD) for ten generations to increase genome homozygosity. By the F17 generation, lines have a unique mixed genome from both parental strains that are homozygous at each locus.

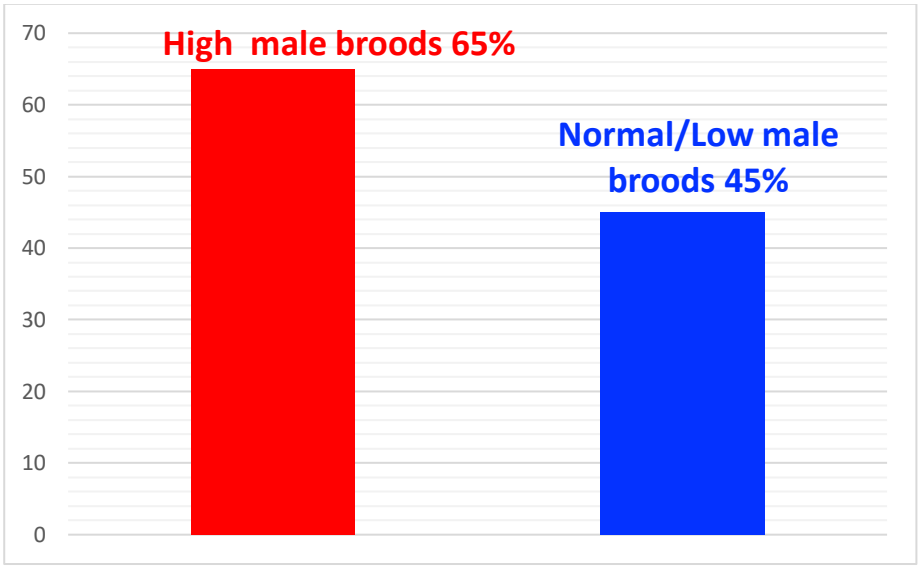

Figure 4.3: Sorting RIAILs lines by phenotype.
From the total number of RIAILs, 65% of lines produced a high number of males, and 45% of lines produced a low number of males when crossed with wt APS7 feamales in separate crosses.

In separate crosses, males form 65% of the lines produced unusual high number of males when crossed with wildtype female and males from 45% of the lines produced the normal low proportion of male brood after an outcross with wildtype APS7 females (Figure 4.3 and 4.4). During an outcross, APS7 *A. freiburgensis* produces on average 18% male brood, with sometimes variations between 20-25% (Table 1.1) [69]. Therefore, a threshold of 25% of male brood after an outcross with wt APS7 female was considered as a cut off between (LM) and (HM) (Figure 4.4). Number of XO and XX progeny resulted from each RIAIL separate cross are outlines in (Table B.1), probability of 0.18 (average number of male broods produced by wildtype cross) was used to calculate binomial and beta distribution for each cross (Table B.1). Production of a high number of males by males from (HM) is attributed to males' ability to produce a functional nullo-X sperm. The novelty of our model organism offers an easy to score phenotype. By scoring the sex ratio, it is possible to determine the kind of divisions occurring in the male germline. Production of functional nullo-X sperm by males isolated from HM lines was determined from the sex ratio when crossed with wildtype females. Production of functional nullo-X sperm resulted in a higher percentage of male progeny than wildtype crosses, close to 50% and sometimes higher, after an outcross with females (Figure 4.4).

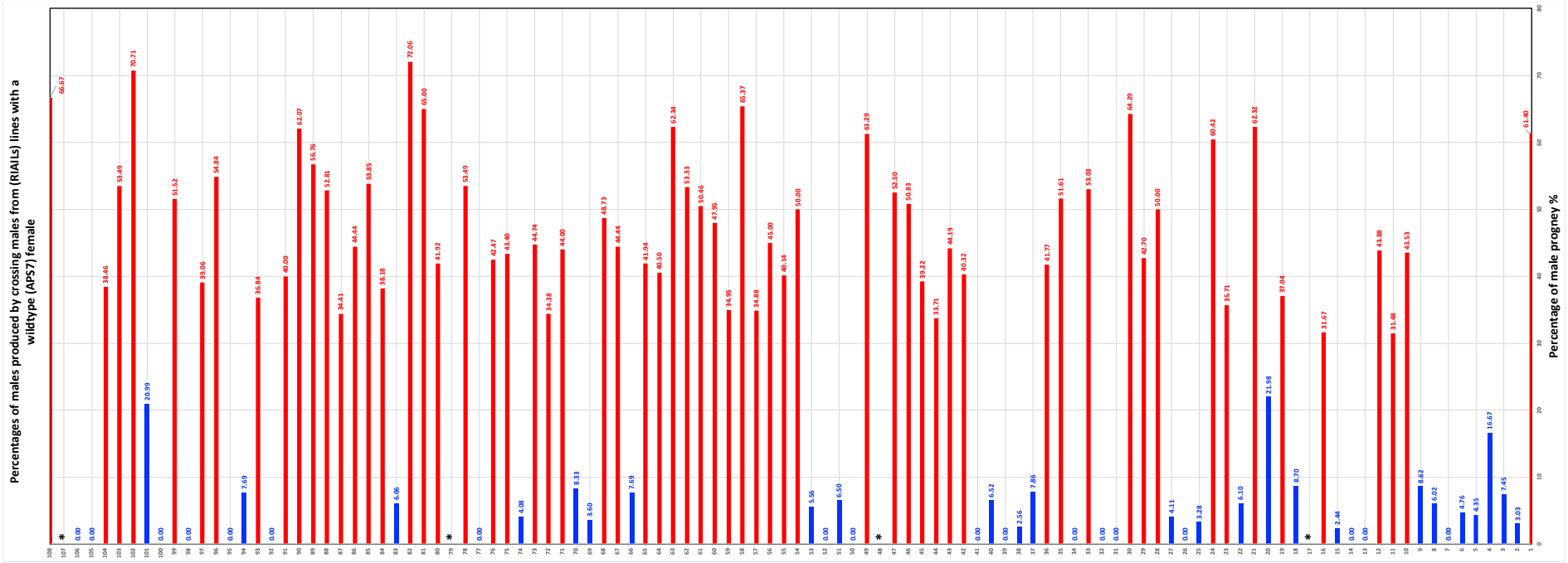

Figure 4.4: Percentage of males produced after males from RIALs crossed with wild type females in separate crosses.
Males from HM lines produced a high number of males after an outcross with APS7 wt female. Whereas, males from LM lines produced low/normal numbers of males. A threshold of 25% of male brood was considered as cut off between HM and LM. Red color represents HM, blue clour LM, and * crosses data not available. Table B.1 outlines number of XX and XO progeny from each separate cross.

4.3.2. Bulk segregant analysis identified quantitative trait loci on the X chromosome of *A. freiburgensis* associated with asymmetric cell division

4.3.2.1. Data collection for bulk segregant analysis and identification of genetic variants

The whole genome was extracted from the APS14 maternal strain and all RIAILs separately (Figure 4.5). DNA pools from lines producing high male progeny and another two DNA pools from lines producing a low number of male progeny were generated. Each pool is composed of an equal amount of DNA pooled together from 10 different lines (Table B.2) (Figure B.1). The four DNA pools and the APS14 maternal samples were sequenced by NGS. FastQC examination of raw reads showed poor quality score, especially towards the end of reads. Besides, two peaks for GC content were observed with the lowest peak representing bacterial contaminants (Figure B.2) [178]. Trimming of low-quality reads improved the per-base sequence quality by trimming and filtering out low-quality reads (Figure B.2) (Table B.3).

Trimmed reads alignment to reference (APS7) genome revealed different mapping percentages depending on the presence of contaminant reads in each sample after sequencing (Table 4.2). Alignment to reference genome eliminated contaminant reads by only aligning nematode reads to the APS7 reference genome and discarding bacterial reads. FastQC test on alignment bam file illustrated one GC peak corresponding to nematode reads, in comparison to the FastQC test of raw and trimmed reads (Figure B.2). Alignment bam files from L-pools and H-pools were merged into one bam file called LowBulk (LB) and HighBulk (HB). Variants between each bulk and APS7 reference genome were called separately (Table 4.3). Then, VCF files were merged using to a single VCF file. Merging VCF files combined the vcf records at each position by multi-sample aggregation. Hence, the number of combined Low Bulk and High Bulk variants at each position in the combined VCF file were 399319, significantly reduced than the total number of variants called separately for each bulk (Table 4.3).

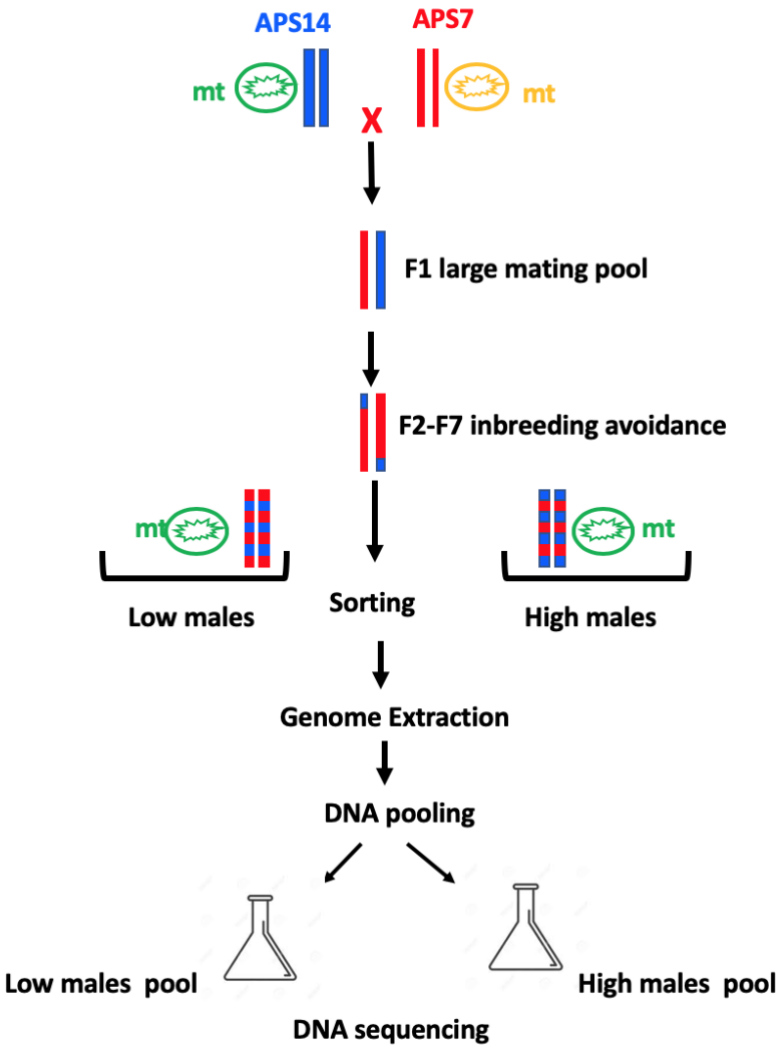

Figure 4.5: Data collection for bulk segregant analysis.
RIAILs chromosomes at F17 will by a hybrid mix between APS14 and APS7 genome; however, it will be homozygote at each locus. RIAILs were sorted into high males or low males, depending on the production of males. The genome was extracted from all lines separately. DNA from lines with similar phenotypes was pooled together to generate high males pool and low males pool. Finally, DNA pools were sequenced using NGS technology in high depth.

Table 4.2: Alignment results using BWA of trimmed reads.

Sample	Total QC passed reads	Number of mapped reads	Percentage of mapping
APS14	215883207	76501280	35.44%
Pool1	195745572	131954473	67.41%
Pool2	182728793	132138960	72.31%
Pool3	186390896	144178811	77.35%
Pool4	183971885	148638391	80.79%

Table 4.3: Number of variants called for each bulk.
Consolidating called variants from both bulks into a combined VCF file significantly reduces the number of variants in the combined file to 399319.

Bulk	Total Number of variants	SNPs	Insertions	Deletions	Indels
Low Bulk	1371822	329604	30197	24702	460
High Bulk	1451138	335409	30131	25216	373

4.3.2.2. SNPs filtering eliminates low confidence SNPs from the BSA analysis

Low confidence SNPs were filtered based on read depth. SNPs with high read depth that may be located in a repetitive region and SNPs with low coverage were also filtered out [179]. To assess the quality of SNPs and define filtering thresholds, histograms were plotted for reads depth, per bulk SNP-index, and reference allele frequency (Figure B.3). Histogram plots of per bulk SNP-index illustrate peaks at each end of SNP-index of 0 and 1. Histogram plots for reads depth and reference allele frequency determined the threshold used to filter low confidence SNPs (Table 4.4). SNPs plot after filtering low confidence, SNPs appeared to be more normally distributed and without a peak at each end of SNP-index of 0 and 1 (Figure 4.6).

Table 4.4: Threshold used for each variable to filter low confidence SNPs and the number of SNPs filtered at each step.

Filtering by	Threshold	Number of SNPs filtered
Reference allele frequency	0.2 <=REF_FRQ <=0.8	133682
Total sample read depth	Total DP >= 500	14876
Total sample read depth	Total DP <= 1750	6808
Per sample read depth	DP >= 40	29
Genotype quality	GQ >= 99	3426
Difference between bulks	<= 100	45480
Original Number of SNPs	**Filtered**	**Remaining**
399319	204301	195018

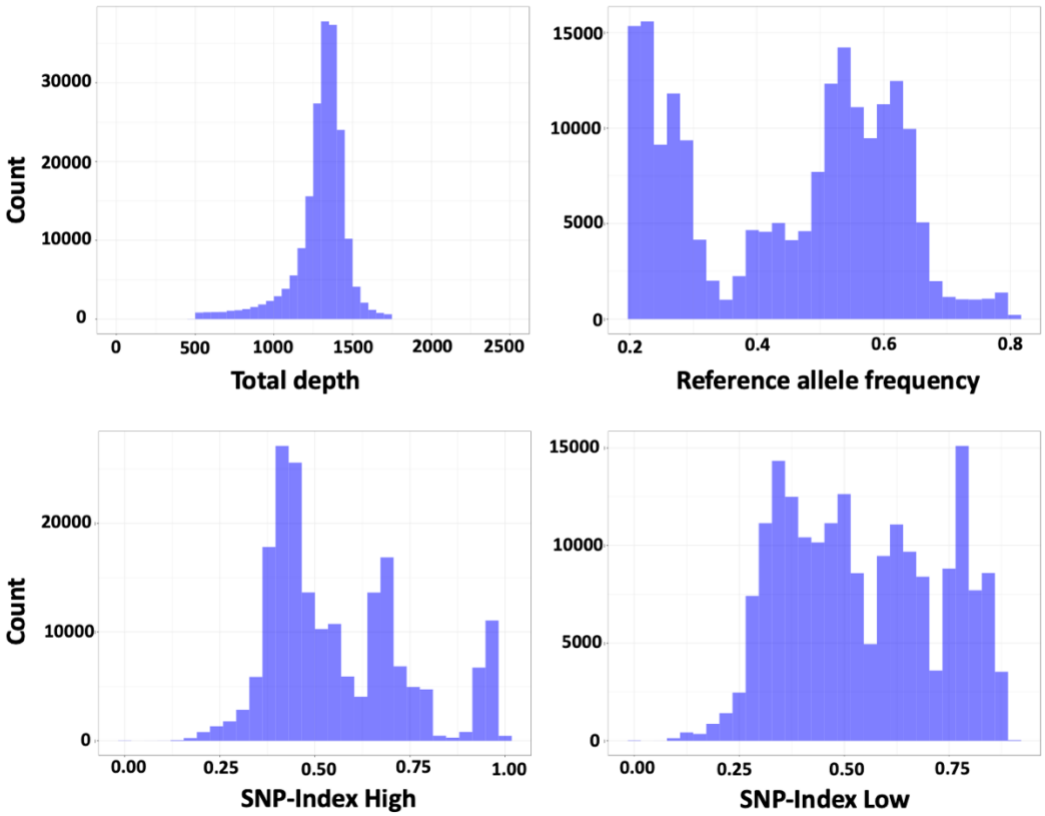

Figure 4.6: Histogram plots of SNPs after filtering low confidence SNPs. SNPs with a total read depth between 500 and 1750 were maintained. Per bulk, SNP-index is moderately distributed normally around SNP-index value of 0.5. Peaks at each end of 0 and 1 in from the per-bulk SNP index plots were filtered out.

4.3.2.3. BSA analysis identified 4 QTLs associated with asymmetry in the male germline

Four Quantitative Trait Loci (QTLs) were identified on scaffolds number 5, 6, 25, and 26, and they were named QTL1-4, respectively. QTL2 (mean p-value 5.90E-05 and mean Q-value 0.000876097) on scaffold 6 was the largest by size (3278726bp) with 12096 SNPs (3689 average SNPs per Mb). QTL1 (mean p-value 4.18E-05 and mean Q-value 0.000668699) on scaffold 5 was the second largest by size (2035319bp), with 6847 SNPs (3364 average SNPs per Mb). QTL3 (mean p-value 5.22E-05 and mean Q-value 0.000791481) located on scaffold 25 with a size of 278182bp containing 187 SNPs. QTL4 (mean p- 1.55E-05 and mean Q-value 0.000606695) located on scaffold 26 was the shortest candidate region reported with a size of 138237bp containing 108 SNPs (Table 4.5) (Figure 4.7) (Figure 4.8).

Table 4.5: Four QTLs were identified on different scaffolds with a significant mean p-value and mean q-value.

QTL	QTL1	QTL2	QTL3	QTL4
Scaffolds	5	6	25	26
start	9035	45748	33889	16474
end	2044354	3324474	312071	154711
length	2035319	3278726	278182	138237
nSNPs	6847	12096	187	108
avgSNPs_Mb	3364	3689	672	781
peakDeltaSNP	0.35907495	0.43719216	0.42908529	0.44841324
posPeakDeltaSNP	9035	864832	33889	154711
avgDeltaSNP	0.35576673	0.38135858	0.42831606	0.44834105
maxGprime	308.859984	357.049435	282.212248	359.015893
posMaxGprime	9035	866623	33889	16474
meanGprime	301.680279	294.89346	281.616387	358.980606
sdGprime	18.0352498	48.8814072	0.39200526	0.03002877
AUCaT	228109358	517066524	37880374.9	29535392.9
meanPval	4.18E-05	5.90E-05	5.22E-05	1.55E-05
meanQval	0.0006687	0.0008761	0.00079148	0.0006067

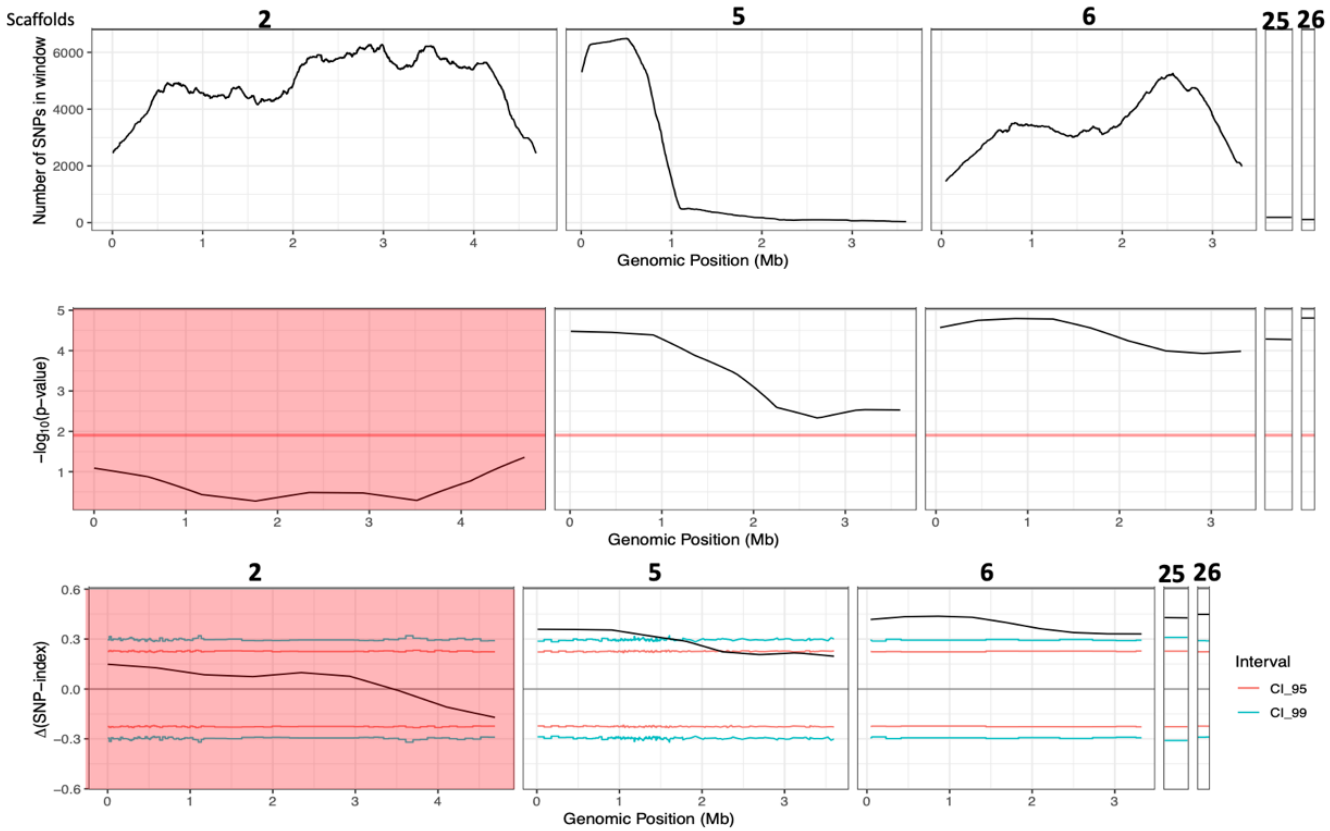

Figure 4.7: BSA-QTL analysis Identified QTLs on four different scaffolds.
Highlighted scaffold 2 in red contains non-significant QTLs compared to other QTLs. In each scaffold, the number of SNPs in each window was plotted against the genomic position in (Mb). Scaffolds 25 and 26 are smaller than 1Mb compared to other scaffolds. QTLs in scaffolds 5, 6, 25 and 26 have a P-value that is above the threshold. Besides, calculated delta-SNP-index indicates significant QTLs in scaffolds 5, 6, 25, and 26 where the calculated delta-SNP-index is above the confidence intervals, 95%) (red) and 99% (green).

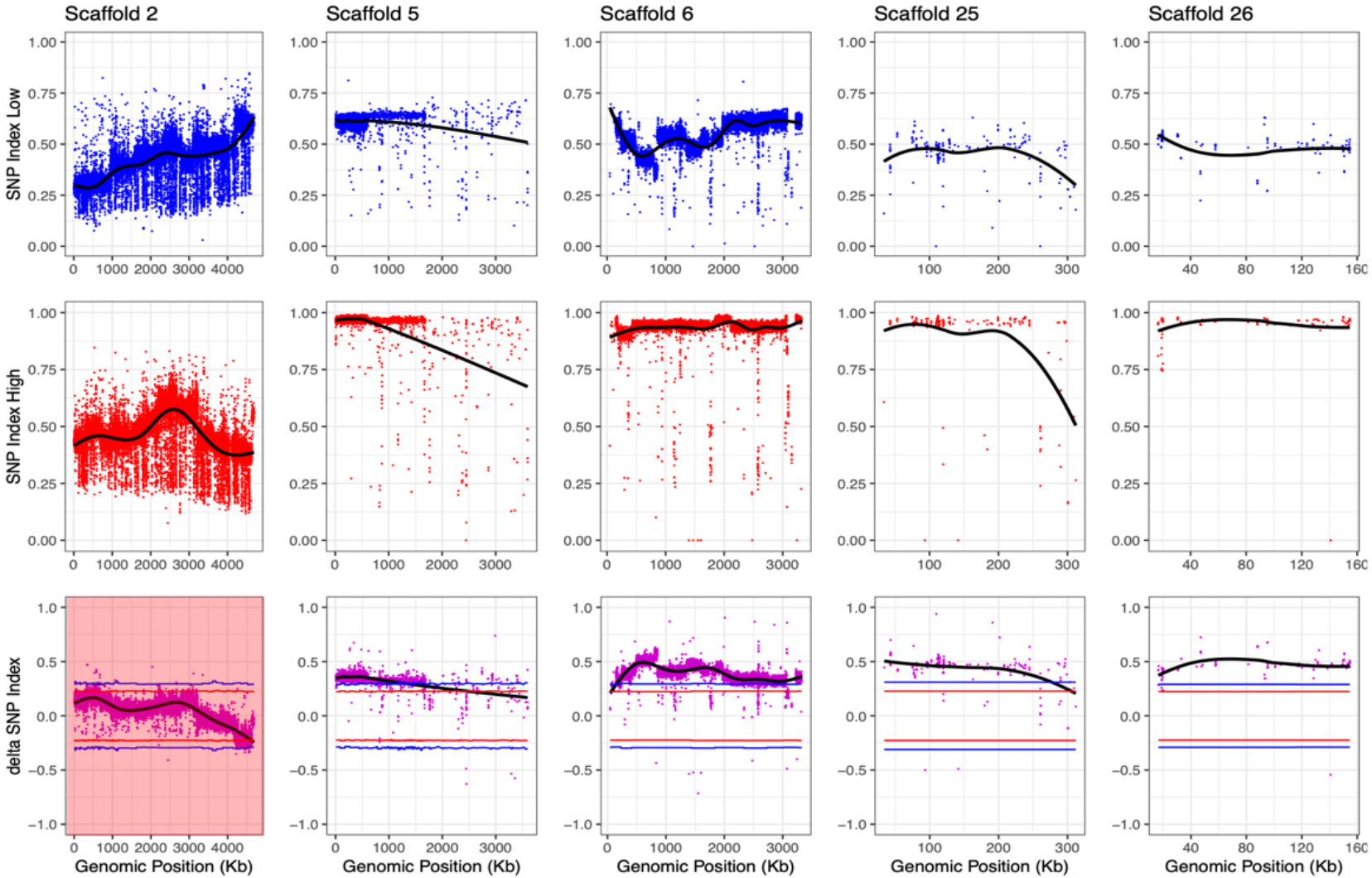
Scaffold 2
Scaffold 5
Scaffold 6
Scaffold 25
Scaffold 26
SNP Index Low
SNP Index High
delta SNP Index
Genomic Position (Kb)

Figure 4.8: delta-SNP-index of SNPs from scaffolds 5,6,25 and 26 revealed a region of significance.
Highlighted scaffold in red does not contain a region of significance compared to the other four scaffolds QTLs. Calculated delta SNP-index for scaffolds 5,6,25 and 26 are above confidence intervals 95% (red) and 99% (blue).

4.3.3. Macrosynteny revealed that identified QTLs are on *A. freiburgensis* X chromosome

The 45 Mb *A. freiburgensis* APS7 genome was assembled into 75 scaffolds. Therefore, it is challenging to determine the chromosomes identified QTLs belong without a genetic linkage map. However, scaffolds were mapped to chromosomes through whole-genome alignment of *A. freiburgensis* APS7 genome with the genome of the related species *A. rhodensis* APS4. The general gene composition of each chromosome is highly conserved in nematodes [180-182]. Synteny to *A. rhodensis* and *c. elegans* enabled assigning *A. freiburgensis* scaffolds representing the X chromosome. *A. rhodensis* APS4 genome has been previously organized into seven linkage groups, each representing a chromosome. *A. rhodensis* APS4 whole-genome alignment with *c. elegans* genome identified linkage group-5 (lg5) to represent the X chromosome in *A. rhodensis* (Figure 4.10). Whole-genome alignment of *A. freiburgensis* APS7 with *A. rhodensis* APS4 identified APS7 scaffolds that align with *A. rhodensis* APS4 linkage group 5 (Figure 4.9). Scaffolds 5,6,25 and 26 with identified QTLs aligned with the X chromosome of *A. rhodensis.*

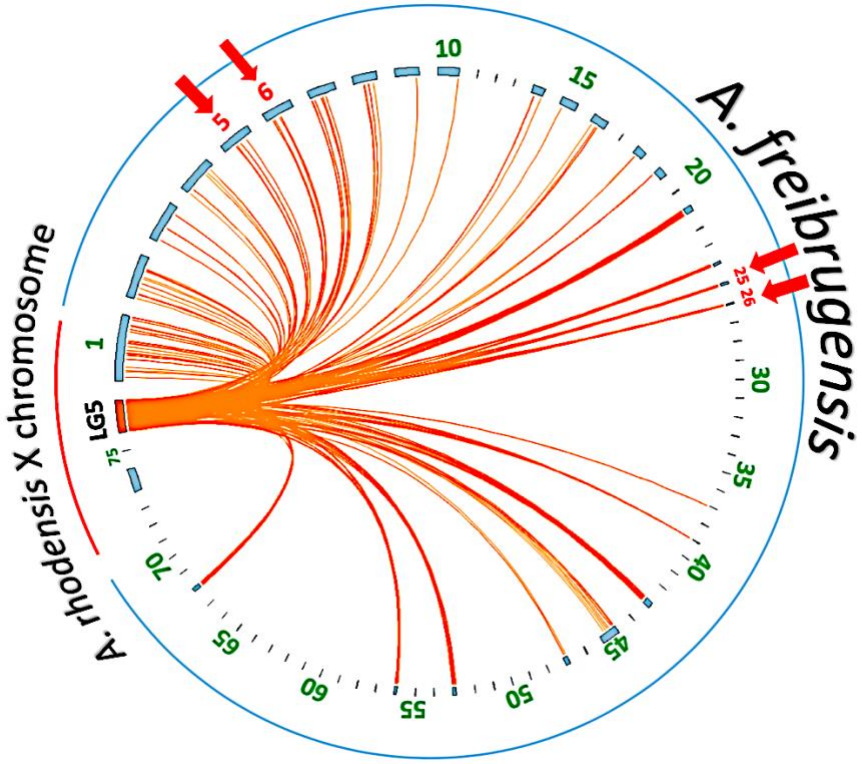

Figure 4.9: Identified QTLs located on *A. freiburgensis* scaffolds share orthologues sequences with *A. rhodensis* X chromosome (LG5).
Whole-genome alignment between X chromosome (LG5) of *A. rhodensis* and *A. freiburgensis* indicates that scaffolds 5, 6, 25 and 26 where QTLs were identified share orthologues sequences. This is a significant indication that identified QTLs are in the X chromosome of *A .freiburgensis*.

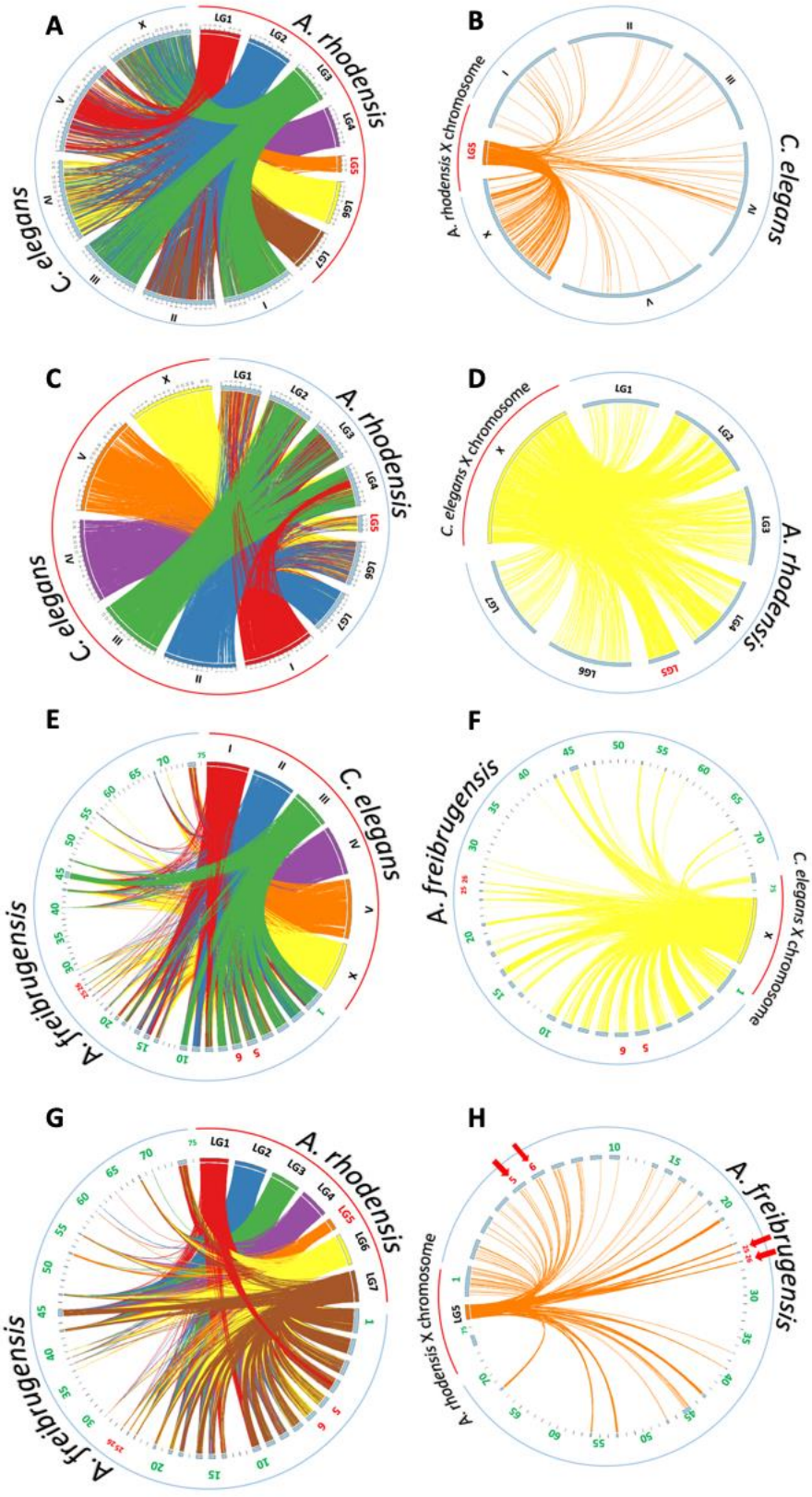

Figure 4.10: Orthologous sequences between *c. elegans* vs. *A. rhodensis* and *A. rhodensis* vs. *A. freiburgensis* identified *A. freiburgensis* scaffolds belonging to the X chromosome.
Red arrows and scaffolds labeled in red indicate the location of identified QTLs.

3.3.4. Predicting the effect of SNPs called between *A. freiburgensis* RIAILs parental strains narrowed down the search for candidate genes

In order to identify candidate genes from the identified QTLs, only transcripts with missense mutations were considered for the analysis. Initially, 1728880 variants were called between APS14 and APS7 reference genome. However, when low confidence SNPs were filtered based on depth, genotype quality, and filtering out heterozygote SNPs, 320312 true variants were maintained. From the true overall variants, there were 277788 SNPs, 22521 insertions, 19992 deletions, and 11 Indels (Table 4.6). The variant rate between APS14 and APS7 reference genome is one variant in every 161 bases, the ratio between missense and silent mutations is 0.3415 (missense/silent ratio), and the ratio between SNPs transitions to transversions is 1.61(transitions/transversions) (Table B.5) (Table B.6).

SnpEff software was used to predict the effect of SNPs called on transcripts to only consider transcripts with non-synonymous mutations. The total number of transcripts in the APS7 genome is 18532. SnpEff predicted 9452 transcripts have non-synonymous mutations, 238 transcripts with a stop codon gained, and 192 with both missense variants and stop codon gained. QTL1 has 250 transcripts with missense mutations, of which 219 transcripts had a blast hit with nematode RefSeq-protein database, and 14 transcripts with stop codon gained, of which 13 transcripts had a blast hit. In qtl1 the highest deltaSNP index (deltaSNP 0.673076923, P-value 3.47E-05 and Q-value 0.000606695) at scaffold five positions 339811 is an insertion of 198bp long approximately 18688bp upstream of the non-muscle myosin transcript, that contains missense variants and variants causing stop codon. The insertion is over-represented in the high bulk with SNPindex of (0.950549451) compared to the low bulk (Table 4.7).

QTL2 is the largest candidate region in size containing 315 transcripts with missense variants in APS14, of which 271 have a blast hit, and eight transcripts with stop codon gained, of which seven transcripts have a blast hit. An insertion of 224bp at scaffold 6 position 2008276 was overrepresented in high bulk (SNP-index 0.918439716) with the highest delta-SNP-index in QTL2 (deltaSNP 0.904694012, P-value 4.85E-05 and Q-value 0.000753638) (Table 4.7).

There were 23 transcripts with missense variants in qtl3, with 16 of them correspond to a protein from the nematode RefSeq-protein database. The smallest candidate region qtl4 harbours 12 transcripts with missense mutations, the identity of 8 of those transcripts has been identified with search against nematode RefSeq-protein database (Table 4.7).

Table 4.6: Number of variants called and filtered between APS14 and APS7 reference genome.

Variant calling stage	Number of SNPs	Insertions	Deletions	Indels	Total	Percentage kept
Initial variants called	344301	29282	26823	40	1728880	100%
Filtering by genotype quality (QUAL >= 50) and (GQ>= 99)	320034	25820	24049	34	369937	21.4%
Filter by depth >=100	297905	24147	22412	26	344490	19.92%
Filtering out heterozygote SNPs	277788	22521	19992	11	320312	18.52%

Table 4.7: Variants' effect on transcripts in each QTL as reported by snpEff.

	Qtl1	Qtl2	Qtl3	Qtl4
Number of variants reported with effect	21496	17477	1833	2194
Number of variants causing mis-sense variants	938	794	85	73
Number of variants with stop gained	15	8	0	1
Total Number of Transcripts	843	1225	83	55
Number of transcripts with missense variants	250	315	21	12
Number of transcripts with missense variants have blast hits	219	271	16	8
Number of transcripts with stop gained	14	8	0	1

Number of transcripts with stop gained have blast hit	13	7	0	0

4.3.5. All RIAILs inherited mitochondria from the maternal line APS14

Assembled APS7 mitochondrial genome was loaded into genious software and aligned with the APS14 variant file. Variants on the mitochondrial genome between APS14 and APS7 were discovered. A molecular marker to differentiate between both mitochondria was designed. Primers were designed on both ends of a SNP site that also a restriction enzyme cut site. Amplified fragment is digested by restriction enzyme in one strain but not the other. The size of the digested fragment determines the strain of the investigated mitochondria (Table B). A molecular marker for *A. freiburgensis* mitochondria revealed that all of the investigated RIAILs had inherited the mitochondria from maternal line APS14 (Figure 4.11) (Figure 4.12).

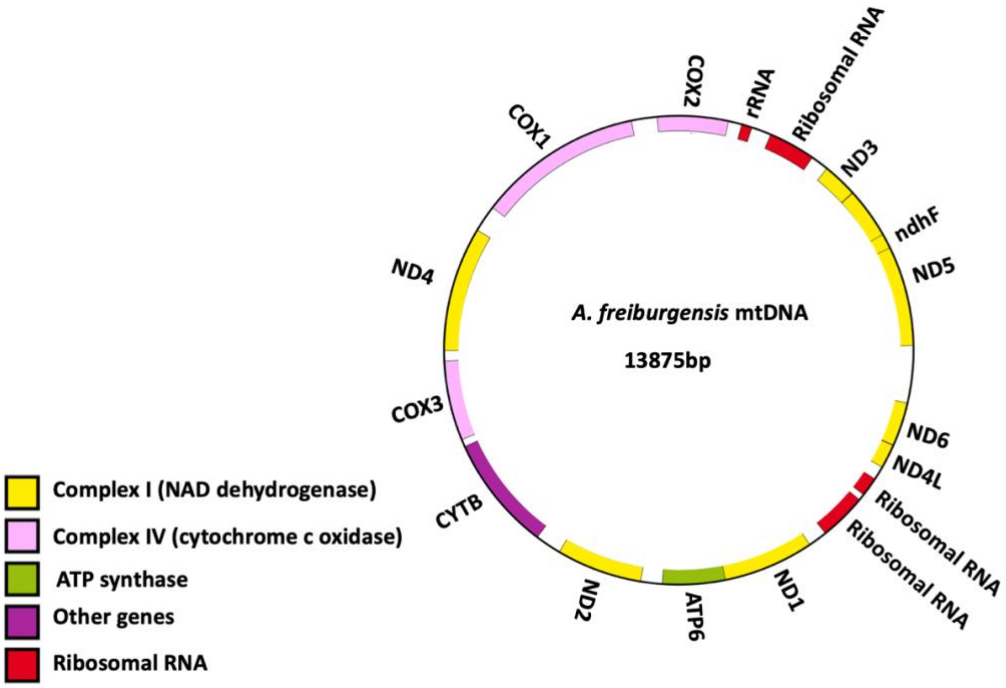

Figure 4.11: Schematic map of the APS7 assembled mitochondria.
SNPs between APS7 and APS14 mitochondria used to design molecular markers to determine the origin of mitochondria in each RIAIL.

4.3.6. Investigation of candidate genes non-muscle myosin and myosin XVIII shows no direct role in the asymmetric segregation of mitochondria

Candidate genes non-muscle myosin and myosinXVIII were identified on QTL1. SNPs contained on both genes were predicted by SnpEff to cause misesne mutations (Table 4.8). I hypothesised that non-muscle myosin, myosinXVIII and mitochondria have to be from the same strain in LM-RIAILs to achieve the wildtype phenotype. Wherase, in HM-RIAILs non-muscle myosin, myosinXVIII and mitochondria will be inherited from different *A. freiburgensis* strains. Incompatibility between myosin and mitochondria is possible to generate the transgressive phenotype in HM-RIAILs. Therefore, Molecular markers were designed on SNPs close or within non-muscle myosin and myosinXVIII to determine their inheritance in RIALS.

Molecular markers used to genotype non-muscle myosin and myosinXVIII located on QTL1, indicate that myosin and mitochondria do not have to be from the same strain in LM-RAILs to achieve the wildtype phenotype (Figure 4.12). On the other hand, Mitochondria in HM-RIAILs segregte to the nullo-X sperm even when mitohonria, non-muscle myosin and myosinXVIII were from the same strain. There is still a limitation in terms of cytological analysis to determine whether anaphase II mitochondria in the spermatogensis of HM-RIAILs segregate symmetrically. However, this conclusion could be true based on the fact that males from HM-RIAILs produce a functional nullo-X sperm.

This experiment indicates that inheritance of both myosin genes has no direct role in the underlying phenotype. However, non-muscle myosin and myosinXVIII were always inherited together in all investigated RIAILs indicating that they segregate together during recombination. An X chromosome marker located away from QTL1 was also genotyped. Genotyping X chromosomes marker and both myosin genes, which are located on the X, indicate that the X chromosome in RIAILs is composed of different rearrangements of haplotype blocks from both *A. freiburgensis* strains (Figure 4.12).

Table 4.8: Non-muscle myosin and myosinXVIII were identified on QTL1. table contains combine data from SnpEff and blast2go. SnpEff determined that transcripts within QTL1 contain missesne variants and blast2go determined the identity of those transcripts by blasting them agianst protein databse.

Gene Name	**Non-muscle Myosin**	**Myosin XVIIIA**
Transcript Id	gene-3.0-mRNA-4	gene-9.5-mRNA-1
Bio-type	Protein coding	Protein coding
Length	1470	2091
Missense variants	1	3
E-value	9.24E-107	1.05E-174
Function	actin binding	motor activity; actin binding; myosin complex

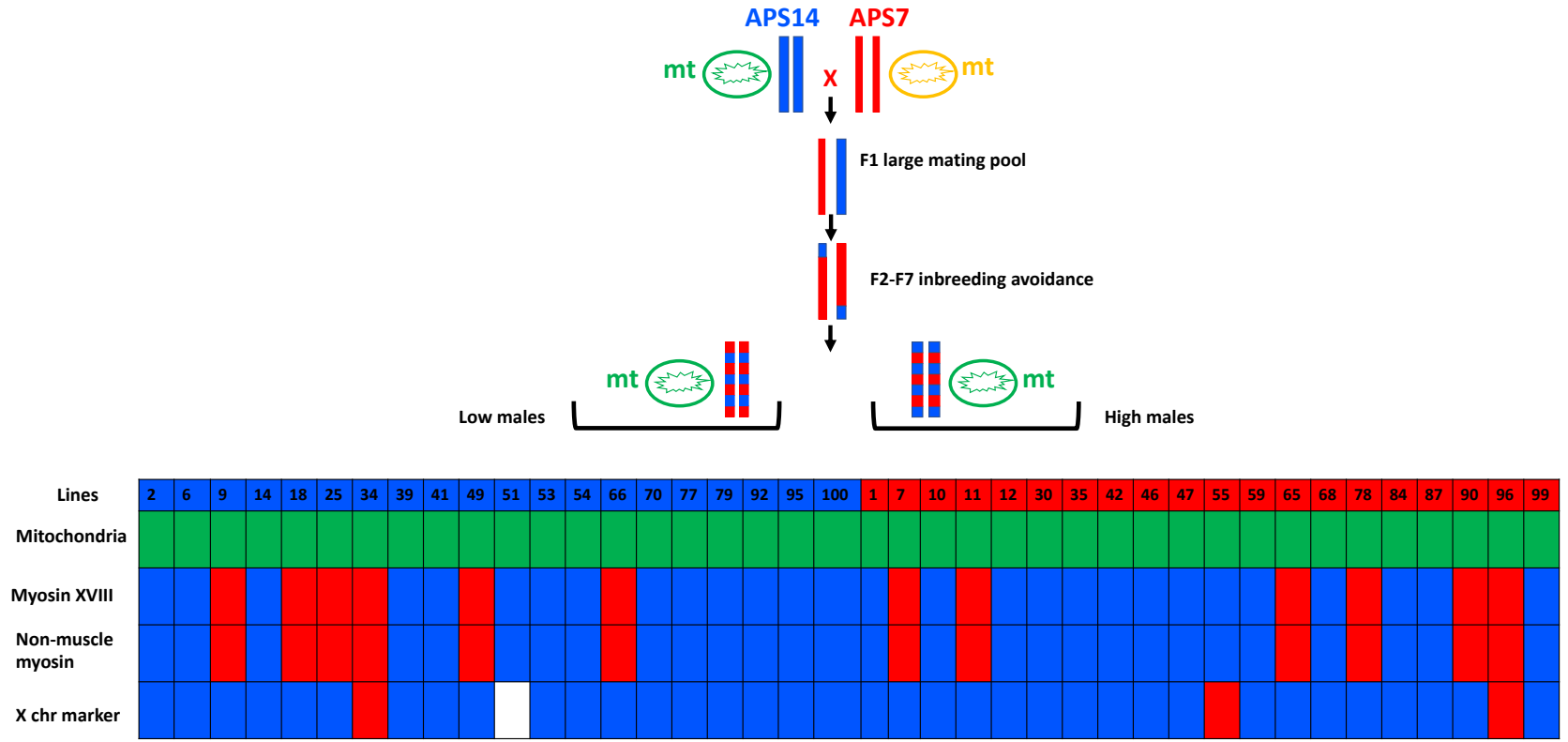

Figure 4.12: Inheritance of mitochondria, myosinXVIII, and non-muscle myosin in RIAILs.
Inheritance of non-muscle myosin and myosinXVIII is not related to the transgressive phenotype and mitochondrial inheritance. However, in all investigated RIAILs, both myosins are inherited together. Both myosins are located on QTL1, and their inheritance together indicates that they segregated together during recombination. Red APS7, blue APS14, and green APS14 mitochondria

4.4. Discussion

4.4.1. X chromosome haplotype block mosaic shuffling in RIAILs resulted in a transgressive phenotype, where males produce viable nullo-X sperm

RIAILs were constructed using *A. freiburgensis* paternal APS7 and maternal APS14 polymorphic strains. Genotyping mitochondrial genome from 40 RIAILs indicated that all the investigated RIAILs inherited the mitochondria from their maternal APS14 strain (Figure 4.12). Intercrosses between lines in an inbreeding avoidance scheme to avoid consanguineous mating (IA-RIAILs) led to an increase in haplotype breakpoints in the RIAILs genome introduced by meiotic recombination (Figure 4.1). As a result, the RIAILs genome was a varied mix from the two APS7 and APS14 parental strains. In some RIAILs, mosaic shuffling of its genome from two parental strain might have disrupted the wildtype interaction of a group of linked polygenes resulting in a new transgressive phenotype, where lines produced a high number of males.

BSA analysis identified 4 QTLs associated with X chromosome segregation and spatial localization of cytoplasmic components in *A. freiburgensis* male spermatogenesis. Macrosynteny between *A. freiburgensis* and *A. rhodensis* genome revealed that identified QTLs allign with *A. rhodensis* LG5, that shares homologs with *c. elegans* X chromosome (Figure 4.9). Therefore, it is posible that in wildtype *A. freiburgensis* male spermatogenesis, epistatic interaction between a linked group of polygenes, located on the X chromosome, and sperm components maintains asymmetric co-segregation of sperm components exclusively with the X chromosome (Figure 4.13). In lines were wildtype epistatic interaction between X chromosome polygenes and sperm components is lost, an extreme transgressive phenotype is observed, where males from those lines produce a high number of males during an outcross with a wildtype female. The wildtype epistatic interaction was lost probably due to RIAILs genome mosaic shuffling of haplotype blocks from both APS7 and APS14 *A. freiburgensis* strains. *A. freiburgensis* as a model organism enables the determination of the type of divisions occurring in males germline through brood count of sex ratios after an outcross with a wildtype female. Males from lines producing a high number of males also produced a high number of males during an outcross with a wildtype

female. The production of a high number of males by those males indicates their ability to produce functional nullo-X sperm. Therefore, I hypothesise that males from lines producing a high number of males, lack the wildtype epistatic interactions between X chromosome polygenes and sperm components that maintain asymmetric segregation in the second anaphase, due to the RIAILs genome mosaic mix (Figure 4.13). As a result, sperm components in males from lines producing a high number of males segregate symmetrically during the second anaphase, irrespective of the X chromosome, leading to the production of functional nullo-X sperm. Production of functional nullo-X sperm varies between lines, some lines produced males as high as 80%, and other lines did not produce males at all (Figure 4.4). Several environmental and biological factors contributed to the variation of production of functional nullo-X sperms between males from RIAILs constrained us from displaying RIAILs phenotype in a continuous graph. Percentages of nullo-X sperms produced by males from RIAILs, represented by male brood count after an outcross, are influenced by the age of individuals involved in the cross, period of the cross, temperature, varying percentages of nullo-X produced between females and sperm competition [183, 184]. Therefore, RIAILs were sorted into two discrete groups, a high males group, and a low males group. Since wildtype females predominantly produce X-bearing oocytes, the only explanation for the production of a high number of males from HM-RIAILs is their ability to produce functional nullo-X sperm. However, the production of nullo-X sperm from HM-RIAILs was not observed through cytology and remained an area for future investigation.

Since the spermatogensis of HM-RIAILs has not yet been invetigated by cytologicaly analysis, It is possible that nullo-X sperm in HM-RIAILs is produced in a similar spermatogeneis to that of *c. elegans* (Figure 1.8). However, I do not favour that hypothesis, since the diminitive size of the *Auanema* male spermatocyte compared to *c. elegans* spermatpcyte does not have enough material for the formation of two centrual residual bodies and 4 sperm [58]. Moreover, central residual bodies did not form during *Arh-mas*-1spermatogensis when sperm components (MSP and mitochondria) segregated symmetrically (Figure 2.13 and 2.14). There were incidances of residual body formation (Figure 2.13), but it was very rare compared to other symmetic divisions that resolved into only two cells,

and it is not yet clear if sperms detached completely from the central residual body. From the observations of wildtype *Auanema* male spermatognenesis, the investigation of *Auanema Arh-mas-1* spermatogenesis and the fact that *Auanema* male spermatocyte is smaller than *c. elegans*, I would favour the notion that nullo-X sperm in HM-RIAILs is a result of symmetric segregation of cytoplasmic components in anaphase II. Indeed there is still limitations of cytlogical analysis of HM-RIAILs spermatognesis to draw a final conclusion of how the nullo-X sperm is produced. However, conclusions drawn from the RIAILs-BSA analysis are still strong hypotheses completely worth investigating in the future.

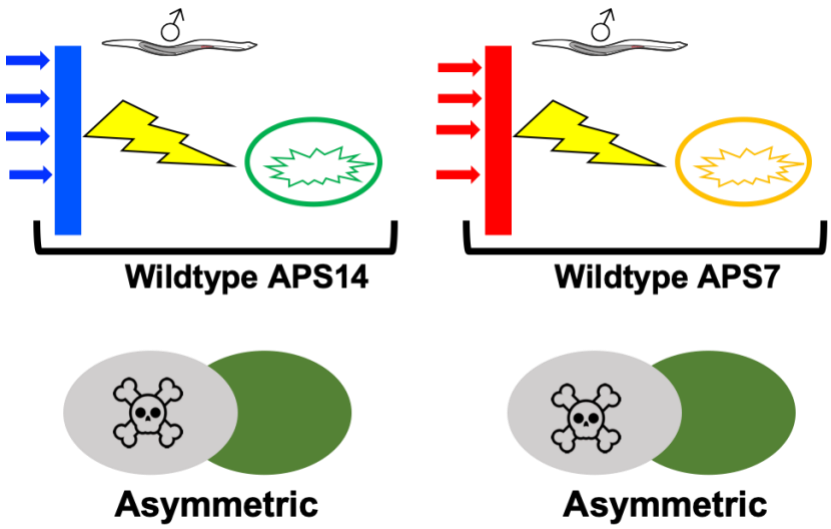

Figure 4.13: Wildtype epistatic interactions between a group of polygenes on the X chromosome and sperm components.
Results from RIAIL-BSA analysis are compatible with the hypothesis that asymmetric segregation of sperm components exclusively with the X chromosome in wildtype *A. freiburgensis* males is maintained by epistatic interaction between X chromosome polygenes and sperm components (mitochondria). Four candidate regions discovered associated with the X chromosome of *A. freiburgensis* to be responsible for the investigated phenotype, red arrows in APS7 and blue arrows in APS14.
I expect that during the second anaphase of male spermatogenesis, sperm components segregate exclusively with the X chromosome. It is possible that epistatic interaction between genetic elements on the X chromosome maintains its polarising cue of sperm components to co-segregate with the X chromosome.

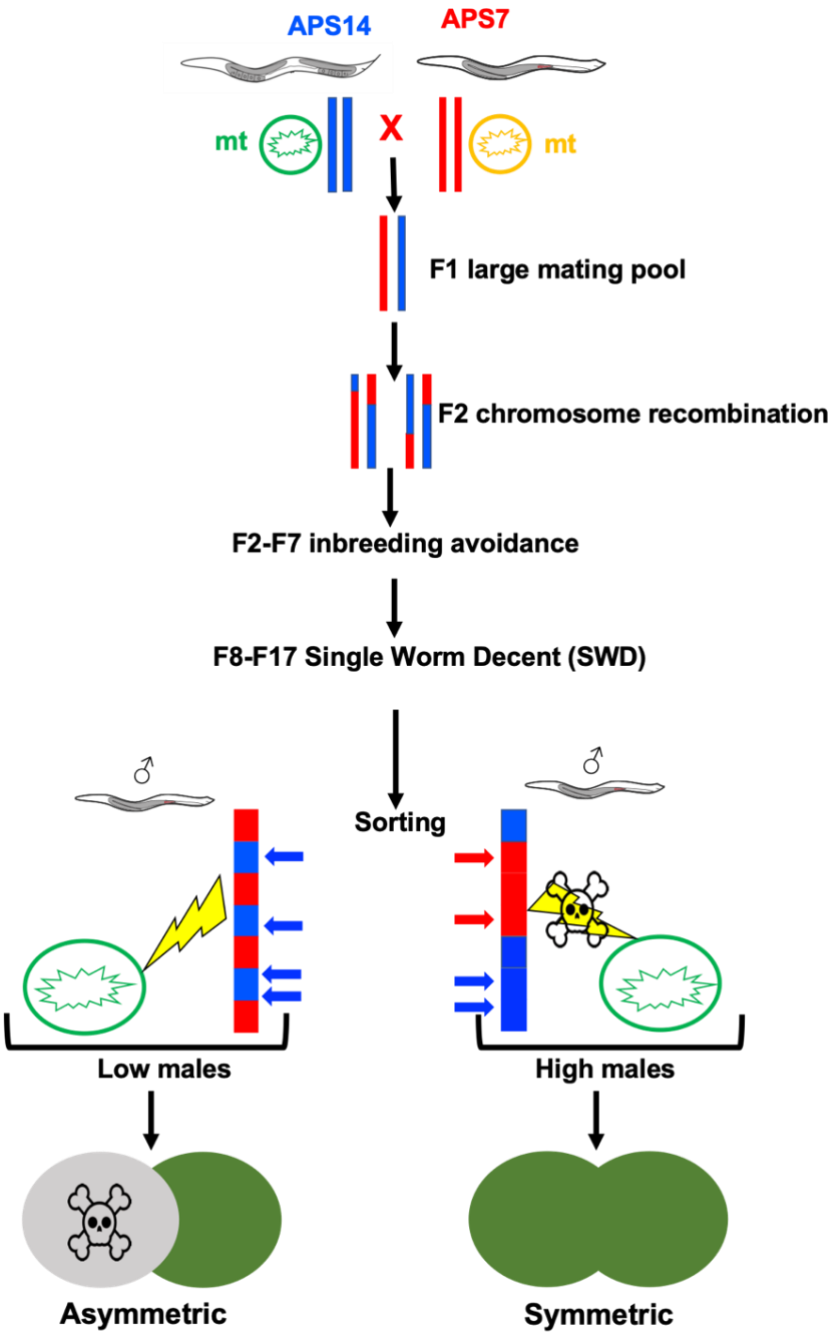

Figure 4.14: X chromosome mosaic mix in males from HM RIAILs lost its wildtype role leading to the formation of nullo-X sperm.
It is possible that in wildtype males epistatic interaction between X chromosome polygenes, represented by the four identified QTLs, and sperm components, represented by the mitochondria, is lost in males from HM lines, due to X chromosome haplotype blocks mix from APS7 and APS14 genome. Lack of this epistatic interaction results in symmetric segregation of sperm components in the second anaphase leading to the production of nullo-X sperms. On the other hand, in males from LM lines, wildtype epistatic interaction between X chromosome polygenes and sperm components is maintained, leading to asymmetric segregation of sperm components with the X chromosome to exclusively produce X bearing sperm. Red arrows represent qtls from APS7 and blue arrows represent Qtls from APS14.

4.4.2. Investigating candidate genes

Identified QTLs responsible for X chromosome segregation and subsequent localization of cytoplasmic components during anaphase II of male spermatogenesis contains many transcripts with missense mutations (Table 4.7). Gene ontology analysis using blast2go helped to identify the identity of those transcripts. Due to the large number of transcripts with missense mutations identified in each QTL, the lack of complete genome of *A. freiburgensis* that is organised into chromosomes, and preliminary annotation of *A. freiburgensis* genome, it was challenging to narrow down the number of genes to a specific set of genes with a direct role with the observed phenotype.

Genomic regions identified using BSA-QTL analysis were associated with a male-specific phenotype, as RIAILs were segregated into discrete groups HM lines and LM lines. However, RIALs DNA used in the analysis was not extracted exclusively from males. DNA was extracted from plates, including females and hermaphrodites. RIAILs hermaphrodite and female phenotype was not considered mainly, and therefore characterised for each RIAIL, because my investigation only concerned with RIAILs males. Since lines were a result of a single hermaphrodite that was inbred for ten generations by SWD when RIAILs were made, it is rational to conclude that hermaphrodites from lines producing a high number of males also produce a high number of males. It was also clear that hermaphrodites from lines producing a high number of males also produced a high number of males during the maintenance of lines; isolated hermaphrodites from HM lines into a fresh plate produced a high number of male progeny. *Auanema* hermaphrodites generally produce diplo-X sperms and a nullo-X oocyte, hence predominantly produce XX progeny [81, 83]. As a result of X chromosome nondisjunction during hermaphrodite spermatogenesis, hermaphrodite spermatogenesis sometimes produces haplo-X sperm leading to the production of XO males. Production of a high number of males from HM hermaphrodites indicates that the rate of X chromosome nondisjunction in HM hermaphrodites spermatogenesis is higher than LM and wildtype hermaphrodites. Therefore, identified QTLs are not only associated with male ability to produce nullo-X sperm; they are also associated with a hermaphroditic rate of X

chromosome nondisjunction during spermatogenesis. This explains the large number of transcripts with missense mutations reported in those QTLs.

Non-muscle myosin (myosin II) and myosin XVIII were identified on QTL1 to have missense variants (Table 4.8). Thus, they were investigated for their direct role in X chromosome segregation and subsequent localization of cytoplasmic components. The role of myosin II and myosin VI are required for residual body formation and spermatids budding during *c. elegans* spermatogenesis. The role of Myosin II in *c. elegans* spermatogenesis was illustrated to regulate and mediate RB expansion [185]. Residual body expansion and budding of *c. elegans* spermatids are mediated by the polarised movement of myosin II to opposite directions. Furthermore, myosin II mediates the segregation of cytoplasmic components between *c. elegans* residual body and spermatids. Mitochondria are believed to be connected with astral microtubules that are physically linked to the cell cortex. Myosin II ensures that mitochondria are not partitioned to the central RBs by omitting astral mitochondria from the central region to spermatids buds during RB expansion [185]. Myosin VI-mediated cytokinesis eventually separate spermatids from the central residual body [186, 187]. Mutant spermatocyte lacking myosin VI cannot efficiently segregate sperm components, including; mitochondria and MSP, to the differentiating spermatid [186]. Lack of myosin VI affects the complete separation of budding spermatids, where spermatids expand, but no complete separation is observed [186]. Initially, myosin II-mediated segregation excludes mitochondria and MSP to spermatids; however, spermatids do not separate when myosin VI is absent. Subsequently, mitochondria and MSP withdraw to RB. Excision of spermatids by myosin VI-mediated cytokinesis is precisely timed to maintain MSP and mitochondria within spermatids [185]. Lack of myosin VI or myosin II does not cause a global segregation failure as chromosomal segregation is not affected [186]. Non-muscle myosin (Myosin II) coassembles with myosin XVIII into mixed polarised filaments [188]. Myosin XVIII lacks motor activity, and their cellular function highlighted to be co-assembly and regulation of Myosin II [188].

Investigation of Myosin II and Myosin XVIII revealed no immediate role with mitochondrial inheritance. All RIAILs inherited the mitochondria from the

APS14 maternal strain. Mitochondria segregated asymmetrically with the X chromosome in anaphase II of males form LM-RIAILs. As a result, males from LM-RIAILs produced low males during an outcross, due to the exclusive formation of only X bearing sperm. Whereas, mitochondria segregate symmetrically in males from HM-RIAILs irrespective of X chromosome inheritance. Therefore, males from HM produce high males during outcross, due to the formation of functional nullo-X sperm. Inheritance of APS14 mitochondria in RIAILs was not affected by the inheritance of myosin II and myosin XVIII. Mitochondria in HM-RIAILs segregated symmetrically even when myosin II and myosin XVIII were inherited from the same strain as the mitochondria. In LM-RIAILs mitochondria segregated asymmetrically even when myosin II and myosin XVIII were inherited from a different strain, indicating that movement of myosin II and myosin XVIII was polarised and mediated segregation of mitochondria exclusively with the X-bearing sperm. The polarised mono-oriented movement of mitochondria mediated by myosin II and myosin XVIII exclusively to the X-bearing sperm in LM-RIAILs, indicates that the X chromosome polarising cue acts upstream myosin II and myosin XVIII. Another genetic component on the X chromosome initiates the polarisation of actomyosin complex, constituting myosin II and myosin XVIII. When the polarising signal on the X and actomyosin are interacting, i.e. from the same strain, actomyosin polarises and mediates the cosegregation of sperm components with the X chromosome. However, when the polarising signal is from another strain and actomyosin are not interacting, actomyosin will not polarise leading to symmetric segregation of sperm components.

In all the genotyped RIAILs, myosin II and myosin XVIII were inherited together, always from the same strain. Inheritance of both myosin together indicates their segregation together during meiotic recombination. Genotyping RIAILs for *A. freiburgensis* X chromosome specific-marker together with myosin II and myosin XVIII, which are located on the X chromosome, indicates mosaic shuffling of RIAILs X chromosome from both parental genomes (Figure 4.12). It is expected that all the identified QTLs are located on the X chromosome and the RIAILs generation resulted in X chromosome mosaic shuffling. Therefore, I expect that a combined inheritance of different genetic elements from all

identified QTLs is required to maintain wildtype asymmetric segregation of mitochondria. In this thesis, I have only investigated the direct role of genes from QTL1 in the cytoplasmic spatial organisation during sperm formation of RIAILs males. BSA analysis identified 4 QTLs involved in creating the extreme transgressive phenotype represented by HM-RIAILs. Therefore, the genotype of all identified QTLs should have been investigated in RIAILs to determine the pattern of inheritance of identified QTLs in both HM and LM RIAILs. Genotyping of all QTLs in RIAILs will determine which of the QTLs are physically linked and consequently inherited together in RIAILs. It will also determine which of those identified QTLs are required to work together in epistatic interaction to maintain the wildtype phenotype in LM-RIAILs.

Molecular network controlling the asymmetric portioning of sperm components with the X chromosome was not completely determined in this thesis and remain an area for future investigation. However, from the results obtained in this study I expect genetic signal expressed by the X chromosome during the second meiosis of male spermatogenesis to influence the polarisation of the actomyosin complex, and consequently the unipolar segregation of MSP and mitochondria with the X chromosome occurs. The first sign of asymmetric cell division in wildtype *Auanema* males spermatogenesis is the lagging of the X chromosome. Once the lagging-X chromosome is included into one anaphase plate MSP and mitochondria exclusively segregate with the cell inheriting the X chromosome. In wildtype *Auanema* male spermatogenesis X chromosome possibly initiates polarisation of actomyosin complex, constituting non-muscle myosin, which elongate dividing spermatocytes and ensures mitochondria and MSP segregation with the X chromosome. During *c. elegans* spermatogenesis equal segregation of mitochondria and MSP is mediated by non-muscle myosin and complete excision of spermatids by cytokinesis is meditated by Myosin VI [185, 186, 189]. I expect the same mechanism to occur during *Auanema* spermatogenesis, however the function of non-muscle myosin will be restricted unipolarly mono-oriented to the X bearing pole. In wildtype *Auanema* male and LM-RIAILs, X chromosome polarising signal influences the unipolar polarisation of non-muscle myosin towards the X-bearing pole, as a consequence mitochondria and MSP segregate with X bearing pole. Then, myosin IV-mediated cytokinesis ensures final

separation of the X-bearing sperm with essential components and the sister cell exhibits the role of residual body (RB) with DNA. However, in HM-RIAILs actomyosin complex constituting non-muscle myosin fails to polarise unipolarly and exclusively with the X bearing pole, because X chromosome mosaic mix disrupts its polarising cue. The polarising signal on the X chromosome in HM-RIAILs will not be able to mediate the polarisation of the actomyosin complex, there will be incompatibility because of its inheritance from a different *A. freiburgensis* strains. As a result, mitochondria and MSP will fail to separate exclusively to the X-bearing pole and distribute symmetrically. When myosin VI-mediated cytokinesis separates the two daughter cells, both cells will contain mitochondria, MSP and essential cytoplasmic components important for sperm function and motility. Hence, a functional nullo-X sperm is produced leading to production of high number of males by males from HM-RIAILs (Figure 4.15).

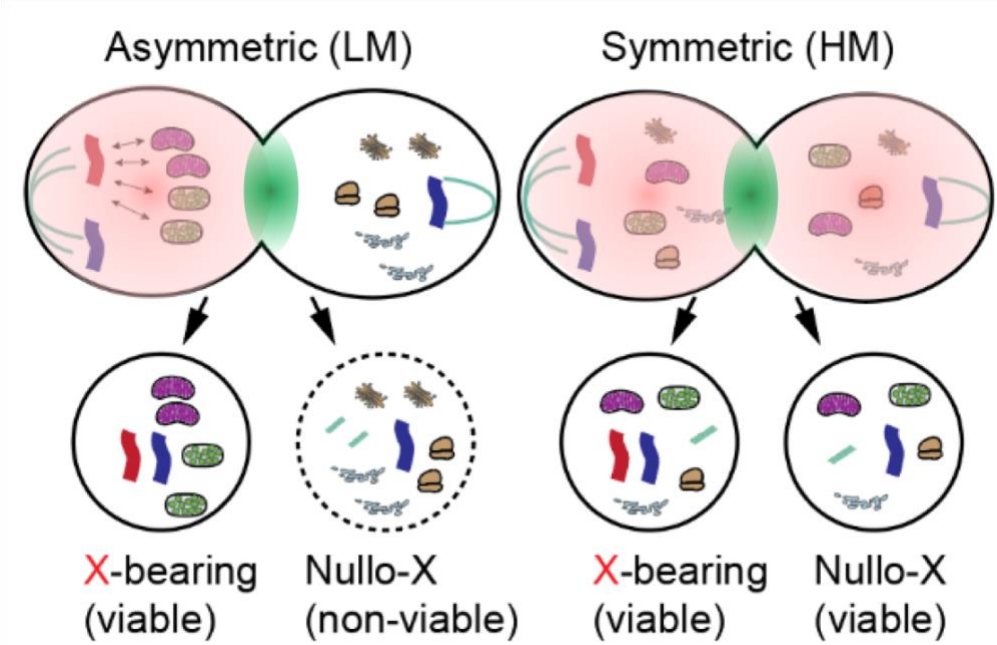

Figure 4.15: Schematic draw of myosin II (red) and myosin IV (green) localization in anaphase II of males from RIAILs spermatogenesis.
In LM-RIAILs X chromosome (red) polarising signal causes unipolar polarisation of non-muscle myosin (myosin II), resulting in active transportation of mitochondria and MSP to the pole inheriting the X chromosome. Following myosin VI-mediated cytokinesis mitochondria and MSP will exclusively segregate with the cell inheriting the X chromosome. Whereas, in HM line X chromosome fails to polarise the non-muscle myosin, as a result mitochondria and MSP distribute symmetrically in the dividing secondary spermatocyte. Following myosin VI-mediated cytokinesis X-bearing and nullo-X sperm will be viable containing MSP and mitochondria.

The genome of all RIAILs has been sequenced individually to create a genetic map for *A. freiburgensis* genome. A future work of a genetic map construction will organise *A. freiburgensis* 75 scaffolds into linkage groups. Using genome from individual RIAILs will enable the identification of QTLs associated with the RIAILs transgressive phenotype. BSA-QTL analysis on the new *A. freiburgensis* genome will identify QTL on the linkage group corresponding to the X chromosome. Inheritance of candidate genes within identified QTLs can be investigated in all RIAILs since all the RIAILs will be genotyped against the same APS7 reference genome. SNPs close to or on candidate genes can be investigated in all RIAILs to identify genes involved in causing the transgressive phenotype in HM-RIAILs.

Chapter 5

Investigating mito-nuclear interaction through X chromosome introgression into polymorphic mitochondrial and autosomal background

Summary

In this chapter I will outline attempts to introgress the X chromosome from one *A. freiburgenis* into the autosomal and cellular background of another strain. The unique X chromosome inheritance pattern in *Auanema*, where the X chromosomes in sons is inherited paternally, will enable the generation of males with an X chromosome from one strain while autosomes and the cellular background will be from another strain. Spermatogenesis of those males will provide a model system to study mito-nuclear interactions. Since I hypothesized that the X chromosome is a polarising signal in *Auanema* male spermatogenesis incompatibility, between X chromosomes, autosomes and mitochondria in those males is expected. Attempts to introgress the X chromosome from one *A. freiburgenis* strain into the background of another did not follow expected paternal transmission as in *A. rhodensis*. However, we have identified differences in the meiosis between *A. freiburgensis* and *A. rhodensis*, despite belonging to the same genus. In contrast to *A. rhodensis*, where X chromosome in sons is always inherited from the father, paternal X chromosome transmission in *A. freiburgensis* occur in age-controlled crosses, during the first day of adulthood.

5.1. Introduction

5.1.1. Reciprocal communication between mitochondria and nuclear genome

Mitochondria derived from bacterial ancestor co-evolved with its host organism through an endosymbiosis event occurred in the estimation of more than 1.45

billion years ago [190]. The primary function of mitochondria is the maintenance of energy supply [191]. Despite having its own genome, 98% of mitochondrial proteins, essential for mitochondrial function, are encoded by the nuclear genome [191]. Due to mitochondria's limited-expression capability, it cannot be reconstructed de novo. Thus, proteins required for mitochondrial genome replication, transcription, and translation are encoded in the nuclear genome [191, 192].

Mitochondria are not only crucial for the production of ATP but serve other critical cellular functions. Mitochondria are involved in apoptosis, synthesising essential molecules (heme and phospholipids), and intervenes in numerous signaling pathways [28, 191]. Mitochondrial retrograde signaling or retrograde regulation is a general term for signaling pathways mediated by the mitochondria. Mitochondria signaling pathways to the nucleus impacts a variety of cellular and organismal activities under normal and pathophysiological conditions [27]. Intracellular signaling mediated by mitochondria implicates life expectancy, development, disease, environmental adaptation and epigenetics [27, 193]. Signaling from mitochondria has a direct role in activating cellular apoptotic programs and in the cellular immune system [28, 29, 193]. On the other hand, factors encoded in the nuclear genome have been implicated in regulating mitochondria copy number [192]. Quantity and activity of mitochondria are controlled by nuclear transcription regulatory networks according to energy demand in different cells under a variety of physiological conditions [194]. Therefore, coordinated expression and reciprocal communication between two sets of genes encoded by mitochondria and nucleus is crucial for mitochondria biogenesis and to maintain cellular hemostasis [191].

5.1.2. Mito-Nuclear co-evolution is crucial to maintain cellular homeostasis

Mitochondria originated from free-living bacteria co-evolved with its eukaryotic host thorough an endosymbiosis event [195]. Through this process, a large number of genes, once coded by the mitochondria, translocated to the nucleus [195, 196]. The majority of mitochondrial function genes are encoded by the nuclear genome; the only subset of these crucial genes is encoded by the mitochondria [196]. In higher eukaryotes, out of approximately 1500 genes

encoding for mitochondria, only 37 genes of which are within the mtDNA [195, 196]. This explains why the majority of mitochondria-associated disorders are not due to mutation in the mtDNA but rather mutation in the nuclear genes encoding mitochondrial functions [195]. Mitochondria contain a high rate of mutation that enables its genome to evolve ten times faster than the nuclear genome [197]. The difference in mutation rate between mtDNA and nDNA could lead to functional mutation in the mitochondrial genome that halts mitochondrial function resulting in most cases to disease-causing mutations [198]. Therefore, co-evolution between nDNA and mtDNA is required to maintain cellular homeostasis [198].

Previous studies reported incompatibility between the mitochondrial genome and nuclear genome between two different wild strains in male-female nematode *Caenorhabditis nouraguensis* [199]. Incompatibility between the two genomes results in a natural reproductive barrier within the species leading to a significant rate of embryonic lethality [199]. In *A. rhodensis,* males naturally inherit paternal X chromosomes, while autosomes and mitochondria are inherited maternally [83]. This unique pattern of X chromosome inheritance in *Auanema* renders it a good model to study mito-nuclear interactions in males.

5.1.3. *A. freibrugensis* as a model to study mito-nuclear interaction

In this chapter, I will outline attempts and challenges to introgress the X chromosome from one *Auanema* strain into the background of another strain to study mito-nuclear interaction. Production of males that have an X chromosome from one strain and cellular background from another is made possible because of the *Auanema* X chromosome unique inheritance pattern, in which the X chromosome in sons is inherited paternally. In *A. rhodensis*, F1 males resulting from a cross between two *A. rhodensi* strains inherit the X chromosome paternally [83]. This unique inheritance pattern is explained by the males' exclusive production of X-bearing sperms and because *A. rhodensis* females produce nullo-X oocyte, in rarer events of X chromosome nondisjunction (Figure 1.6) [83]. In crosses between *A. rhodensis* male and hermaphrodite, cross-progeny males inherit the X chromosome paternally. This is due to the predominant production of nullo-X oocytes by the hermaphrodites (Figure 1.6 and 1.7) [83].

To study mito-nuclear interaction a strain can be generated with X chromosome from one strain while mitochondria and half of the autosomes from another. F1 males resulting from *Auanema* outcross will be backcrossed with their maternal strain for several generations. Thus, those lines will have the paternal X in the genetic and cellular background of the maternal strain. If the X chromosome is a polarising signal, incompatibility is possible between the X chromosome, autosomes and mitochondria from the two highly divergent genotypes. My hypothesis is that this incompatibility will result in the asymmetric segregation of mitochondria in the second meiosis of male spermatogenesis, and consequently, a functional nullo-X sperm will be produced. The production of functional nullo-X sperm is expected to result in the generation of a high number of males during an outcross. X chromosome introgression experiment was conducted in *A. freiburgensis* instead of *A. rhodensis* because previous sequencing data indicate higher genetic diversity between *A. freiburgensis* strains. Generation of F2-derived RILs from two different strains of each species resulted in the formation of a transgressive phenotype in *A. freiburgenis* RILs but not *A. rhodensis* RILs [200].

Unfortunately, the introgression of the X chromosome into the background of another strain was not successful. However, in this chapter, I will outline the attempts made to introgress the X chromosome, discuss possible reasons for the unsuccessful introgression, and suggest amendments to the introgression scheme for future experiments.

5.2. Methods

5.2.1. X chromosome introgression using wildtype APS7 female crossed with APS14 male

A. freiburgensis APS7 female was crossed with APS14 male. F1 males resulting from the outcross were isolated and backcrossed with *A. freiburgensis* APS7 females in separate crosses. Male progenies resulting from each cross were mated back to the maternal strain to establish lines of repeated crosses for 10 generations.

5.2.2. Mutagenesis screening

A. freiburgensis produces hermaphrodites, which are convenient for mutagenesis screens because they harbour male and female gametes within the same individual, avoiding setting up crosses. Hermaphrodites can be identified already at larval stages, because every dauer becomes a hermaphrodite. Dauers in *A. freiburgensis* are produced in response to a crowding pheromone signal experienced by the maternal generation [201]. Therefore, it is essential to culture a minimum of ~10 nematodes in a single plate to initiate a crowding a signal and produce F1 dauers. After mutagenesis, mutagenised P0 hermaphrodites were isolated into fresh plates ten hermaphrodites per plate. Then, F1 dauers were isolated into a single plate each and let to develop to hermaphrodites. Placing a single F1 dauer into a fresh plate will result in F2 females. Morphological mutants recovered from the F2 generation produced in a non-crowding condition will be females. It is difficult to maintain a recessive morphological mutant from F2 females. Therefore, ~20 F2 mutant females were isolated into a separate plate to simulate crowding and left to lay eggs for ~24 h before being moved to a fresh new plate. Dauers produced by the F2 mutant females were isolated to a single plate each and left to develop to hermaphrodites and reproduce. A hermaphrodite that is homozygous for the morphological mutation will produce 100%, mutant progeny.

5.3. Results and discussion

5.3.1. X chromosome introgression into the cellular background of polymorphic wildtype females is age-dependent

In *A. freiburgensis*, a cross between XO males and XX females predominantly result in XX animals [69]. This unusual sex ratio skew is attributed to *Auanema's* male ability to produce X-bearing sperm exclusively. In the rare instance of X chromosome nondisjunction in female *Auanema*,a nullo-X oocyte is produced that leads to the generation of males, when fertilised by male X-bearing sperm. Given this unique paternal transmission of X chromosome to sons in *Auanema*, it should be possible to introgress the X from the paternal strain into the genetic and cellular background of the maternal strain. To do this, an APS7 female was crossed with APS14 male to generate males with the APS14 paternal X chromosome, but cellular background (including mitochondria) and autosomes from the APS7 female. This mixed background strains, will help to investigate a possible mito-nuclear incompatibility. In case there is an incompatibility between X chromosome, autosomes and mitochondria, those males will produce functional nullo-X sperm, and consequently, a high number of males during an outcross. X chromosome will fail to attract subcellular compartments during male spermatogenesis, leading to asymmetric segregation of mitochondria to daughter cells. Males resulting from a cross between APS14 male and APS7 female were backcrossed to their maternal mother for successive generations (Figure 5.1). However, genotyping males, after several generations of crosses, indicated that they inherited the maternal X chromosome rather than the paternal X as previously suggested.

Further investigation of X chromosome inheritance in age-controlled crosses on the first day of adulthood by Thomas Murrell (Personal communication) indicated that sons resulting from APS7 female crossed with APS14 male inherited paternal X chromosome. However, the reciprocal cross inherited the maternal X chromosome and produced very few males if none. Since APS14 X chromosome transmission to sons is age-dependent, it may have affected previous attempts to introgress the APS14 X chromosome into the mitochondria and cellular background of APS7 female for several generations.

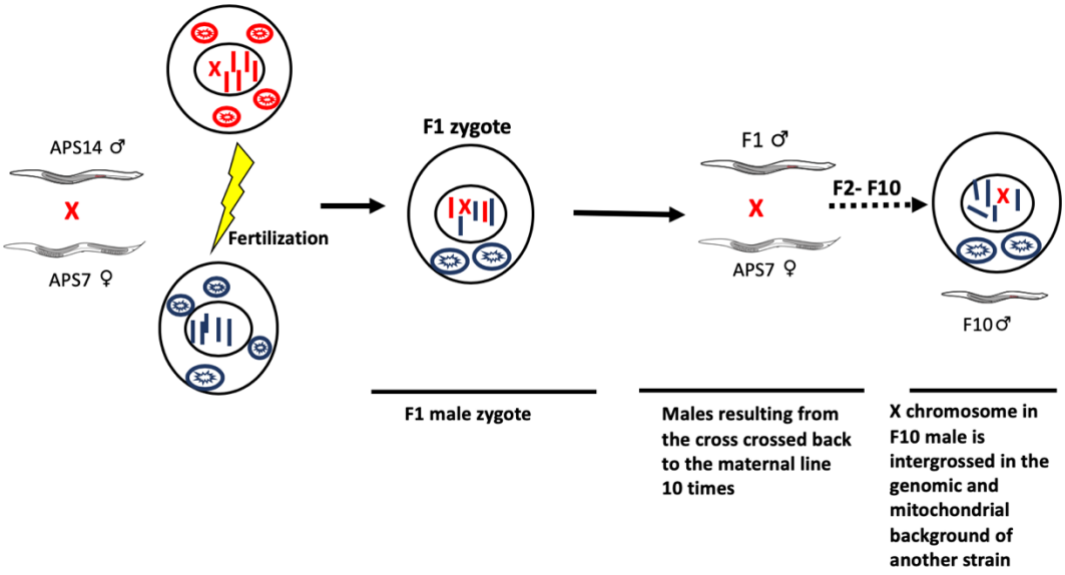

Figure 5.1: APS14 males X chromosomes introgression into the background of APS7 female.
Males resulting from a cross between APS14 male and APS7 female were backcrossed to their maternal mother for successive generations.

5.3.1. Investigating *A. freiburgensis* hermaphrodite meiosis

A. rhodensis hermaphrodites predominantly produce diplo-X sperm and nullo-X oocyte [83]. Therefore, a cross between a male and a hermaphrodite will always produce male cross progeny. Since hermaphrodites predominantly produce nullo-X oocyte, introgression of the polymorphic X chromosome in male cross progeny will be almost certain. We hypothesised that *A. freiburgensis* hermaphrodite meiosis is similar to *A. rhodensis* since it generally produces XX animals when it self-fertilises [69]. To investigate *A. freiburgensis* hermaphrodite meiosis, EMS-mutagenesis was preformed to identify morphologically mutant *A. freiburgensis* hermaphrodite, any morphological mutant with distinctive body morphology will be good. If *A. freiburgensis* hermaphrodites predominantly produce nullo-X oocyte, then I hypothesised that a cross between wildtype male and a morphologically mutant hermaphrodite would only produce males' cross progeny, that are heterozygous for the morphological mutation but wildtype looking (Figure 1.7C). A homozygous morphologically mutant hermaphrodite will produce homozygous mutant progeny through self-fertilisation, but if crossed with a wildtype male it will produce only males' cross progeny that are a wildtype looking but heterozygous for the mutation (Figure 1.7C).

A. freiburgensis (APS7) Morphological mutants were recovered from EMS-chemical wide mutagenesis. In the first mutagenesis, 290 F1 plates were screened and identified one roller, two uncs, and one dumpy. However, it was difficult to maintain the mutations by moving a mutated animal to a fresh new plate. Moving a mutated animal to a fresh new plate produced mutants and wildtype nematodes. It seemed as the mutation was not penetrant enough. Despite changing the temperature to check if the mutation was temperature-dependent, mutated animals continued to produce wildtype and mutated animals. This problem persisted until I lost the mutants. Research in the development of *A. freiburgensis* revealed that *A. freiburgensis* hermaphrodites in uncrowded plates produce females and crowding conditions dauer/hermaphrodites [69]. Therefore, F1 *A. freiburgensis* hermaphrodites isolated in an individual plate only produced females. It was challenging to maintain mutation using female mutants mated with wild type or heterozygote males since they will produce a mixture of mutant and wild type animals in the next generation. A new screen design was introduced, once a mutation was found, several mutated females were moved to a single plate to induce crowding and increase the chance of dauer formation that is homozygous for the mutation. Homozygote dauers for the mutation produced by impregnated females will be separated to separate plates to maintain a homozygous line of the mutation.

In the second EMS mutagenesis, 250 F1 plates were screened by Thomas Murrell (Personal communication) to identify a mutant that exhibited a transparent phenotype. Recovered mutant lacked the dark pigmentation identified in wt animals. Recovered F2 female mutants were isolated into a separate plate approx, ten animals per plate (Figure 5.2). This procedure was conducted to induce dauer formation and produce daures that are homozygous for the mutation. Dauers were isolated to separate plates to develop to hermaphrodites. A homozygous hermaphrodite for the mutation will produce a population that is homozygous for the mutation. The mutant was named *A. freiburgensis* APS28 *clear-1* [*(Afr-clr-1-brz-4)*]. Those mutants were morphologically different from wildtype; however, they reproduced normally.

A cross between *A. freiburgensis clear-1* and wildtype male failed to produce male cross progeny that are wildtype. In all crosses, *A. freiburgensis clear-1* hermaphrodite only produced *Afr-clr-1* clear mutants demonstrating difficulties in crossing the two sexes.

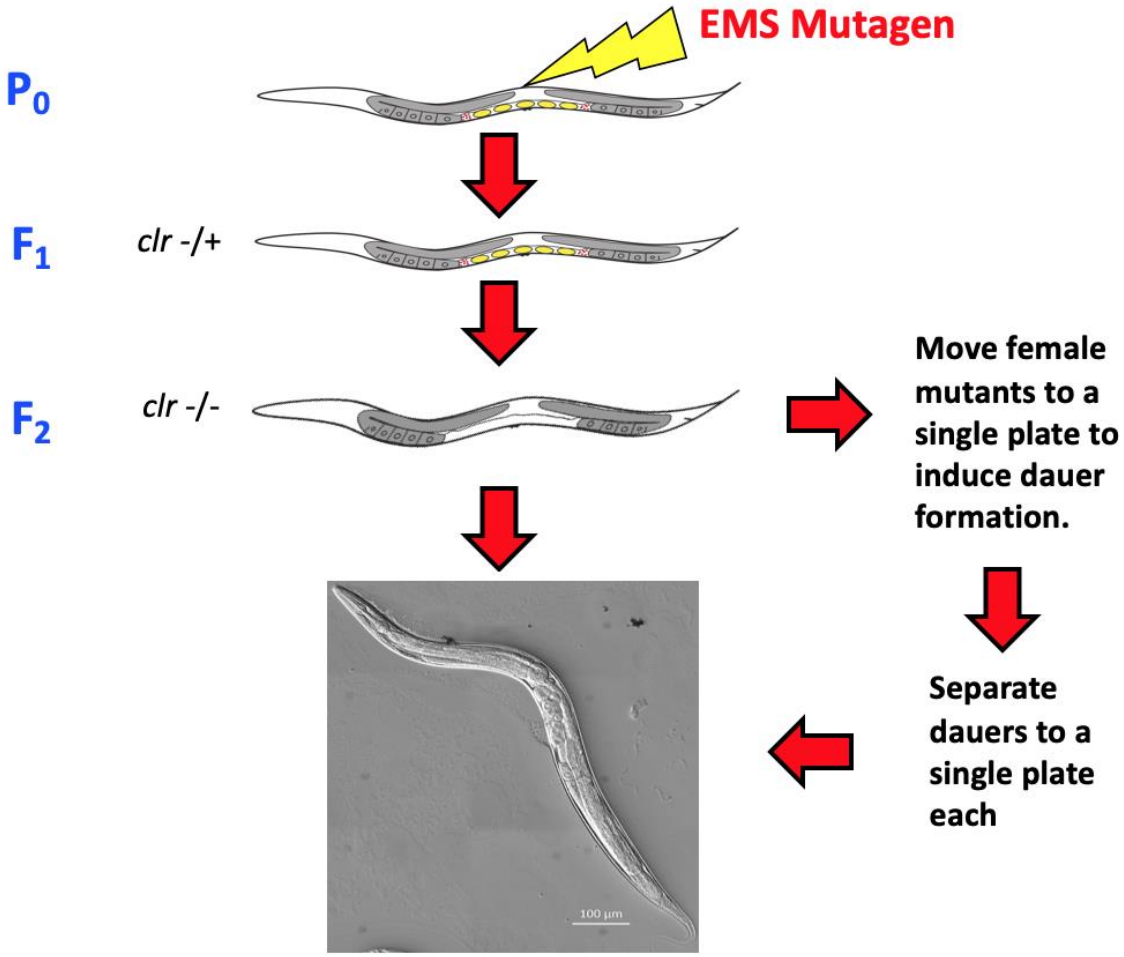

Figure 5.2: EMS-mutagenesis screen identified *A. freiburgensis clear-1* mutant.
A. freiburgensis clear-1 were recovered in the F2 generation from a mugginsed P0. *A. freiburgensis* generally produce females in isolation; therefore, recovered F2 female mutants were isolated to a single plate to induce crowding condition and produce dauers. Dauers were isolated to a separate plate each and left to develop to hermaphrodites, a homozygous hermaphrodite for the mutation will generate only mutant animals.

5.4. Conclusion

X chromosome introgression from one strain into the cellular and autosomal background of another strain in *A. freiburgensis* did not follow the expected pattern. Even though *A. freiburgensis* and *A. rhodensis* belong to the same genus, the meiosis in the two species is not similar. *A. freiburgensis* has more genetic diversity than *A. rhodensis* since F2-derived RILs in *A. freiburgensis* generated a new transgressive phenotype but not in *A. rhodensis*. Therefore, I hypothesised that the introgression of the X chromosome from one strain into the molecular and cellular background of another strain in *A. freiburgensis* would have a significant effect due to the genetic diversity between APS7 and APS14 strain.

Paternal to son X chromosome transmission in *A. freiburgensis* only occurs in age-controlled crosses, on the first day of adulthood between APS7 female and APS14 male but not in the reciprocal cross. As a result, it was challenging to introgress the X chromosome from one strain into the cellular background of another for several generations.

The X chromosome introgression experiment was designed to investigate if genes expressed by the X chromosome interact with autosomes and mitochondria in wildtype *A. freiburgensis* strains to achieve the asymmetric segregation of sperm components with the X chromosome. However, BSA analysis on RIAILs identified four candidate regions just on the X chromosome, to be responsible for the asymmetric segregation of sperm components with the X chromosome. Polygenes expressed only on the X responsible for asymmetric segregation of sperm components. When this group of polygenes located on the X chromosome are able to interact sperm components co-segregate with the X chromosome. However, when the interaction between the group of polygenes located on the X chromosome is disrupted by RIAILs X chromosome mosaic shuffling, sperm components segregate symmetrically. Even if I managed to introgress the X chromosome from APS14 strain into the mitochondrial and autosomal background of APS7, I do not expect a significant change to those males' spermatogenesis. As long as the group of polygenes located on the X chromosome are from the same strain and able to interact, sperm components will co-segregate asymmetrically with the X chromosome.

A. freiburgensis can still be used as a model to investigate mito-nuclear interactions and its effect on embryonic lethality as in *C. nouraguensis* [199]. APS14 female crossed with APS7 males will produce females with APS14 mitochondria and Some chromosomes from APS7. Females resulting from the cross backcrossed to their paternal line for several generation will have mitochondria from one strain introgressed in the genetic background of another strain. Mito-nuclear interaction effect on embryonic lethality can be investigated using those females. This experiment is not related to the investigation of X chromosome as a polarising signal. However, it a suggestion of a future project that stemmed from my investigation in this thesis.

Chapter 6

Conclusions and future directions

6.1. Conclusions

6.1.1. *Auanema* nematode is a unique model to study asymmetric cell division

Auanema nematode is a unique model offers an easy-to-score phenotype to study asymmetric cell division, where divisions occurring in the second meiosis of males spermatogenesis can be determined by ratio of sex progeny of that male. Wildtype *A. rhodensis* male produce low number of males when crossed with a female, 1.6-2.3 % of the total cross progeny are male [69]. Similarly, *A. freiburgensis* male produces skewed sex ratio during an outcross, where male progeny ratio is around 18% [69]. This remarkable production of skewed sex ratio is attributed to the production of only one kind of sperm, an X bearing sperm (Figure 1.10). During the second anaphase of *Auanema* male spermatogenesis, sperm components important for sperm function and motility exclusively segregate to the pole inheriting the lagging-X chromosome (Figure 1.9 and 1.10). Investigation in this study identified X chromosome as a polarising signal causing asymmetric segregation of sperm components exclusively with the X chromosome. X chromosome of *Auanema* harbours genomic region involved in mono-orientation of sperm components exclusively with the lagging-X in the second anaphase of male spermatogenesis.

6.1.2. In all examples of *A. rhodensis* spermatogenesis, including masculiniser mutant, sperm components co-segregate with the X chromosome

In all *A. rhodensis* spermatogenesis examples, sperm components in anaphase II always co-segregate with the X chromosomes. During the spermatogenesis of *A. rhodensis* OX (male), XX (hermaphrodite), and XX masculinisers, sperm components important for sperm function and motility segregate exclusively to the sperm inheriting X chromosomes, while the cell without the X (nullo-X cell)

inherits discarded materials and behave as a residual body. Spermatogenesis in *A. rhodensis* hermaphrodite predominantly produce duplo-X sperm; where, in the second anaphase of hermaphrodite spermatogenesis, sperm components segregate asymmetrically exclusively with the pole inheriting duplo-X chromosomes, while tubulin is discarded in the nullo-X cell (Figure 3.1). To investigate further if the X chromosome is a polarising signal in XX spermatocyte, a masculiniser (*Arh-mas-1*) an XX pseudomale was generated using EMS chemical mutagenesis (Figure 3.3). A masculiniser mutant was generated in *A. rhodensis* rather than in *A. freiburgensis* simply because all previous cytological studies on male spermatogenesis were undertaken on *A. rhodensis* male, however males from both species exclusively produce X-bearing sperm as indicated by the brood skewed sex ratio after an outcross. Sexing and genotyping of *Arh-mas-1* brood indicates that *Arh-mas-1* spermatogenesis produces X-bearing, nullo-X and duplo-X sperms in different proportions (Figure 3.9). In the second anaphase of *A. rhodensis Arh-mas-1* spermatogenesis MSP and mitochondria in anaphase II either segregate symmetrically with X chromosomes or asymmetrically to the cell that inherits X chromosomes. In the event of asymmetric segregation mitochondria and MSP segregate to the cell with the more significant DNA mass, due to its inheritance of X chromosomes, while the other nullo-X cell takes the role of a residual body and inherits discarded materials such tubulin (Figure 3.12 and 3.14). Multiple patterns of lagging-X chromosomes were observed in *Arh-mas-1* male anaphase II including, 1X, 2X, 3X and 4X lagging-X chromosomes (Figure 3.15). Patterns of lagging-X chromosomes observed in the second anaphase are dependent on the way unpaired X chromosomes segregate in the first anaphase (Figure 3.14). Multiple segregation patterns of X chromosome in anaphase I and anaphase II are expected depending on whether sister chromatids of unpaired X chromosomes split and segregate equally or the X chromosome segregate without splitting (Figure 3.14). The unequal segregation of X chromosomes in the first anaphase is manifested by the unequal distribution of DNA between two secondary spermatocyte (Figure 3.12A). However, different patterns of X chromosomes segregation in the second anaphase were determined by the number and structure of lagging-X chromosome. Structure of the lagging-X was determined because lagging-X chromosome from two sister chromatids has bigger DAPI surface area compared to lagging-X chromosome from a single

chromatid (Figure 3.14). In conclusion, in the event of asymmetric segregation in anaphase II during *Arh-mas-1* spermatogenesis sperm components always segregate with the cell inheriting the lagging-X chromosomes, while the nullo-X cell behaves as a residual body, were cellular materials are discarded.

The first sign of asymmetric segregation in anaphase II of *A. rhodensis* spermatogenesis is the lagging of X chromosomes. MSP and mitochondria remain positioned in the central region of the dividing cell as long as lagging-X chromosomes are centrally positioned. However, once lagging-X chromosomes are incorporated into one anaphase plate, MSP and mitochondria segregate exclusively to the cell inheriting the lagging-X. Lagging-X chromosomes in anaphase result from equi-merotelic kinetochores (equi Latin roots term for equal), where those kinetochores has equal number of microtubules oriented towards both poles [202-205]. Chromosomes lags due to the equal pulling force experienced by equi-merotelic kinetochores from both poles [202]. The highlight of meiosis is that every one round of DNA replication is followed by two rounds of chromosome segregation, resulting in reduction in ploidy [206]. During meiosis one, sister chromatids co-segregate together enabling the separation of homologues chromosomes. However, in the second meiosis, sister chromatids separate [206]. In the first meiosis co-segregation of sister chromatids in a range of different organisms is suggested to be due to fusion of sister kinetochores [207, 208]. Fused kinetochores in meiosis I harbours more microtubules binding elements than kinetochores from meiosis II, therefore, forming a stronger attachment with microtubes and direct sister chromatids to co-segregate together [206]. In the first anaphase of *A. rhodenis* male spermatogenesis, X chromosome sister kinetochores were separated despite fusion and sister chromatids segregate equally. The separation of X chromosome sister kinetochores in meiosis I is probably due to their weak cohesion as a result of *A. rhodensis* small X chromosome (3.6 Mb) [200]. Kinetochores in nematodes are holocentric extending along each chromatid [209, 210]. Therefore, the small *A. rhodensis* X chromosomes will have weaker sister kinetochores cohesion in the first meiosis compared to other big chromosomes. In the second anaphase of *A. rhodenis* male spermatogenesis, X chromosome (from a single chromatid) will have a merotelic kinetochore, where equal number of microtubules will be oriented to both poles.

As a result lagging X chromosome is observed in the second anaphase of male spermatogenesis. Since all chromosomes in the second metaphase are from two sister chromatids but only X chromosome is from a single chromatid, only X chromosome will have a merotelic kinetochore causing it to lag during the second anaphase (Figure 3.1). In *A. rhodenis Arh-mas-1*spermatogenesis segregation of X chromosome does not follow a predictable pattern as in male or hermaphrodite spermatogenesis. Multiple variations are expected in *A. rhodenis Arh-mas-1* spermatogenesis depending on the segregation of X chromosome sister kinetochores in the first meiosis. Sister kinetochores of the unpaired X chromosomes either segregate and separate equally or co-segregate together. In the second anaphase a variation of lagging-X chromosomes were observed depending on the number of X chromosome inherited from the first meiosis.

6.1.3. RIAILs genome mosaic shuffling resulted in a transgressive phenotype

Auanema short life cycle and its amenability for genetic to generate Recombinant Inbred Advanced Intercross lines (RIAILs) was utilised to map genomic regions of the underlying phenotype (Figure 4.2). The genomic region regulating X chromosome mediated asymmetric segregation of sperm components in *Auanema* male was mapped by generating *A. freiburgensis* RIAILs. *A. freiburgensis* mating dynamics enables the production of highly advanced RIAILs; Males cross with females increased haplotype breakpoints introduced by meiosis and inbreeding by hermaphrodite selfing brought all introduced breakpoints into homozygosity. At the end of the inbreeding scheme, genome of RIAILs was a mosaic mix from *A. freiburgensis* APS7 and APS14 parental genome. In some RIAILs, mosaic shuffling of its genome disrupted the wildtype interaction of a linked group of polygenes resulting in the production of a novel transgressive phenotype, where 64% of RIAIL lines produced a high number of males. *A. freiburgensis* provides easy-to-score phenotype, where the kind of divisions occurring in male germline can be determined from its brood sex ratio after an outcross (Figure. 4.4). Males from HM-RIAILs lines produced a high number of males after an outcross with a wildtype female due to their ability to produce functional nullo-X sperm. Mosaic shuffling of its genome disrupted the wildtype epistatic interaction between the X chromosome and sperm components leading to symmetric segregation of sperm

components irrespective of lagging-X chromosome orientation, consequently viable nullo-X sperm produced. *A. freiburgensis* RIAILs were not organised into a continuous phenotype, in terms of their production of nullo-X sperms, because there were many environmental variables that affected scoring the exact ratio of nullo-X sperms produced. Production of nullo-X sperm was determined from the ratio of male broods resulting from males from RIAILs cross with wildtype female. However, in addition to production of functional nullo-X sperms by males from HM-RIAILs production of males in each cross is influenced by the ratio of nullo-X oocyte produced by wild type females in each cross, the age of individuals involved in the cross and the period of the cross. Therefore, RIAILs phenotype was sorted into two discrete phenotypes; high male RIAILS and low male RIAILs. The wildtype interaction between X chromosome and sperm components is disrupted in HM-RIAILs because of their genome mosaic shuffling results in symmetric segregation of sperm components producing a functional nullo-X sperm, that led to production of high number of males during an outcross. Whereas, in LM-RIAILs genome shuffling retained the wildtype phenotype of asymmetric segregation of sperm components with the X bearing sperm, exclusively producing X-bearing sperm. Genomic mapping using bulk segregant analysis (BSA) was conducted to correlate observed phenotype with the genotype rather than Genomic linkage map (GLM), Even though whole genome was extracted from all RIAILs lines separately and APS14 maternal strain. Bulk segregant analysis offers a cheaper, faster and affective approach to map genomic regions of interest.

6.1.4. BSA analysis identified candidates regions on the X chromosome

X chromosome of *A. freiburgensis* harbours genomic regions essential for establishing unipolar segregation of sperm components with the X chromosome. Four candidate regions belonging to four different scaffolds were identified to underlie the observed transgressive phenotype in RIAILs using BSA analysis (Figure 4.8). Macrosynteny analysis with closely related *A. rhodensis* genome revealed that identified scaffolds with candidate regions belong to the X chromosome of *A. freiburgensis* (Figure 4.9). Therefore, genetic elements on four location on the X chromosome of *A. freiburgensis* epistatically interact together to

achieve asymmetric segregation of sperm components with the X chromosome. Disruption of this epistatic interaction by shuffling X chromosome with haplotype blocks from two different *A. freiburgensis* strains results in symmetric segregation of sperm components in HM-RIAILs. X chromosome in HM-RIAILs fails to establish its wildtype function of guiding and reorganising sperm components to exclusively segregate with the X-bearing pole. Molecular network controlling the asymmetric portioning of sperm components with the X chromosome were not completely determined in this thesis and remain an area of investigation in the future. I expect genetic elements expressed by the X chromosome during the second meiosis of male spermatogenesis to influence the polarisation of the actomyosin complex to achieve the unipolar segregation of MSP and mitochondria with the X chromosome (Figure 4. 15).

The unique inheritance of X chromosome in *Auanema*, where X chromosome in sons is inherited paternally, enables the production of males that have X chromosome from one strain, while autosomes and cellular background will be from another stain. However, the introgression of *A. freiburgensis* APS14 X chromosome into the background of *A. freiburgensis* APS7 female did not follow the expected pattern. Paternal X chromosome transmission only occurs in age-controlled crosses, on the first day of adulthood (Thomas Murrell, Personal communication). As a result, it was challenging to produce *A. freiburgensis* male with X chromosome introgresed into the background of a polymorphic strain to study X chromosome interaction with mitochondria. However, mixing the genome of the two *A. freiburgensis* strains through the generation of highly recombinant RIAILs resulted in a transgressive phenotype. 59% of RIAILs produced unusual high percentage of males indicating that the wildtype mito-nuclear interaction in males from those lines have been disrupted, and hence, those males are able to produce nullo-X sperm. BSA analysis identified candidate regions only on the X chromosome to be involved in X chromosome segregation and spatial rearrangement of cytoplasm during *Auanema* spermatogenesis. Interaction between a group of polygenes on the X chromosome was disrupted by the RIAILs genome mosaic shuffling resulting in a transgressive phenotype. Therefore, if the complete X chromosome from one strain is introgressed into the genetic background of another strain, it will not have a drastic effect to its

spermatogenesis, as long as the group of polygenes on the X are from the same strain and able to interact.

In multicellular organisms intrinsic factors controlling the polarity of asymmetric cell division are poorly understood without the influence of an extrinsic factor. Our understanding of asymmetric cell division in stem cells and vertebrate relies in transferring the knowledge gained from studying asymmetric cell division in model organisms. This study highlights a new intrinsic mechanism to control polarisation during asymmetric cell division, where X chromosome polarises cytoplasm unipolarly, and establishes *Auanema* as a model organism to study asymmetric cell division. The molecular network involved in creating the asymmetric segregation of cytoplasmic components was not entirely characterised in this study. However, this is a new study that highlights sex chromosome (X chromosome) to be involved in creating an intrinsic polarisation signal for asymmetric cell division in multicellular organisms.

6.2. Future Directions

In this study genomic region underlies asymmetric segregation of sperm components asymmetric with the X chromosome during *Auanema* spermatogenesis was located on the X chromosome. Identifying the molecular mechanism involved in creating the asymmetry will help our current understanding of asymmetric cell division or possibly outline a new mechanism of asymmetric cell division. In order to precisely determine the location of QTLs that were mapped provisionally using BSA analysis, a genetic linkage map (GLM) must be produced to provide chromosome resolution. Individual RIAILs genome was recently sequenced using Illumina sequencing (30 X coverage) to generate linkage map and precisely determine *A. freiburgensis* chromosomes resolution. BSA analysis combined with QTL analysis using data from individual RIAILs on the new *A. freiburgensis* genome, organised to linkage group, will determine the prices location and size of candidate regions. Candidate genes identified from BSA and QTL analysis can be investigated for their role in the underlying phenotype depending on their inheritance in individual RIAILs.

Inheritance of candidate genes in RIAILs can be investigated by the inheritance of SNPs on or close to the candidate gene, using data from the vcf file of each RIAIL line. Candidate genes identified will be knocked out using CRISPR/Cas9 to generate mutant, and assay the phenotypic consequence on sex ratio following male outcross [211].

Live imaging of organelles, X chromosome and Myosin and cytoskeleton in wildtype *Auanema* male will determine the timing of events during cell divisions. *A. rhodensis* secondary spermatocyte division takes about 2 hours as determine by the vital dye Hochest used to label the DNA. This is long enough time for temporal resolution to take into accounts exposure time and different optical sections. Until recently nematode male spermatocyte couldn't be cultured outside the gonad [212]. Recently a protocol has been established to culture spermatocyte *in vitro*[185]. Live *in vitro* culture of *Auanema* spermatocyte will enable live tracking of cellular events following X chromosome segregation. Mitochondria can be tracked by generating *A. rhodensis* transgenic line with fluorescent-marked mitochondrial protein; GFP reporter for Cox-4, a mitochondrial cytochrome c oxidase subunit. Chromosomes including the X chromosome can be labelled by a fusion of mCherry protein with histone H2B (*his-58*) under the control of a germline promoter of the gene *pi1-1*. X chromosome can be recognised easily since it is the only chromosome that lags during anaphase [58, 59, 92]. Non-muscle myosin can be tracked in cultured spermatocyte *in vitro* by fusion with GFP reporter generating *A. rhodensis* males expressing GFP::NMY-2[185]. Myosin VI can be tracked *in vitro* by generating a transgenic *A. rhodensis* male expressing GFP::SPE-15 [185]. Furthermore, conducting live imaging of HM-RIAILs male spermatocyte expressing GFP::NMY-2 will validate our prediction that non-muscle myosin II fails to polarise and actively transport mitochondria and MSP exclusively to the X-bearing pole. Whereas, non-muscle myosin polarisation in LM-RIAILs will be similar to that of wildtype male. Those transgenic lines can be created using CRISPR/Cas9 a method recently described for *Auanema* [211].

Appendix A

Table A.1: *A. rhodensis* X chromosome markers.

Marker	APS4 allele	APS6 allele	Restriction enzyme	Allele that gets cut	Primers	Size of undigested amplicon	sizes after digestion
9686	CATCTG	CATATG	NdeI	APS6	UW231/UW232	666	533 / 133
7963	GGTC	GGCC	HaeIII	APS6	UW239/UW242	450	290 / 160
12469	GTAC	GCAC	RsaI	APS4	UW235/UW236	400	327 / 73

Primers

UW231

Orientation Forward

Sequence 5’-TGTCCTGACCCGCGTGTTGA-3’

UW232

Orientation Reverse

Sequence 5’-AACTGAGTTTGCAGCCCTGT-3’

UW239

Orientation Froward

Sequence 5’-TGGTGGGGCTTGGAGTTCGA-3’

UW240

Orientation Reverse

Sequence 5’-ACGGCTGATGTTGACGCTC-3’

UW235
Orientation Forward
Sequence 5’-TGCAAGGCAGACGTCCCTTG-3’
UW236
Orientation Reverse
Sequence 5’-CCAATTCTTCGCTTATTGCCCG-3’

Appendix B

Table B.1: Males from RIAILs crosses with wildtype APS7 females.
Table outlines RIAILs lines number, its corresponding phenotype, number of XX and XO progeny produced in each separate cross. Binomial distribution for the probability of 0.18 (ratio of males produced in wildtype crosses) was calculated for all the lines using number of males as number of success and total number of progeny as (n). Beta distribution of probability of 0.18 was calculated using number of males as α and number of females as β. Binomial and Beta distribution were calculated to assess the success and failure of the proportion of males in each line, using the wt male ratio of 0.18 as probability (p). Line numbers labelled with yellow indicates that crosses data are not available, while genome is available, and * indicates where data are missing. Cells shaded in green indicates that beta distribution was not calculated because number of success α is equal to 0.

Line number	Males Production High/normal	XX	XO (Number of sucesses)	Total (n)	Binomial.dist (probablity of 0.18)	Beta (probablity of 0.18)
1	High	22	35	57	3.8123E-13	2.05477E-13
2	Normal	64	2	66	0.000211865	3.81673E-05
3	Normal	87	7	94	0.001989928	0.001159855
4	Normal	40	8	48	0.148414842	0.371610473
5	Normal	154	7	161	1.59282E-07	4.63747E-08
6	Normal	140	7	147	1.33863E-06	4.35342E-07
7	Normal	33	0	33	0.001431717	
8	Normal	78	5	83	0.001039336	0.000443403
9	Normal	106	10	116	0.002130773	0.00159399
10	High	48	37	85	3.35201E-08	3.14962E-08
11	High	37	17	54	0.006672026	0.00956626
12	High	55	43	98	2.11846E-09	1.97429E-09
13	Normal	33	0	33	0.001431717	
14	Normal	49	0	49	5.98245E-05	
15	Normal	40	1	41	0.002633968	0.000356906
16	High	41	19	60	0.00423835	0.006078788
17	Normal	*	*	*	*	*
18	Normal	84	8	92	0.005907506	0.004375498
19	High	68	40	108	1.46635E-06	1.73652E-06
20	Normal	71	20	91	0.063302783	0.181033464
21	High	26	43	69	3.82313E-16	2.00473E-16

22	**Normal**	77	5	82	0.001191128	0.000516032
23	**High**	117	65	182	6.52441E-09	8.25615E-09
24	**High**	19	29	48	6.72421E-11	3.73118E-11
25	**Normal**	59	2	61	0.000487544	9.55484E-05
26	**Normal**	73	0	73	5.10989E-07	
27	**Normal**	70	3	73	0.000336163	8.72216E-05
28	**High**	26	26	52	1.23497E-07	9.40841E-08
29	**High**	106	79	185	4.31549E-15	4.22126E-15
30	**High**	20	36	56	2.29772E-14	1.12651E-14
31	**Normal**	42	0	42	0.000239984	
32	**Normal**	85	0	85	4.72256E-08	
33	**high**	31	35	66	1.17324E-10	8.20143E-11
34	**Normal**	103	0	103	1.32687E-09	
35	**High**	15	16	31	1.85982E-05	1.33225E-05
36	**high**	46	33	79	5.39277E-07	5.35562E-07
37	**Normal**	129	11	140	0.000332039	0.000217321
38	**Normal**	76	2	78	2.74128E-05	4.13598E-06
39	**Normal**	63	0	63	3.71769E-06	
40	**Normal**	43	3	46	0.017421476	0.007751505
41	**Normal**	47	0	47	8.89715E-05	
42	**high**	37	25	62	2.29847E-05	2.37693E-05
43	**high**	48	38	86	1.3655E-08	1.25673E-08
44	**high**	59	30	89	0.000167959	0.000225793
45	**high**	93	60	153	4.1689E-10	4.59107E-10
46	**high**	59	61	120	2.91411E-16	2.19413E-16
47	**high**	19	21	40	6.94053E-07	4.87935E-07
48	**Normal**	*	*	*	*	*
49	**High**	24	38	62	4.15487E-14	2.2498E-14
50	**Normal**	40	0	40	0.000356906	
51	**Normal**	230	16	246	9.53767E-08	4.83829E-08
52	**Normal**	36	0	36	0.000789403	
53	**Normal**	51	3	54	0.005818965	0.002137704
54	**High**	35	35	70	9.28886E-10	7.11941E-10
55	**High**	88	59	147	2.01245E-10	2.14283E-10
56	**high**	22	18	40	5.66692E-05	4.9744E-05
57	**High**	28	15	43	0.003948041	0.004848931
58	**High**	71	134	205	1.96091E-50	9.34272E-51
59	**High**	67	36	103	1.8994E-05	2.43899E-05
60	**high**	38	35	73	3.77598E-09	3.08214E-09
61	**High**	54	55	109	1.19801E-14	9.11405E-15
62	**High**	28	32	60	5.90705E-10	4.08543E-10
63	**High**	29	48	77	7.50154E-18	3.93525E-18

64	High	119	81	200	6.43257E-14	6.7942E-14
65	High	54	39	93	4.9195E-08	4.87927E-08
66	Normal	60	5	65	0.010523685	0.006182772
67	High	40	32	72	1.50125E-07	1.36487E-07
68	High	81	77	158	1.04163E-18	8.38713E-19
69	Normal	107	4	111	3.77161E-06	8.58945E-07
70	Normal	66	6	72	0.010892774	0.007320412
71	High	28	22	50	1.41563E-05	1.29138E-05
72	High	21	11	32	0.012845783	0.015696605
73	High	21	17	38	9.74611E-05	8.60611E-05
74	Normal	47	2	49	0.003390029	0.000841671
75	High	30	23	53	1.20352E-05	1.12089E-05
76	High	42	31	73	7.60761E-07	7.36988E-07
77	Normal	78	0	78	1.89444E-07	
78	High	20	23	43	1.34919E-07	9.2275E-08
79	Normal	*	*	*	*	*
80	High	115	83	198	3.24319E-15	3.26028E-15
81	High	42	78	120	8.22512E-30	3.95974E-30
82	High	19	49	68	2.48928E-22	9.20501E-23
83	Normal	62	4	66	0.003430168	0.001443648
84	High	34	21	55	0.00022676	0.000250992
85	High	18	21	39	4.02043E-07	2.71451E-07
86	High	40	32	72	1.50125E-07	1.36487E-07
87	High	61	32	93	7.06215E-05	9.23576E-05
88	High	42	47	89	1.08477E-13	7.66599E-14
89	High	16	21	37	1.23458E-07	7.63252E-08
90	High	22	36	58	1.10557E-13	5.83355E-14
91	High	54	36	90	5.94074E-07	6.28574E-07
92	Normal	32	0	32	0.001745996	
93	High	48	28	76	5.10588E-05	6.01564E-05
94	Normal	36	3	39	0.042074104	0.022938784
95	Normal	70	0	70	9.26765E-07	
96	High	28	34	62	6.45125E-11	4.26645E-11
97	High	39	25	64	4.20474E-05	4.5437E-05
98	High	89	0	89	2.13517E-08	
99	High	16	17	33	1.06574E-05	7.671E-06
100	Normal	84	0	84	5.75922E-08	
101	Normal	128	34	162	0.047963483	0.175988727
102	High	29	70	99	2.06413E-30	8.06902E-31
103	High	20	23	43	1.34919E-07	9.2275E-08
104	high	32	20	52	0.000280444	0.000306612
105	Normal	79	0	79	1.55344E-07	

106	**Normal**	84	0	84	5.75922E-08	
107	**high**	*	*	*	*	*
108	**High**	21	42	63	2.25295E-17	1
109	**High**	Switched to line 33			*	*
110	**High**	Switched to line 73			*	*
probability	**0.18**					
	DNA available but not the line					
*	**data not available**					
	beta distribution not calculated number of success = 0					

Table B.3: DNA pools and their constituting lines.
Pools were constructed by pipetting a volume from each line containing 150ng of DNA, from total Qubit fluorometer concentration measured in the lab, to make up a total concentration of 1.5ug of DNA of each pool. The reported concentration for each pool was reported to us by the sequencing company upon receiving the samples.

Sample	Lines constituting the pool	Phenptype	Amount received in (ug)	Volume (uL)
APS14	Maternal line	Maternal line (LM)	5.5	120
Pool1	5,9,54,77,74,2,13,14,17,20	LM	2.7	175
Pool2	61,23,24,28,29,30,33,36,45,57	HM	3.6	77
Pool3	35,42,46,55,56,59,63,65,72,87	HM	4.5	120
Pool4	6,8,15,18,25,37,40,69,95,27	LM	2.3	80

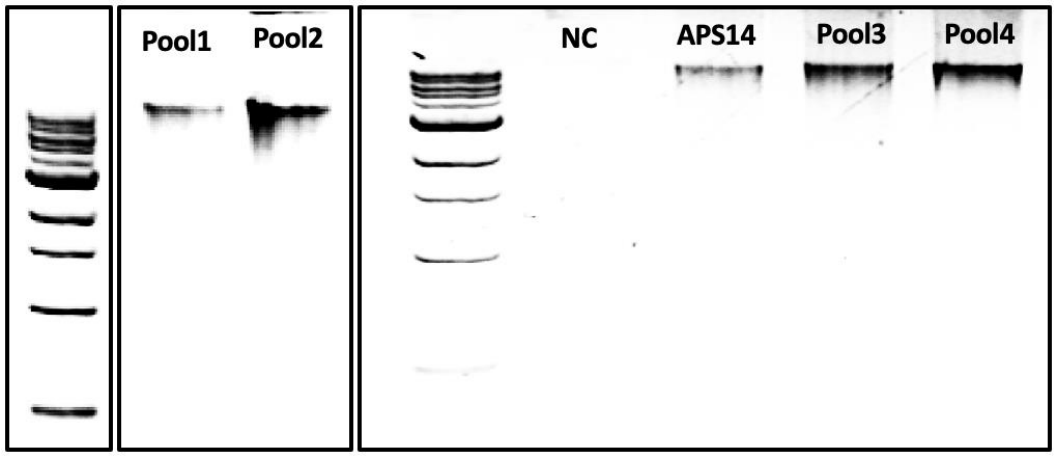

Figure B.1: Gel image assessing the quality of RIAILs DNA pools.
Pools DNA was constructed from RIAILs with a similar phenotype. Four DNA pools were created 2 HM-Pools (1 & 4) and 2 LM-Pools (2 & 3). Besides, DNA from maternal line APS14 was extracted for sequencing.

Table B.2: Number of reads in all DNA samples and results of trimming low-quality reads.
The table represents the number of reads as reported by FastQC Html file.

Sample	strain	Library type	Raw reads	Trimmed reads	Kept %
APS14-1	APS14	PE	111466603	107728015	96.64
APS14-2	APS14	PE	111466603	107728015	96.64
Pool1-1	RIAILs	PE	101559334	97655752	96.15
Pool1-2	RIAILs	PE	101559334	97655752	96.15
Pool2-1	RIAILs	PE	95145518	91069393	95.71
Pool2-2	RIAILs	PE	95145518	91069393	95.71
Pool3-1	RIAILs	PE	97615600	92874421	95.14
Pool3-2	RIAILs	PE	97615600	92874421	95.14
Pool4-1	RIAILs	PE	95361733	91739956	96.20
Pool4-2	RIAILs	PE	95361733	91739956	96.20

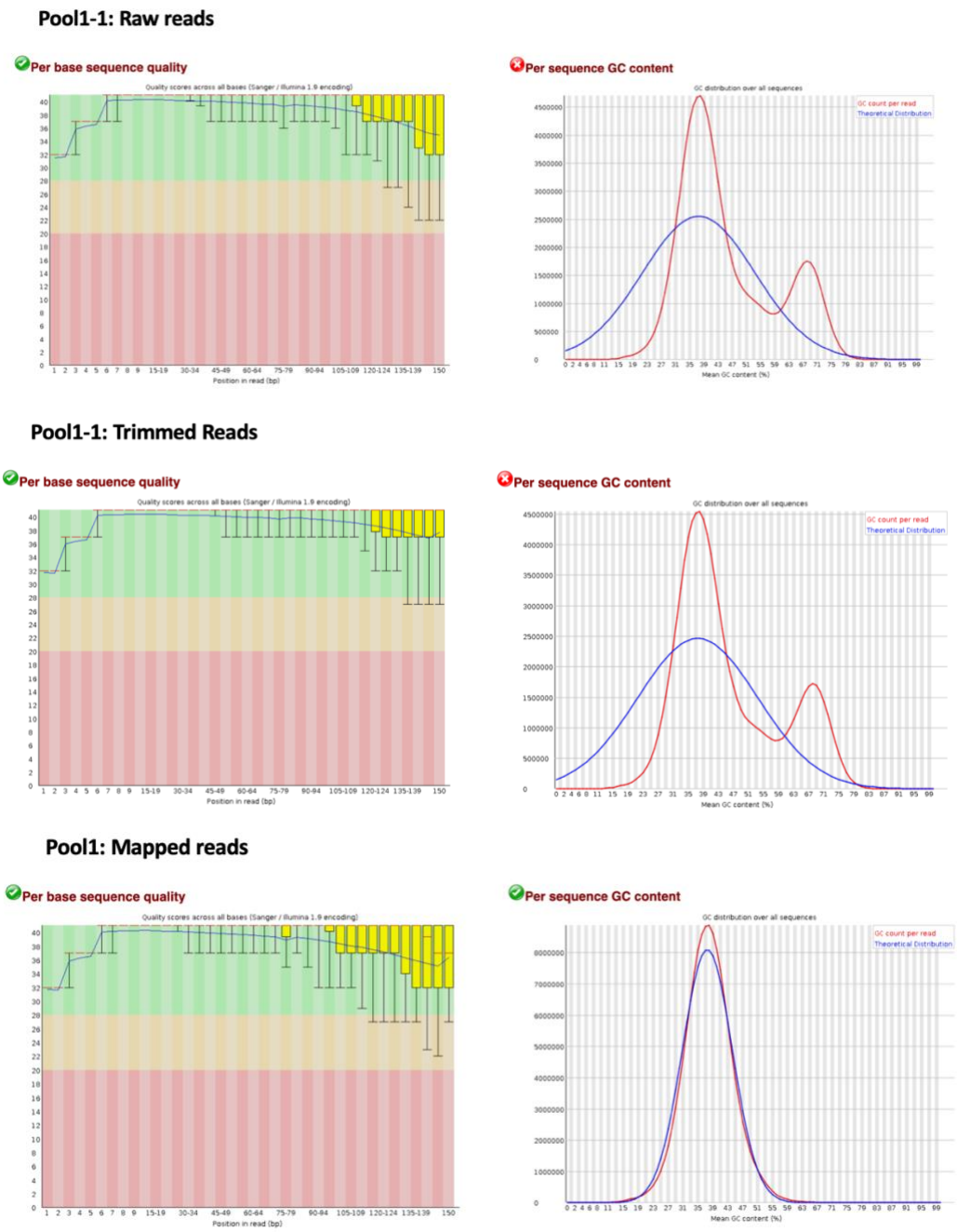

Figure B.2: Quality check using FastQC of raw reads, trimmed reads, and mapped reads against the APS7 genome.
Quality score across all bases for pool1-1 raw reads improved after trimming the reads using trimmomatic; however, the per sequence GC content revealed two GC peaks, the lower peak represents GC content for nematode reads, and the higest peak represent the GC content of bacterial contaminant. After mapping trimmed reads to the reference APS7 genome, only nematode sequences aligned to the reference and bacterial reads were eliminated. Therefore, FastQC of the aligned file revealed one GC content peak after aligning trimmed reads with the APS7 genome.

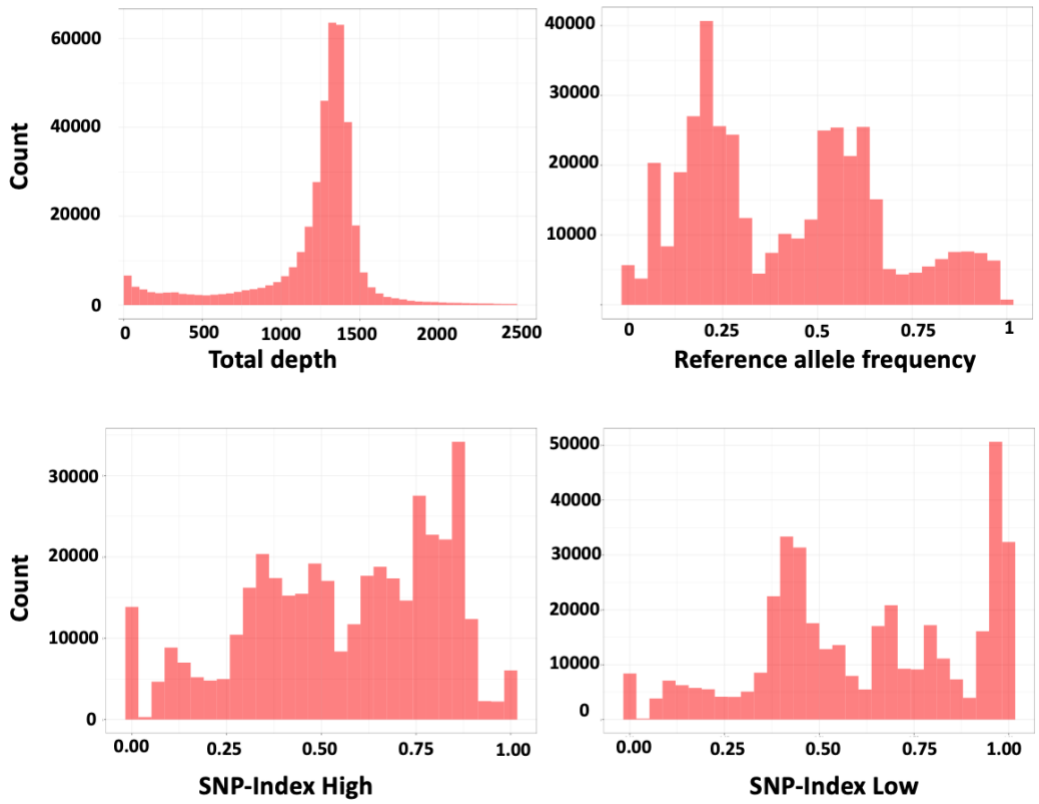

Figure B.3: Histogram Plots of total read depth, reference allele frequency, and per bulk SNP-Index.
Per bulk, SNP-index has a small peak at 0 and 1. SNP-index of 0 indicates that the reads at that SNP position have the reference allele. SNP-index of 1 indicates that all the reads at that SNP position have the alternative allele. Filtering low confidence, SNPs will eliminate small peaks at 0 and 1 from both bulks SNP-index.

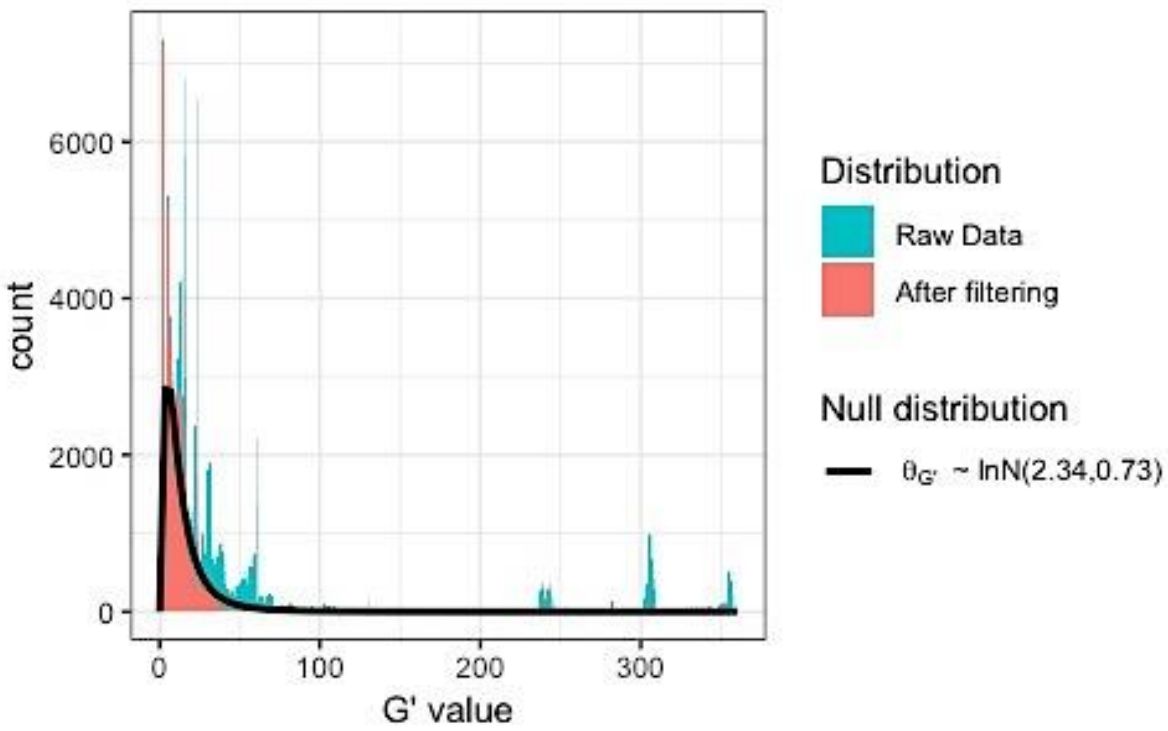

Figure B.4: G' Value distribution.
P-value is calculated from the null distribution of G'. The graph illustrates that the null distribution of filtered G' values (red) is close to log-normally distribution compared to raw data (blue).

Table B.4: Percentages of SNP effects by impact between APS14 and APS7 reference genome.

Number of effects by impact

Type (alphabetical order)	Count	Percent
HIGH	2,075	0.113%
LOW	104,887	5.728%
MODERATE	24,971	1.364%
MODIFIER	1,699,119	92.795%

Table B.5: Number of effects and percentages by functional class reported by SnpEff.

Number of effects by functional class

Type (alphabetical order)	Count	Percent
MISSENSE	24,276	25.402%
NONSENSE	211	0.221%
SILENT	71,079	74.377%

Missense / Silent ratio: 0.3415

Table B.6: Number of effects by their type and location within the genome.

Number of effects by type and region

Type

Type (alphabetical order)	Count	Percent
3_prime_UTR_truncation	2	0%
3_prime_UTR_variant	45,164	2.423%
5_prime_UTR_premature_start_codon_gain_variant	3,565	0.191%
5_prime_UTR_truncation	2	0%
5_prime_UTR_variant	28,209	1.513%
bidirectional_gene_fusion	8	0%
conservative_inframe_deletion	147	0.008%
conservative_inframe_insertion	166	0.009%
disruptive_inframe_deletion	241	0.013%
disruptive_inframe_insertion	275	0.015%
downstream_gene_variant	634,780	34.054%
exon_loss_variant	4	0%
frameshift_variant	1,127	0.06%
initiator_codon_variant	3	0%
intergenic_region	166,895	8.953%
intragenic_variant	5	0%
intron_variant	224,227	12.029%
missense_variant	24,154	1.296%
non_coding_transcript_variant	83	0.004%
splice_acceptor_variant	196	0.011%
splice_donor_variant	424	0.023%
splice_region_variant	33,481	1.796%
start_lost	65	0.003%
stop_gained	247	0.013%
stop_lost	104	0.006%
stop_retained_variant	133	0.007%
synonymous_variant	70,946	3.806%
upstream_gene_variant	629,374	33.764%

Region

Type (alphabetical order)	Count	Percent
DOWNSTREAM	634,780	34.668%
EXON	95,231	5.201%
GENE	8	0%
INTERGENIC	166,895	9.115%
INTRON	194,632	10.63%
SPLICE_SITE_ACCEPTOR	187	0.01%
SPLICE_SITE_DONOR	411	0.022%
SPLICE_SITE_REGION	32,529	1.777%
TRANSCRIPT	88	0.005%
UPSTREAM	629,374	34.372%
UTR_3_PRIME	45,146	2.466%
UTR_5_PRIME	31,771	1.735%

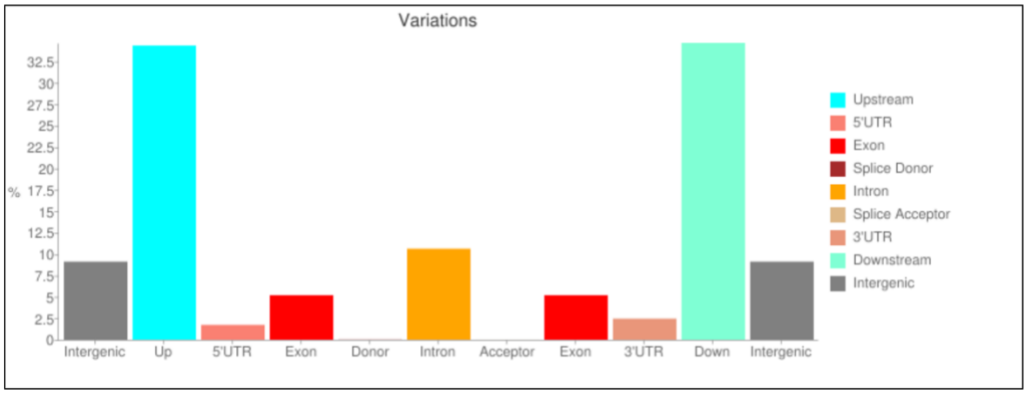

Figure B.5: Bar chart illustrating the percentage of APS14 SNP effects by location within the genome:

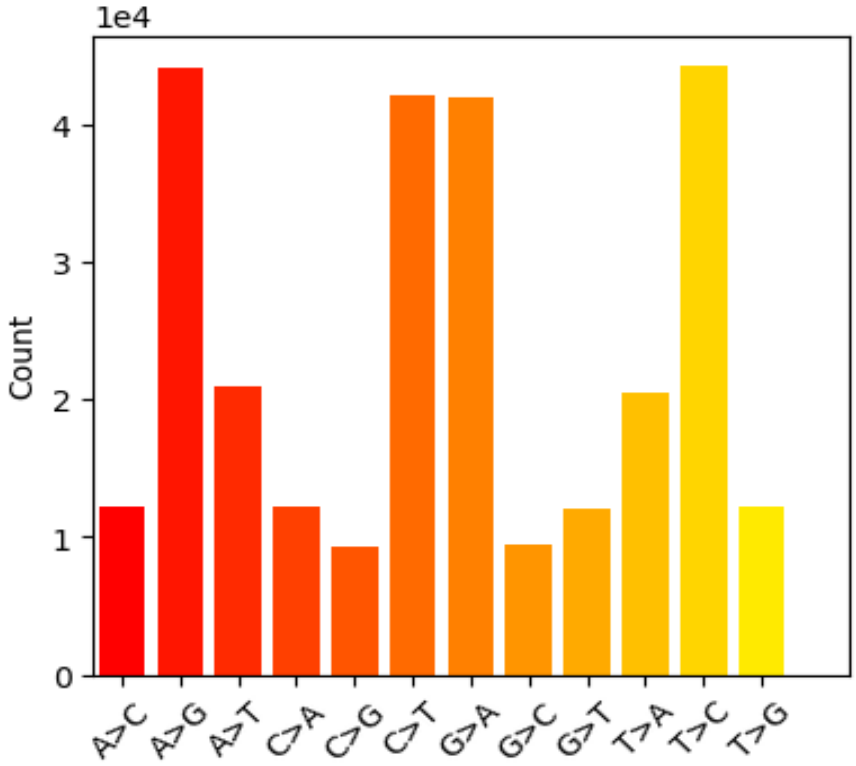

Figure B.6: Bar chart represents APS14 SNPs substitutions count with other bases.

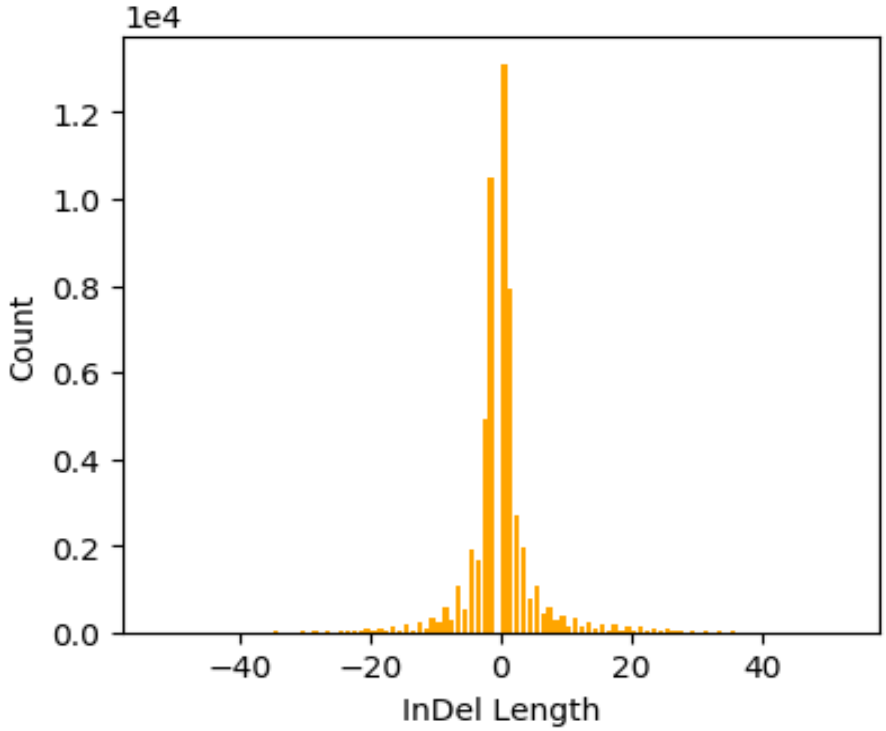

Figure B.7: APS14 InDel length plotted against the count.
InDel length count normally distributes around InDel length of 0, with the highest InDel count close to 0.

Table B.7: Markers used to investigate RIAILs inheritance of mitochondria, Non-muscle myosin, and Myosin XVIII.

Marker	Experiment(s) Used	Primers	Restriction Enzyme and buffer	Amplicon size (bp)	Sizes of digested fragments (bp)
X Chromosome	RIAIL analysis	UW594 & UW595	BamHI & Buffer E	909	637 & 272
Mitochondria	RIAIL analysis	UW580 & UW581	AluI & Buffer B	582	352 & 230
Non-muscle Myosin	RIAIL analysis	UW602 & UW603	HindIII & Buffer E	617	70 & 547
Myosin XVIII	RIAIL analysis	UW600 & UW601	RsaI & Buffer C	623	80 & 543

Primer sequences (5'- 3'):

- **UW265**- CAGCTGGTCTTGTCGCCAGAAAG
- **UW280**- ACTTCATTCAAATCTGCTTGAAC
- **UW594**- TGGAGCTTCTACAGTCAAGACACCA
- **UW595**- CGTCGTCACGGAAGCAGCTT
- **UW580**- ACTAGAGGTGCTGAAAAACCA
- **UW581**- AGGTACAGCAGGATTTTTACGT
- **UW600**- AAACCCGGCGTTGATACTGT
- **UW601**- CTGAGCTCAGCAAAGTTCGC
- **UW602**- ACACGTTTTCCCCACGATGA
- **UW603**- ATCACTTTGCGACTGGGAGG

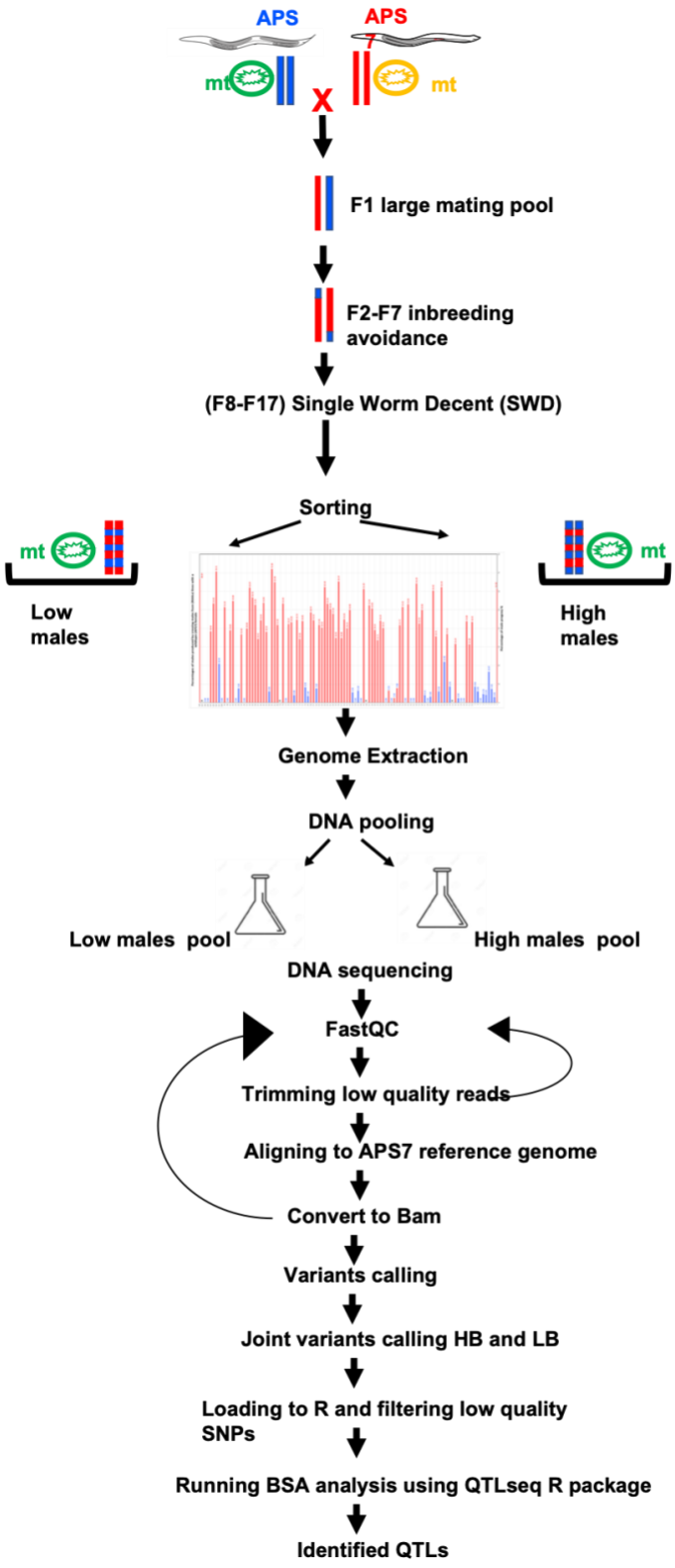

Figure B.8: A map of all the steps taken from RIAILs construction to the identification of QTLs.

Appendix C

Table C.1: Marker used to investigate X chromosome pattern of inheritance in *A. freiburgensis.*

Marker Name	Primers	Restriction Enzyme and buffer	Amplicon size (bp)	Sizes of digested fragments (bp)
X Chromosome	UW265 & UW280	HindIII & Buffer E	385	75 & 310

Primer sequences (5'- 3'):

- **UW265**- CAGCTGGTCTTGTCGCCAGAAAG
- **UW280**- ACTTCATTCAAATCTGCTTGAAC

Bibliography

1. Kaltschmidt, J.A. and A.H. Brand, *Asymmetric cell division: microtubule dynamics and spindle asymmetry.* Journal of Cell Science, 2002. **115**(11): p. 2257.
2. Horvitz, H.R. and I. Herskowitz, *Mechanisms of asymmetric cell division: two Bs or not two Bs, that is the question.* Cell, 1992. **68**(2): p. 237-55.
3. Doe, C.Q., *Neural stem cells: balancing self-renewal with differentiation.* Development, 2008. **135**(9): p. 1575-87.
4. Gonczy, P., *Mechanisms of asymmetric cell division: flies and worms pave the way.* Nat Rev Mol Cell Biol, 2008. **9**(5): p. 355-66.
5. Hawkins, N. and G. Garriga, *Asymmetric cell division: from A to Z.* Genes Dev, 1998. **12**(23): p. 3625-38.
6. Venkei, Z.G. and Y.M. Yamashita, *Emerging mechanisms of asymmetric stem cell division.* The Journal of cell biology, 2018. **217**(11): p. 3785-3795.
7. Fuentealba, L.C., et al., *Asymmetric mitosis: Unequal segregation of proteins destined for degradation.* Proc Natl Acad Sci U S A, 2008. **105**(22): p. 7732-7.
8. Berika, M., M.E. Elgayyar, and A.H.K. El-Hashash, *Asymmetric cell division of stem cells in the lung and other systems.* Frontiers in Cell and Developmental Biology, 2014. **2**: p. 33.
9. Kahney, E.W., et al., *Symmetry from Asymmetry or Asymmetry from Symmetry?* Cold Spring Harb Symp Quant Biol, 2017. **82**: p. 305-318.
10. Shlyakhtina, Y., K.L. Moran, and M.M. Portal, *Asymmetric Inheritance of Cell Fate Determinants: Focus on RNA.* Noncoding RNA, 2019. **5**(2).
11. Fuller, M.T. and A.C. Spradling, *Male and Female Drosophila Germline Stem Cells: Two Versions of Immortality.* 2007. **316**(5823): p. 402-404.
12. WHITMAN, C.O., *Memoirs: The Embryology of Clepsine.* 1878. **s2-18**(71): p. 215-315.
13. Conklin, E.G., *Mosaic development in ascidian eggs.* 1905. **2**(2): p. 145-223.
14. Rhyu, M.S., L.Y. Jan, and Y.N. Jan, *Asymmetric distribution of numb protein during division of the sensory organ precursor cell confers distinct fates to daughter cells.* Cell, 1994. **76**(3): p. 477-91.
15. Shahriyari, L. and N.L. Komarova, *Symmetric vs. Asymmetric Stem Cell Divisions: An Adaptation against Cancer?* PLOS ONE, 2013. **8**(10): p. e76195.
16. Knoblich, J.A., *Asymmetric cell division: recent developments and their implications for tumour biology.* Nat Rev Mol Cell Biol, 2010. **11**(12): p. 849-60.
17. Fennell, D.A. and D.M. Jablons, *13 - Stem Cells and Lung Cancer: In Vitro and In Vivo Studies*, in *IASLC Thoracic Oncology (Second Edition)*, H.I. Pass,

D. Ball, and G.V. Scagliotti, Editors. 2018, Content Repository Only!: Philadelphia. p. 117-120.e2.
18. Kahn, M., *Chapter Seven - Wnt Signaling in Stem Cells and Cancer Stem Cells: A Tale of Two Coactivators*, in *Progress in Molecular Biology and Translational Science*, J. Larraín and G. Olivares, Editors. 2018, Academic Press. p. 209-244.
19. Neumuller, R.A. and J.A. Knoblich, *Dividing cellular asymmetry: asymmetric cell division and its implications for stem cells and cancer.* Genes Dev, 2009. **23**(23): p. 2675-99.
20. Chagastelles, P.C. and N.B. Nardi, *Biology of stem cells: an overview.* Kidney International Supplements, 2011. **1**(3): p. 63-67.
21. Morrison, S.J. and J. Kimble, *Asymmetric and symmetric stem-cell divisions in development and cancer.* Nature, 2006. **441**(7097): p. 1068-1074.
22. Gómez-López, S., R.G. Lerner, and C. Petritsch, *Asymmetric cell division of stem and progenitor cells during homeostasis and cancer.* Cellular and molecular life sciences : CMLS, 2014. **71**(4): p. 575-597.
23. Cicalese, A., et al., *The tumor suppressor p53 regulates polarity of self-renewing divisions in mammary stem cells.* Cell, 2009. **138**(6): p. 1083-95.
24. Colaluca, I.N., et al., *NUMB controls p53 tumour suppressor activity.* Nature, 2008. **451**(7174): p. 76-80.
25. Katajisto, P., et al., *Asymmetric apportioning of aged mitochondria between daughter cells is required for stemness.* Science (New York, N.Y.), 2015. **348**(6232): p. 340-343.
26. Rizzuto, R., et al., *Mitochondria as sensors and regulators of calcium signalling.* Nature Reviews Molecular Cell Biology, 2012. **13**(9): p. 566-578.
27. Butow, R.A. and N.G. Avadhani, *Mitochondrial Signaling.* Molecular Cell. **14**(1): p. 1-15.
28. Wang, X., *The expanding role of mitochondria in apoptosis.* Genes Dev, 2001. **15**(22): p. 2922-33.
29. Duchen, M.R., *Mitochondria and calcium: from cell signalling to cell death.* The Journal of physiology, 2000. **529 Pt 1**(Pt 1): p. 57-68.
30. McFaline-Figueroa, J.R., et al., *Mitochondrial quality control during inheritance is associated with lifespan and mother-daughter age asymmetry in budding yeast.* Aging Cell, 2011. **10**(5): p. 885-95.
31. Ramadasan-Nair, R., et al., *Mitochondrial alterations and oxidative stress in an acute transient mouse model of muscle degeneration: implications for muscular dystrophy and related muscle pathologies.* The Journal of biological chemistry, 2014. **289**(1): p. 485-509.
32. Stauch, K.L., P.R. Purnell, and H.S. Fox, *Aging synaptic mitochondria exhibit dynamic proteomic changes while maintaining bioenergetic function.* Aging, 2014. **6**(4): p. 320-334.
33. Hughes, A.L. and D.E. Gottschling, *An early age increase in vacuolar pH limits mitochondrial function and lifespan in yeast.* Nature, 2012. **492**(7428): p. 261-5.

34. Green, D.R., L. Galluzzi, and G. Kroemer, *Mitochondria and the autophagy-inflammation-cell death axis in organismal aging.* Science, 2011. **333**(6046): p. 1109-12.
35. Park, C.B. and N.G. Larsson, *Mitochondrial DNA mutations in disease and aging.* J Cell Biol, 2011. **193**(5): p. 809-18.
36. Higuchi-Sanabria, R., et al., *Role of asymmetric cell division in lifespan control in Saccharomyces cerevisiae.* FEMS yeast research, 2014. **14**(8): p. 1133-1146.
37. Lu, B., L.Y. Jan, and Y.N. Jan, *Asymmetric cell division: lessons from flies and worms.* Curr Opin Genet Dev, 1998. **8**(4): p. 392-9.
38. Spana, E.P., et al., *Asymmetric localization of numb autonomously determines sibling neuron identity in the Drosophila CNS.* Development, 1995. **121**(11): p. 3489-94.
39. Betschinger, J., K. Mechtler, and J.A. Knoblich, *Asymmetric segregation of the tumor suppressor brat regulates self-renewal in Drosophila neural stem cells.* Cell, 2006. **124**(6): p. 1241-53.
40. Lee, C.Y., et al., *Brat is a Miranda cargo protein that promotes neuronal differentiation and inhibits neuroblast self-renewal.* Dev Cell, 2006. **10**(4): p. 441-9.
41. Guo, M., L.Y. Jan, and Y.N. Jan, *Control of daughter cell fates during asymmetric division: interaction of Numb and Notch.* Neuron, 1996. **17**(1): p. 27-41.
42. Lu, B., et al., *Partner of Numb colocalizes with Numb during mitosis and directs Numb asymmetric localization in Drosophila neural and muscle progenitors.* Cell, 1998. **95**(2): p. 225-35.
43. Wodarz, A., et al., *Bazooka provides an apical cue for Inscuteable localization in Drosophila neuroblasts.* Nature, 1999. **402**(6761): p. 544-7.
44. Schober, M., M. Schaefer, and J.A. Knoblich, *Bazooka recruits Inscuteable to orient asymmetric cell divisions in Drosophila neuroblasts.* Nature, 1999. **402**(6761): p. 548-51.
45. Rolls, M.M., et al., *Drosophila aPKC regulates cell polarity and cell proliferation in neuroblasts and epithelia.* J Cell Biol, 2003. **163**(5): p. 1089-98.
46. Cowan, C.R. and A.A. Hyman, *Centrosomes direct cell polarity independently of microtubule assembly in C. elegans embryos.* Nature, 2004. **431**(7004): p. 92-6.
47. Munro, E. and B. Bowerman, *Cellular symmetry breaking during Caenorhabditis elegans development.* Cold Spring Harbor perspectives in biology, 2009. **1**(4): p. a003400-a003400.
48. Marston, D.J. and B. Goldstein, *Symmetry breaking in C. elegans: another gift from the sperm.* Developmental cell, 2006. **11**(3): p. 273-274.
49. Zonies, S., et al., *Symmetry breaking and polarization of the C. elegans zygote by the polarity protein PAR-2.* Development, 2010. **137**(10): p. 1669.
50. Tsai, M.C. and J. Ahringer, *Microtubules are involved in anterior-posterior axis formation in C. elegans embryos.* J Cell Biol, 2007. **179**(3): p. 397-402.

51. Munro, E., J. Nance, and J.R. Priess, *Cortical flows powered by asymmetrical contraction transport PAR proteins to establish and maintain anterior-posterior polarity in the early C. elegans embryo.* Dev Cell, 2004. **7**(3): p. 413-24.
52. Broadus, J. and C.Q. Doe, *Extrinsic cues, intrinsic cues and microfilaments regulate asymmetric protein localization in Drosophila neuroblasts.* Curr Biol, 1997. **7**(11): p. 827-35.
53. Shen, C.P., et al., *Miranda as a multidomain adapter linking apically localized Inscuteable and basally localized Staufen and Prospero during asymmetric cell division in Drosophila.* Genes Dev, 1998. **12**(12): p. 1837-46.
54. Knoblich, J.A., *Asymmetric cell division during animal development.* Nat Rev Mol Cell Biol, 2001. **2**(1): p. 11-20.
55. Jan, Y.N. and L.Y. Jan, *Asymmetric cell division in the Drosophila nervous system.* Nat Rev Neurosci, 2001. **2**(11): p. 772-9.
56. Wirtz-Peitz, F., T. Nishimura, and J.A. Knoblich, *Linking cell cycle to asymmetric division: Aurora-A phosphorylates the Par complex to regulate Numb localization.* Cell, 2008. **135**(1): p. 161-173.
57. Zhao, P., et al., *Aurora-A Breaks Symmetry in Contractile Actomyosin Networks Independently of Its Role in Centrosome Maturation.* Dev Cell, 2019. **48**(5): p. 631-645.e6.
58. Winter, E.S., et al., *Cytoskeletal variations in an asymmetric cell division support diversity in nematode sperm size and sex ratios.* Development, 2017.
59. Shakes, D.C., et al., *Asymmetric spermatocyte division as a mechanism for controlling sex ratios.* Nat Commun, 2011. **2**: p. 157.
60. Klar, A.J., *Determination of the yeast cell lineage.* Cell, 1987. **49**(4): p. 433-5.
61. Klar, A.J.S., *Differentiated parental DNA strands confer developmental asymmetry on daughter cells in fission yeast.* Nature, 1987. **326**: p. 466.
62. Singh, J., et al., *Cdc23/Mcm10 Primase Generates the Lagging Strand-Specific Ribonucleotide Imprint in Fission Yeast.* bioRxiv, 2018.
63. Staiber, W., *Asymmetric distribution of mitochondria and of spindle microtubules in opposite directions in differential mitosis of germ line cells in Acricotopus.* Cell Tissue Res, 2007. **329**(1): p. 197-203.
64. Bauer, H. and W. Beermann, *Der Chromosomencyclus der Orthocladiinen (Nematocera, Diptera)*, in *Zeitschrift für Naturforschung B*. 1952. p. 557.
65. Staiber, W., *Germline-specific labeling of the somatic chromosomes by protein phosphatase 2A and histone H3S28 phosphorylation in Acricotopus lucidus.* Protoplasma, 2017. **254**(5): p. 1983-1993.
66. Bauer, H., *Rearrangements between germ-line limited and somatic chromosomes in Smittia parthenogenetica (Chironomidae, Diptera).* Chromosoma, 1970. **32**(1): p. 1-10.
67. Staiber, W., *Centrosome hyperamplification with the formation of multiple asters and programmed chromosome inactivation in aberrant spermatocytes during male meiosis in Acricotopus.* Cell and Tissue Research, 2008. **334**(1): p. 81-91.

68. Félix, M.-A., *Alternative morphs and plasticity of vulval development in a rhabditid nematode species.* Development Genes and Evolution, 2004. **214**(2): p. 55-63.
69. Kanzaki, N., et al., *Description of two three-gendered nematode species in the new genus Auanema (Rhabditina) that are models for reproductive mode evolution.* Scientific Reports, 2017. **7**(1): p. 11135.
70. Denver, D.R., K.A. Clark, and M.J. Raboin, *Reproductive mode evolution in nematodes: insights from molecular phylogenies and recently discovered species.* Mol Phylogenet Evol, 2011. **61**(2): p. 584-92.
71. Thomas, C.G., G.C. Woodruff, and E.S. Haag, *Causes and consequences of the evolution of reproductive mode in Caenorhabditis nematodes.* Trends Genet, 2012. **28**(5): p. 213-20.
72. Pires-daSilva, A., *Evolution of the control of sexual identity in nematodes.* Seminars in Cell & Developmental Biology, 2007. **18**(3): p. 362-370.
73. Denver, D.R., K.A. Clark, and M.J. Raboin, *Reproductive mode evolution in nematodes: Insights from molecular phylogenies and recently discovered species.* Molecular Phylogenetics and Evolution, 2011. **61**(2): p. 584-592.
74. Kiontke, K., et al., *Caenorhabditis phylogeny predicts convergence of hermaphroditism and extensive intron loss.* 2004. **101**(24): p. 9003-9008.
75. Hill, R.C., et al., *Genetic Flexibility in the Convergent Evolution of Hermaphroditism in Caenorhabditis Nematodes.* Developmental Cell, 2006. **10**(4): p. 531-538.
76. Bachtrog, D., et al., *Sex determination: why so many ways of doing it?* PLoS Biol, 2014. **12**(7): p. e1001899.
77. Merchant-Larios, H. and V. Diaz-Hernandez, *Environmental sex determination mechanisms in reptiles.* Sex Dev, 2013. **7**(1-3): p. 95-103.
78. Strome, S., et al., *Regulation of the X Chromosomes in Caenorhabditis elegans.* Cold Spring Harbor Perspectives in Biology, 2014. **6**(3): p. a018366.
79. Ercan, S., *Mechanisms of x chromosome dosage compensation.* Journal of genomics, 2015. **3**: p. 1-19.
80. Chaudhuri, J., V. Kache, and A. Pires-daSilva, *Regulation of Sexual Plasticity in a Nematode that Produces Males, Females, and Hermaphrodites.* Current Biology, 2011. **21**(18): p. 1548-1551.
81. Chaudhuri, J., et al., *Mating dynamics in a nematode with three sexes and its evolutionary implications.* Scientific Reports, 2015. **5**: p. 17676.
82. Edwards, A.W., *Carl Dusing (1884) on the regulation of the sex-ratio.* Theor Popul Biol, 2000. **58**(3): p. 255-7.
83. Tandonnet, S., et al., *Sex- and Gamete-Specific Patterns of X Chromosome Segregation in a Trioecious Nematode.* Current Biology, 2018. **28**(1): p. 93-99.e3.
84. Nishimura, H. and S.W. L'Hernault, *Spermatogenesis-defective (spe) Mutants of the Nematode Caenorhabditis elegans Provide Clues to Solve the Puzzle of Male Germline Functions during Reproduction.* Developmental Dynamics, 2010. **239**(5): p. 1502-1514.

85. Ward, S., Y. Argon, and G.A. Nelson, *Sperm morphogenesis in wild-type and fertilization-defective mutants of Caenorhabditis elegans.* The Journal of cell biology, 1981. **91**(1): p. 26-44.
86. Wolf, N., D. Hirsh, and J.R. McIntosh, *Spermatogenesis in males of the free-living nematode, Caenorhabditis elegans.* Journal of Ultrastructure Research, 1978. **63**(2): p. 155-169.
87. Kasimatis, K.R. and P.C. Phillips, *Rapid Gene Family Evolution of a Nematode Sperm Protein Despite Sequence Hyper-conservation.* G3 (Bethesda, Md.), 2018. **8**(1): p. 353-362.
88. King, K.L., et al., *Structure and macromolecular assembly of two isoforms of the major sperm protein (MSP) from the amoeboid sperm of the nematode, Ascaris suum.* J Cell Sci, 1992. **101 (Pt 4)**: p. 847-57.
89. Tarr, D.E. and A.L. Scott, *MSP domain proteins show enhanced expression in male germ line cells.* Mol Biochem Parasitol, 2004. **137**(1): p. 87-98.
90. Kasimatis, K.R., et al., *Proteomic and evolutionary analyses of sperm activation identify uncharacterized genes in Caenorhabditis nematodes.* BMC Genomics, 2018. **19**(1): p. 593.
91. Roberts, T.M., F.M. Pavalko, and S. Ward, *Membrane and cytoplasmic proteins are transported in the same organelle complex during nematode spermatogenesis.* The Journal of cell biology, 1986. **102**(5): p. 1787-1796.
92. Albertson, D.G. and J.N. Thomson, *Segregation of holocentric chromosomes at meiosis in the nematode, Caenorhabditis elegans.* Chromosome Res, 1993. **1**(1): p. 15-26.
93. Shakes, D.C., et al., *Spermatogenesis-specific features of the meiotic program in Caenorhabditis elegans.* PLoS genetics, 2009. **5**(8): p. e1000611-e1000611.
94. Byerly, L., R.C. Cassada, and R.L. Russell, *The life cycle of the nematode Caenorhabditis elegans. I. Wild-type growth and reproduction.* Dev Biol, 1976. **51**(1): p. 23-33.
95. Avery, L., *The genetics of feeding in Caenorhabditis elegans.* Genetics, 1993. **133**(4): p. 897-917.
96. Brenner, S., *The Genetics of CAENORHABDITIS ELEGANS.* Genetics, 1974. **77**(1): p. 71-94.
97. McCaig, C.M., et al., *Germ cell cysts and simultaneous sperm and oocyte production in a hermaphroditic nematode.* Dev Biol, 2017.
98. Kanzaki, N., et al., *Two androdioecious and one dioecious new species of pristionchus (nematoda: diplogastridae): new reference points for the evolution of reproductive mode.* Journal of nematology, 2013. **45**(3): p. 172-194.
99. Hodgkin, J.A. and S. Brenner, *Mutations causing transformation of sexual phenotype in the nematode Caenorhabditis elegans.* Genetics, 1977. **86**(2 Pt. 1): p. 275-87.
100. Hodgkin, J., *More sex-determination mutants of Caenorhabditis elegans.* Genetics, 1980. **96**(3): p. 649-64.
101. Hodgkin, J., *Primary sex determination in the nematode C. elegans</em&gt.* Development, 1987. **101**(Supplement): p. 5.

102. Hansen, D. and D. Pilgrim, *Sex and the single worm: sex determination in the nematode C. elegans.* Mechanisms of Development, 1999. **83**(1): p. 3-15.
103. Harvey, S.C. and M.E. Viney, *Sex Determination in the Parasitic Nematode Strongyloides ratti</em&gt.* Genetics, 2001. **158**(4): p. 1527.
104. Hodgkin, J., *A genetic analysis of the sex-determining gene, tra-1, in the nematode Caenorhabditis elegans.* Genes Dev, 1987. **1**(7): p. 731-45.
105. Hodgkin, J., *Two types of sex determination in a nematode.* Nature, 1983. **304**(5923): p. 267-268.
106. Pires-daSilva, A. and R.J. Sommer, *Conservation of the global sex determination gene tra-1 in distantly related nematodes.* Genes Dev, 2004. **18**(10): p. 1198-208.
107. Donahue, L.M., B.A. Quarantillo, and W.B. Wood, *Molecular analysis of X chromosome dosage compensation in Caenorhabditis elegans.* Proceedings of the National Academy of Sciences, 1987. **84**(21): p. 7600.
108. Myers, S., et al., *A fine-scale map of recombination rates and hotspots across the human genome.* Science, 2005. **310**(5746): p. 321-4.
109. Carmi, I., J.B. Kopczynski, and B.J. Meyer, *The nuclear hormone receptor SEX-1 is an X-chromosome signal that determines nematode sex.* Nature, 1998. **396**(6707): p. 168-173.
110. Gladden, J.M. and B.J. Meyer, *A ONECUT Homeodomain Protein Communicates X Chromosome Dose to Specify Caenorhabditis elegans Sexual Fate by Repressing a Sex Switch Gene.* Genetics, 2007. **177**(3): p. 1621.
111. Gladden, J.M., B. Farboud, and B.J. Meyer, *Revisiting the X:A Signal That Specifies Caenorhabditis elegans Sexual Fate.* Genetics, 2007. **177**(3): p. 1639.
112. Hodgkin, J., *Sex determination in the nematode C. elegans: analysis of tra-3 suppressors and characterization of fem genes.* Genetics, 1986. **114**(1): p. 15-52.
113. Kutscher, L.M. and S. Shaham, *Forward and reverse mutagenesis in C. elegans.* WormBook : the online review of C. elegans biology, 2014: p. 1-26.
114. Flibotte, S., et al., *Whole-genome profiling of mutagenesis in Caenorhabditis elegans.* Genetics, 2010. **185**(2): p. 431-441.
115. Anderson, P., *Methods in Cell Biology* Vol. 48. 1995: Academic press Inc. .
116. Jorgensen, E.M. and S.E. Mango, *The art and design of genetic screens: Caenorhabditis elegans.* Nat Rev Genet, 2002. **3**(5): p. 356-369.
117. Hodgkin, J., H.R. Horvitz, and S. Brenner, *Nondisjunction Mutants of the Nematode CAENORHABDITIS ELEGANS.* Genetics, 1979. **91**(1): p. 67-94.
118. Vargas, E., et al., *Autosomal Trisomy and Triploidy Are Corrected During Female Meiosis in Caenorhabditis elegans.* Genetics, 2017. **207**(3): p. 911-922.
119. Lant, B. and W.B. Derry, *Fluorescent visualization of germline apoptosis in living Caenorhabditis elegans.* Cold Spring Harb Protoc, 2014. **2014**(4): p. 420-7.

120. Lu, Z.J., et al., *Identification of ATP synthase beta subunit (ATPB) on the cell surface as a non-small cell lung cancer (NSCLC) associated antigen.* BMC Cancer, 2009. **9**: p. 16.
121. Lu, Z., et al., *[Preparation of monoclonal antibody against lung cancer and identification of its targeting antigen].* Sheng Wu Yi Xue Gong Cheng Xue Za Zhi, 2010. **27**(1): p. 147-51.
122. O'Rourke, E.J., et al., *C. elegans major fats are stored in vesicles distinct from lysosome-related organelles.* Cell metabolism, 2009. **10**(5): p. 430-435.
123. Yen, K., et al., *A Comparative Study of Fat Storage Quantitation in Nematode Caenorhabditis elegans Using Label and Label-Free Methods.* PLOS ONE, 2010. **5**(9): p. e12810.
124. Perez, M.F. and B. Lehner, *Vitellogenins - Yolk Gene Function and Regulation in Caenorhabditis elegans.* 2019. **10**(1067).
125. Ezcurra, M., et al., *C. elegans Eats Its Own Intestine to Make Yolk Leading to Multiple Senescent Pathologies.* Current Biology, 2018. **28**(16): p. 2544-2556.e5.
126. D'Hulst, C., et al., *Fast Quantitative Real-Time PCR-Based Screening for Common Chromosomal Aneuploidies in Mouse Embryonic Stem Cells.* Stem Cell Reports, 2013. **1**(4): p. 350-359.
127. Ly, K., S.J. Reid, and R.G. Snell, *Rapid RNA analysis of individual Caenorhabditis elegans.* MethodsX, 2015. **2**: p. 59-63.
128. Broman, K.W., *The Genomes of Recombinant Inbred Lines.* Genetics, 2005. **169**(2): p. 1133-1146.
129. Gao, A.W., et al., *Natural genetic variation in C. elegans identified genomic loci controlling metabolite levels.* Genome research, 2018. **28**(9): p. 1296-1308.
130. Michelmore, R.W., I. Paran, and R.V. Kesseli, *Identification of markers linked to disease-resistance genes by bulked segregant analysis: a rapid method to detect markers in specific genomic regions by using segregating populations.* Proceedings of the National Academy of Sciences of the United States of America, 1991. **88**(21): p. 9828-9832.
131. Pollard, D.A., *Design and construction of recombinant inbred lines.* Methods Mol Biol, 2012. **871**: p. 31-9.
132. Hagiwara, W.E., et al., *Transgressive segregation due to linked QTLs for grain characteristics of rice.* Euphytica, 2006. **150**(1): p. 27.
133. Burga, A., et al., *Fast genetic mapping of complex traits in C. elegans using millions of individuals in bulk.* Nature Communications, 2019. **10**(1): p. 2680.
134. Slatkin, M., *Linkage disequilibrium--understanding the evolutionary past and mapping the medical future.* Nature reviews. Genetics, 2008. **9**(6): p. 477-485.
135. Rockman, M.V. and L. Kruglyak, *Breeding Designs for Recombinant Inbred Advanced Intercross Lines.* Genetics, 2008. **179**(2): p. 1069-1078.
136. Darvasi, A. and M. Soller, *Advanced intercross lines, an experimental population for fine genetic mapping.* Genetics, 1995. **141**(3): p. 1199-207.

137. Snoek, B.L., et al., *A multi-parent recombinant inbred line population of C. elegans allows identification of novel QTLs for complex life history traits.* BMC Biology, 2019. **17**(1): p. 24.
138. Meneely, P.M., A.F. Farago, and T.M. Kauffman, *Crossover distribution and high interference for both the X chromosome and an autosome during oogenesis and spermatogenesis in Caenorhabditis elegans.* Genetics, 2002. **162**(3): p. 1169-77.
139. Pattabiraman, D., et al., *Meiotic recombination modulates the structure and dynamics of the synaptonemal complex during C. elegans meiosis.* PLOS Genetics, 2017. **13**(3): p. e1006670.
140. Dernburg, A.F., et al., *Meiotic Recombination in C. elegans Initiates by a Conserved Mechanism and Is Dispensable for Homologous Chromosome Synapsis.* Cell, 1998. **94**(3): p. 387-398.
141. Wright, S., *Systems of Mating. II. the Effects of Inbreeding on the Genetic Composition of a Population.* Genetics, 1921. **6**(2): p. 124-143.
142. Ross, J.A., et al., *Caenorhabditis briggsae recombinant inbred line genotypes reveal inter-strain incompatibility and the evolution of recombination.* PLoS Genet, 2011. **7**(7): p. e1002174.
143. Muller, H.J., *THE RELATION OF RECOMBINATION TO MUTATIONAL ADVANCE.* Mutat Res, 1964. **106**: p. 2-9.
144. Liu, S., et al., *Intragenic Meiotic Crossovers Generate Novel Alleles with Transgressive Expression Levels.* Molecular biology and evolution, 2018. **35**(11): p. 2762-2772.
145. Lu, P., et al., *Analysis of Arabidopsis genome-wide variations before and after meiosis and meiotic recombination by resequencing Landsberg erecta and all four products of a single meiosis.* Genome research, 2012. **22**(3): p. 508-518.
146. Giraut, L., et al., *Genome-wide crossover distribution in Arabidopsis thaliana meiosis reveals sex-specific patterns along chromosomes.* PLoS Genet, 2011. **7**(11): p. e1002354.
147. Leips, J. and T.F.C. Mackay, *Quantitative Trait Loci for Life Span in Drosophila melanogaster: Interactions With Genetic Background and Larval Density.* 2000. **155**(4): p. 1773-1788.
148. Rieseberg, L.H., M.A. Archer, and R.K. Wayne, *Transgressive segregation, adaptation and speciation.* Heredity, 1999. **83**(4): p. 363-372.
149. Zhang, X., et al., *Candidate genes for first flower node identified in pepper using combined SLAF-seq and BSA.* PLoS One, 2018. **13**(3): p. e0194071.
150. Takagi, H., et al., *QTL-seq: rapid mapping of quantitative trait loci in rice by whole genome resequencing of DNA from two bulked populations.* Plant J, 2013. **74**(1): p. 174-83.
151. Zou, C., P. Wang, and Y. Xu, *Bulked sample analysis in genetics, genomics and crop improvement.* Plant biotechnology journal, 2016. **14**(10): p. 1941-1955.
152. Song, J., et al., *Next-Generation Sequencing from Bulked-Segregant Analysis Accelerates the Simultaneous Identification of Two Qualitative Genes in Soybean.* 2017. **8**(919).

153. Halldén, C., et al., *The use of bulked segregant analysis to accumulate RAPD markers near a locus for beet cyst nematode resistance in Beta vulgaris.* Plant Breeding, 1997. **116**(1): p. 18-22.
154. Magwene, P.M., J.H. Willis, and J.K. Kelly, *The Statistics of Bulk Segregant Analysis Using Next Generation Sequencing.* PLOS Computational Biology, 2011. **7**(11): p. e1002255.
155. Livaja, M., et al., *BSTA: a targeted approach combines bulked segregant analysis with next- generation sequencing and de novo transcriptome assembly for SNP discovery in sunflower.* BMC Genomics, 2013. **14**(1): p. 628.
156. Doitsidou, M., S. Jarriault, and R.J. Poole, *Next-Generation Sequencing-Based Approaches for Mutation Mapping and Identification in Caenorhabditis elegans.* Genetics, 2016. **204**(2): p. 451-474.
157. Doitsidou, M., et al., *C. elegans Mutant Identification with a One-Step Whole-Genome-Sequencing and SNP Mapping Strategy.* PLoS ONE, 2010. **5**(11): p. e15435.
158. Andrews, S. *FastQC: a quality control tool for high throughput sequence data*. 2010; Available from: http://www.bioinformatics.babraham.ac.uk/projects/fastqc.
159. Bolger, A.M., M. Lohse, and B. Usadel, *Trimmomatic: a flexible trimmer for Illumina sequence data.* Bioinformatics (Oxford, England), 2014. **30**(15): p. 2114-2120.
160. Li, H., et al., *The Sequence Alignment/Map format and SAMtools.* Bioinformatics (Oxford, England), 2009. **25**(16): p. 2078-2079.
161. Li, H. and R. Durbin, *Fast and accurate short read alignment with Burrows-Wheeler transform.* Bioinformatics, 2009. **25**(14): p. 1754-60.
162. Keel, B.N. and W.M. Snelling, *Comparison of Burrows-Wheeler Transform-Based Mapping Algorithms Used in High-Throughput Whole-Genome Sequencing: Application to Illumina Data for Livestock Genomes.* Frontiers in genetics, 2018. **9**: p. 35-35.
163. Mansfeld, B.N. and R. Grumet, *QTLseqr: An R Package for Bulk Segregant Analysis with Next-Generation Sequencing.* The Plant Genome, 2018. **11**.
164. McKenna, A., et al., *The Genome Analysis Toolkit: a MapReduce framework for analyzing next-generation DNA sequencing data.* Genome research, 2010. **20**(9): p. 1297-1303.
165. Ren, S., et al., *GPU accelerated sequence alignment with traceback for GATK HaplotypeCaller.* BMC Genomics, 2019. **20**(Suppl 2): p. 184.
166. Brouard, J.S., et al., *The GATK joint genotyping workflow is appropriate for calling variants in RNA-seq experiments.* J Anim Sci Biotechnol, 2019. **10**: p. 44.
167. Disratthakit, A., et al., *An optimized genomic VCF workflow for precise identification of Mycobacterium tuberculosis cluster from cross-platform whole genome sequencing data.* Infect Genet Evol, 2019. **79**: p. 104152.
168. Van der Auwera, G.A., et al., *From FastQ data to high confidence variant calls: the Genome Analysis Toolkit best practices pipeline.* Curr Protoc Bioinformatics, 2013. **43**: p. 11.10.1-33.

169. Carson, A.R., et al., *Effective filtering strategies to improve data quality from population-based whole exome sequencing studies.* BMC Bioinformatics, 2014. **15**(1): p. 125.
170. Benjamini, Y. and Y. Hochberg, *Controlling the False Discovery Rate: A Practical and Powerful Approach to Multiple Testing.* Journal of the Royal Statistical Society: Series B (Methodological), 1995. **57**(1): p. 289-300.
171. Kurtz, S., et al., *Versatile and open software for comparing large genomes.* Genome Biology, 2004. **5**(2): p. R12.
172. Delcher, A.L., et al., *Fast algorithms for large-scale genome alignment and comparison.* Nucleic Acids Res, 2002. **30**(11): p. 2478-83.
173. Delcher, A.L., et al., *Alignment of whole genomes.* Nucleic Acids Res, 1999. **27**(11): p. 2369-76.
174. Krzywinski, M., et al., *Circos: an information aesthetic for comparative genomics.* Genome Res, 2009. **19**(9): p. 1639-45.
175. Narasimhan, V., et al., *BCFtools/RoH: a hidden Markov model approach for detecting autozygosity from next-generation sequencing data.* Bioinformatics (Oxford, England), 2016. **32**(11): p. 1749-1751.
176. Cingolani, P., et al., *A program for annotating and predicting the effects of single nucleotide polymorphisms, SnpEff: SNPs in the genome of Drosophila melanogaster strain w1118; iso-2; iso-3.* Fly (Austin), 2012. **6**(2): p. 80-92.
177. Tillich, M., et al., *GeSeq – versatile and accurate annotation of organelle genomes.* Nucleic Acids Research, 2017. **45**(W1): p. W6-W11.
178. Riva, A., et al., *Streamlining DNA Sequencing and Bioinformatics Analysis Using Software Containers.* J Biomol Tech, 2019. **30**(Suppl): p. S38-s39.
179. Altmann, A., et al., *A beginners guide to SNP calling from high-throughput DNA-sequencing data.* Hum Genet, 2012. **131**(10): p. 1541-54.
180. Rodelsperger, C., et al., *Single-Molecule Sequencing Reveals the Chromosome-Scale Genomic Architecture of the Nematode Model Organism Pristionchus pacificus.* Cell Rep, 2017. **21**(3): p. 834-844.
181. Guiliano, D.B., et al., *Conservation of long-range synteny and microsynteny between the genomes of two distantly related nematodes.* Genome Biology, 2002. **3**(10): p. research0057.1.
182. Fradin, H., et al., *Genome Architecture and Evolution of a Unichromosomal Asexual Nematode.* Current Biology, 2017. **27**(19): p. 2928-2939.e6.
183. Bundus, J.D., D. Wang, and A.D. Cutter, *Genetic basis to hybrid inviability is more complex than hybrid male sterility in Caenorhabditis nematodes.* Heredity (Edinb), 2018.
184. Bundus, J.D., R. Alaei, and A.D. Cutter, *Gametic selection, developmental trajectories, and extrinsic heterogeneity in Haldane's rule.* Evolution, 2015. **69**(8): p. 2005-17.
185. Hu, J., et al., *Distinct roles of two myosins in C. elegans spermatid differentiation.* PLOS Biology, 2019. **17**(4): p. e3000211.
186. Kelleher, J.F., et al., *Myosin VI is required for asymmetric segregation of cellular components during C. elegans spermatogenesis.* Curr Biol, 2000. **10**(23): p. 1489-96.

187. Frank, D.J., T. Noguchi, and K.G. Miller, *Myosin VI: a structural role in actin organization important for protein and organelle localization and trafficking.* Current Opinion in Cell Biology, 2004. **16**(2): p. 189-194.
188. Billington, N., et al., *Myosin 18A coassembles with nonmuscle myosin 2 to form mixed bipolar filaments.* Curr Biol, 2015. **25**(7): p. 942-8.
189. Rogat, A.D. and K.G. Miller, *A role for myosin VI in actin dynamics at sites of membrane remodeling during Drosophila spermatogenesis.* J Cell Sci, 2002. **115**(Pt 24): p. 4855-65.
190. Ernster, L. and G. Schatz, *Mitochondria: a historical review.* J Cell Biol, 1981. **91**(3 Pt 2): p. 227s-255s.
191. Ryan, M.T. and N.J. Hoogenraad, *Mitochondrial-nuclear communications.* Annu Rev Biochem, 2007. **76**: p. 701-22.
192. Scarpulla, R.C., *Nuclear Control of Respiratory Chain Expression in Mammalian Cells.* Journal of Bioenergetics and Biomembranes, 1997. **29**(2): p. 109-119.
193. Cherry, C., et al., *2016: A 'Mitochondria' Odyssey.* Trends in Molecular Medicine, 2016. **22**(5): p. 391-403.
194. Fan, W. and R. Evans, *PPARs and ERRs: Molecular Mediators of Mitochondrial Metabolism.* Current opinion in cell biology, 2015. **33**: p. 49-54.
195. Calvo, S., et al., *Systematic identification of human mitochondrial disease genes through integrative genomics.* Nat Genet, 2006. **38**(5): p. 576-82.
196. Adams, K.L. and J.D. Palmer, *Evolution of mitochondrial gene content: gene loss and transfer to the nucleus.* Mol Phylogenet Evol, 2003. **29**(3): p. 380-95.
197. Brown, W.M., M. George, and A.C. Wilson, *Rapid evolution of animal mitochondrial DNA.* Proceedings of the National Academy of Sciences of the United States of America, 1979. **76**(4): p. 1967-1971.
198. Levin, L., et al., *Mito-nuclear co-evolution: the positive and negative sides of functional ancient mutations.* Front Genet, 2014. **5**.
199. Lamelza, P. and M. Ailion, *Cytoplasmic–Nuclear Incompatibility Between Wild Isolates of <em>Caenorhabditis nouraguensis</em&gt.* G3: Genes|Genomes|Genetics, 2017. **7**(3): p. 823.
200. Tandonnet, S., et al., *Chromosome-Wide Evolution and Sex Determination in the Three-Sexed Nematode <em>Auanema rhodensis</em&gt.* G3: Genes|Genomes|Genetics, 2019. **9**(4): p. 1211.
201. Zuco, G., et al., *Sensory neurons control heritable adaptation to stress through germline reprogramming.* bioRxiv, 2018: p. 406033.
202. Thompson, S.L. and D.A. Compton, *Chromosome missegregation in human cells arises through specific types of kinetochore-microtubule attachment errors.* Proceedings of the National Academy of Sciences of the United States of America, 2011. **108**(44): p. 17974-17978.
203. Cimini, D., L.A. Cameron, and E.D. Salmon, *Anaphase spindle mechanics prevent mis-segregation of merotelically oriented chromosomes.* Curr Biol, 2004. **14**(23): p. 2149-55.

204. Brinkley, B.R., et al., *Movement and segregation of kinetochores experimentally detached from mammalian chromosomes.* Nature, 1988. **336**(6196): p. 251-4.
205. Wise, D.A. and B.R. Brinkley, *Mitosis in cells with unreplicated genomes (MUGs): spindle assembly and behavior of centromere fragments.* Cell Motil Cytoskeleton, 1997. **36**(3): p. 291-302.
206. Sarangapani, K.K., et al., *Sister kinetochores are mechanically fused during meiosis I in yeast.* Science (New York, N.Y.), 2014. **346**(6206): p. 248-251.
207. Paliulis, L.V. and R.B. Nicklas, *The reduction of chromosome number in meiosis is determined by properties built into the chromosomes.* J Cell Biol, 2000. **150**(6): p. 1223-32.
208. Corbett, K.D., et al., *The monopolin complex crosslinks kinetochore components to regulate chromosome-microtubule attachments.* Cell, 2010. **142**(4): p. 556-67.
209. Espeut, J., et al., *Natural Loss of Mps1 Kinase in Nematodes Uncovers a Role for Polo-like Kinase 1 in Spindle Checkpoint Initiation.* Cell Reports, 2015. **12**(1): p. 58-65.
210. Maddox, P.S., et al., *"Holo"er than thou: Chromosome segregation and kinetochore function in C. elegans.* Chromosome Research, 2004. **12**(6): p. 641-653.
211. Adams, S., et al., *Liposome-based transfection enhances RNAi and CRISPR-mediated mutagenesis in non-model nematode systems.* Scientific Reports, 2019. **9**(1): p. 483.
212. Fabig, G., et al., *In situ analysis of male meiosis in C. elegans.* Methods Cell Biol, 2019. **152**: p. 119-134.